D I P L O M A R B E I T

M A S T E R ' S T H E S I S

Moisture dependent elastic and viscoelastic properties of wood cell walls

ausgeführt zum Zwecke der Erlangung des akademischen
Grades eines Diplom-Ingenieurs

unter der Anleitung von

Univ. Ass. Dipl.-Ing. Dr. techn. **Thomas Bader**
Proj. Ass. Dipl.-Ing. **Leopold Wagner**

Institut für Mechanik der Werkstoffe und Strukturen
Fakultät für Bauingenieurwesen
Technische Universität Wien

Univ. Prof. Dipl.-Ing. Dr. techn. DDr.h.c. **Josef Eberhardsteiner**

Institut für Mechanik der Werkstoffe und Strukturen
Fakultät für Bauingenieurwesen
Technische Universität Wien

eingereicht an der Technischen Universität Wien
Fakultät für Bauingenieurwesen

von

Clémence Bos

Matr.Nr.: 11 27 533

Wien, im September 2013

.....
Clémence Bos

Danksagung

Zuerst möchte ich mich bei meinen Betreuern, Dr. Thomas Bader und Dipl.-Ing. Leopold Wagner, für die freundliche Betreuung, die geduldigen Erklärungen und die mehrmalige Verbesserung dieser Arbeit bedanken.
Danke auch an meine Eltern und Großeltern, Claire, Philippe, Odile, Michelle et Michel, die ermöglichten, ein umfangreiches Studium zu absolvieren, als das für die meisten Franzosen üblich ist. Für ihre moralische und finanzielle Hilfe bin ich sehr dankbar.
Danke an meine lieben Geschwister Juliette, Vinciane et Martin, die mich alle auf ihre eigene Art und Weise unterstützt haben.
Ich danke auch meinem Freund Jakob für seine weisen Ratschläge und seine gute Laune während meinen zwei Jahren in Wien.
Abschließ end möchte ich mich bei der *Ecole Centrale de Nantes* bedanken, ohne die mein Traum eines ausländischen Studiums wahrscheinlich später oder gar nicht verwirklicht worden wäre. Meine Zeit hier war angenehm, trotz mancher administrativen Schwierigkeiten. Ich habe mich gefreut, unter anderen Heidi, Julie, Peter, Sebastian, Agathe, Fanette, Martin, Lucia und die Materialwissenschaftler kennengelernt zu haben.
Ihnen allen wünsche ich alles Gute für die Zukunft.

Kurzfassung

Das Ziel dieser Arbeit ist die Bestimmung feuchtigkeitsabhängiger elastischer, viskoelastischer und Härte Eigenschaften von Holzzellwänden (S2-Schicht und Mittellamelle). Um eine große Variabilität in den mechanischen Eigenschaften zu untersuchen, wurden fünf verschiedene Holzarten mit verschieden Mikrostrukturen getestet, und zwar: Kiefer, Fichte, Eiche, Buche und Eibe. Zusätzlich wurde eine abgebaute Eichenholzprobe aus dem Vasa-Schiff in Stockholm untersucht. Nanoindentationsversuche wurden in Spätholzzellwänden durchgeführt, um Indentationsmoduli, Härte und Kriecheigenschaften der Zellwände experimentell zu bestimmen. Die Versuche wurden bei verschiedenen relativen Luftfeuchtigkeiten zwischen 10 und 80% realisiert. Es wurden auch Versuche unter Wasser mit Hilfe einer Fluid Cell für den Nanoindenter durchgeführt. Alle Holzarten zeigen eine starke Feuchteabängigkeit ihrer Eigenschaften. Zum Beispiel, der Indentationsmodul in der S2-Schicht von Kieferholzzellen vermindert sich von 20 GPa bei 10% relativer Luftfeuchte (entspricht circa 6% Holzfeuchte) auf 2 GPa unter Wasser (ca. 30 bis 40% Holzfeuchte). Im selben Feuchtebereich erhöhen sich allgemein die Kriecheigenschaften und vermindert sich die Härte aller Holzarten. Die Eibe zeigt ein wesentlich geringeres feuchteabhängiges Verhalten und die untersuchten Nadelhölzer das am stärksten feuchtigkeitsempfindliche Verhalten unter den untersuchten Holzarten. Die Eiche aus dem Vasa-Schiff ist empfindlicher gegenüber Feuchteänderungen als frische Eiche.

Zusätzlich zu den Experimenten wurde eine mikromechanische Modellierung der Holzzellwände durchgeführt. Das Mikromechanikmodell basiert auf einer poromechanischen Formulierung und verbindet die spezifische chemische Zusammensetzung der Schichten und die Holzfeuchte mit effektiven Materialsteifigkeiten. Beide Schichten, d.h. die S2-Schicht und die Mittellamelle, wurden modelliert. Um die Modellierungsvorhersagen mit den Experimenten vergleichen zu können, wurde ein Modell auf Basis anisotroper Indentationstheorie angewandt. Die entsprechende Modellierung beschreibt den Zusammenhang zwischen der schichtspezifischen chemischen Zusammensetzung, dem Feuchtegehalt im Holz und dem Indentationsmodul. Es wurde für die S2-Schicht verwendet, um den Einfluss des Mikrofibrillenwinkels auf den Indentationsmodul zu bestimmen. Die Modellierung zeigt eine Feuchteabhängigkeit der Steifigkeitskomponenten und des entsprechenden Indentationsmoduls. Der Einfluss der Feuchte wird jedoch für die Mittellamelle unterschätzt und für die S2-Schicht überschätzt.

Aus diesem Grund wurden Verbesserungen in der Art, in der Wasser in der mikromechanischen Modellierung berücksichtigt wird, vorgeschlagen. Der Einfluss unterschiedlicher Homogenisierungsmethoden wurde ebenfalls untersucht. Dadurch konnte die Vorhersagequalität des Modells verbessert werden.

Abstract

The aim of this thesis is to determine the moisture dependency of elastic and viscoelastic properties and of the hardness of cell walls (S2-layer and middle lamella) of different wood species. In order to obtain a great variability in mechanical characteristics, five different wood species with different microstructural characteristics were investigated: namely spruce, pine, yew, beech and oak. Additionally, one deteriorated wood from the Vasa ship in Stockholm was tested. Nanoindentation tests were realized on latewood cell walls in order to experimentally measure the indentation moduli, hardness and creep properties of wood cell walls. Experiments were performed in humidity conditions of the surrounding environment between 10 and 80% relative humidity. In addition, nanoindentation tests under water using a fluid cell were done. All wood species showed a great moisture dependency in all measured parameters. For example, the indentation modulus for the S2-layer of pine decreases from 20 GPa at 10% RH (around 6% MC) to 2.9 GPa under water (around 30 to 40% MC). In the same moisture range, the creep properties globally increase, while the hardness decreases. In general, yew has the less moisture-sensitive behaviour and the other softwood species the most moisture-sensitive behaviour among the investigated fresh species. The oak sample from the Vasa ship is even more sensitive to moisture than fresh oak.

In addition to the experiments, a micromechanical model for the wood cell walls was tested over the same moisture content range as in the experiments. Based on micromechanics in the framework of poromechanics, this model links the layer specific chemical composition and its moisture content with the homogenized material stiffness. Both layers were modeled, the S2-layer and the middle lamella. For comparison of model predictions with experiments, anisotropic indentation theory was applied. The corresponding model allows to describe the relationship between the layer specific chemical components, the moisture content and the indentation modulus. This was used for the S2-layer to predict the influence of the microfibril angle on the indentation modulus. The model showed a moisture-dependency of the stiffness components and of the corresponding indentation modulus. However, for most species, this dependency is underestimated for the ML and overestimated for the S2-layer.

Hence, some improvements in the water modeling were implemented in the micromechanical model. This includes the way water is considered in the model as well as different homogenization methods. Also the distribution of water within the cell wall is investigated. Thereby, model predictions could be improved.

Contents

Introduction

Motivation

Wood is a very moisture-sensitive biomaterial since its microstructural components are well known to be hygroscopic. Thus, wood softens when the humidity in the surrounding environment increases. This phenomenon is sometimes useful, like in the basketry industry, where for example the softening of the branches lets the artisan get them into shape. In civil engineering, however, this phenomenon is undesired since it weakens the material and, therefore, increases the deformations of a structure.

Indeed, since wood is a heterogeneous composite, it even has a hierarchical microstructure and the relations between the chemical components and the global structure are very complex. Therefore, the global behaviour of wood strongly depends on the microstructural and micromechanical characteristics, which are moisture dependent. Actually, if the moisture uptake at the molecular scale has an influence on the macro-scale moisture uptake, this effect is also superimposed by the influence of other parameters, such as e.g. the wood density, the cell structure or the total proportion of latewood. Since these other parameters have a high variability within the different wood species, within the trees of one species and within one tree, solely the influence of moisture can hardly be assessed on the macroscale. However, since moisture uptake takes place within the cell wall of wood fibres, the study of cell wall properties is expected to yield enhanced insight into wood moisture-mechanics relationships. In a further step, upscaling the results to the macroscopic level may be possible with a micromechanical model of softwood.

Hence, this thesis is exploring the influence of water on wood from a mechanical point of view and at a microscopic level, using both experiments and a micromechanical simulation. The aim is to identify wood moisture-mechanics relationships for the S2-layer and the middle lamella. Furthermore, microstructural characteristics of wood specimens will be used to develop and verify a micromechanical model for wood cell walls.

Structure of the thesis

The aim of this thesis is to determine the dependency of wood cell wall layers (S2 and middle lamella) on moisture content. This also encompasses to formulate hypotheses on the water absorption within the investigated wood specimens, the moisture repartition between the different cell wall layers and between the cell wall components.

For this purpose, the wood cell walls are tested through nanoindentation measurements, which give results on the elastic, viscoelastic and hardness properties of cell wall layers. Additionally, a micromechanical modeling of the cell walls gives predictions on

elastic properties, which can be compared to the experimental results with a previously developed tool [5].

In a first step, nanoindentation (NI) tests are performed to determine the indentation modulus, the hardness and the creep properties of the main layers of the wood ultrastructure at a number of relative humidities and also under water. Five wood species are investigated, three of them being softwoods and two of them hardwoods. In addition, one deteriorated wood was also investigated, an oak sample from the Vasa ship. The wood samples were tested in their latewood, cut from the heartwood of the tree, and at four different humidity conditions, from 10% RH to 80% RH and under water with the use of a fluid cell. To relate the NI tests with the wood moisture content, the effective proportion in mass of water inside the wood specimen, the desorption curve of five investigated wood species was experimentally determined.

Then, a micromechanical model based on the continuum micromechanics in the framework of poromechanics was used, which was originally developed by Bader et al. [5] in 2010 for the wood cell wall S2-layer. Jäger et al. [30] in 2011 developed a mathematical model for the relationship between the indentation modulus, the microfibril angle and the elastic properties of a wood cell wall layer. Hence, the relationship between indentation modulus - as experimentally investigated - and the chemical composition and wood moisture content of a specific wood sample can be predicted by this modeling approach. Even if the original model heed also a unit cell model of the wood structure up to the macroscopic scale (for softwoods modeling), the work area was here restricted to the wood cell wall. Hence, the S2-model was tested at many various wood moisture contents and adapted for the modeling of the middle lamella. Then, both layer models were improved for considering a broader range of moisture contents, by taking into account the proportions in which water may be absorbed by the different wood cell wall layers and by the different wood components inside one layer.

Chapter 1

Wood-moisture-mechanics relationships

In the following, the relationship between wood microstructure and wood moisture content and its consequences for the mechanical behaviour of wood is discussed. For this purpose, the hierarchical levels of the wood microstructure will be reviewed as well as the origin of moisture uptake in wood. The relevance of these issues for the design of experiments for the investigation of moisture dependent mechanical properties of wood cell walls will be highlighted.

1.1 Hierarchical (micro)structure of wood

There is a great diversity in trees due to the huge variety in natural environments, which represent the growth conditions for trees. This diversity is also visible within a tree, since wood as a material is considered a natural hierarchical composite; a composite well hierarchically organized from its cells to its tree structure. As every biomaterial, before used for industrial or research purposes, trees are living organisms. Hence, tree cells are not only fulfilling the function of mechanical support of the plant body, which is the most interesting function for the engineers, but they also ensure:

- the conduction of water from the roots to the leaves, and
- the storage of tree nutrients.

Therefore, cells are interconnected one with each other, which leads to an anisotropic water absorption on the one hand and a sorption hysteresis on the other hand (see Section 1.2.3). Even more important, trees are also mechanically anisotropic, as the mechanical and vital needs of the tree are oriented in the longitudinal direction. This is also well represented in the hierarchical microstructure of wood, which will be discussed in the following.

1.1.1 Macroscopic structure of wood

At the macroscopic scale, i.e. at the integral level of a tree, a tree is composed of the shoot and the roots. The roots act for water and mineral nutrient uptake, mechanical anchoring and storage of biochemicals. The shoot is composed of the leaves, the branches and the stem, which ensure energy production and, therefore, the growth and the reproduction of the species. Among others, the stem itself is divided in many layers at the macroscopic level (see Figure 1.1):

the pith is located at the center of the stem. It is responsible for the storage and the transport of nutrients and chemicals throughout the tree.

the heartwood is the biggest part of the stem, located around the pith. It is only composed of dead cells and it has an extractives storage function besides its mechanical function.

the sapwood is located between the heartwood and the bark. It conducts water by means of the sap from the roots to the leaves. Its living cells, the parenchymal cells, store carbon for the later use for growth and they transform the nutrients into extractives at its inner border.

the (vascular) cambium is a thin layer between the sapwood and the bark. It produces new cells and, because of the annual climatic changes and their influence on the cell shape, annual rings are created.

the bark is protecting the tree against temperature changes and radial mechanical loads. It can be divided into the inner and outer bark.

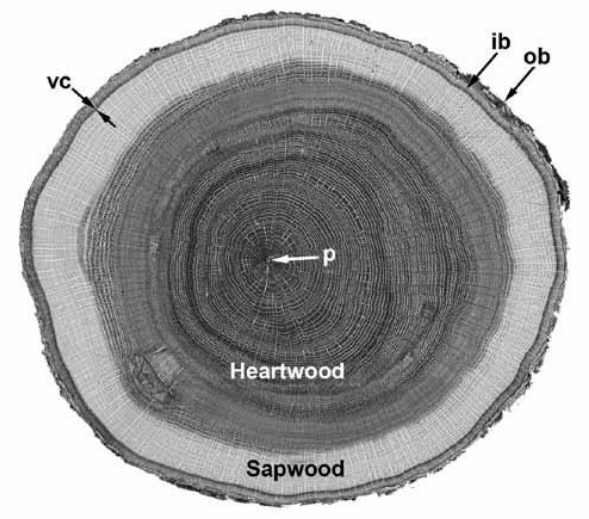

Figure 1.1: Transversal section of wood. From outside to inside: *ob* is the outside bark, *ib* the inner bark, *vc* the cambium and *p* the pith (from [20]).

All measurements and models in this thesis refer to heartwood, except for spruce, for which the sample comes from the sapwood.

Wood sections and wood axes

In mechanics, it is important to define the axes and the main planes for the definition of mechanical and physical properties. In Figure 1.2[1], the longitudinal axis is parallel to the stem, the radial axis is in the direction of wood rays from the pith to the bark. These axes idealize the tree using a cylindrical coordinate system. The tangential axis is tangent to the bark and perpendicular to the radial direction. The main sections of a tree stem are plotted in Figure 1.3. The radial section is the section in the longitudinal and radial directions. The tangential direction is tangential to the annual rings. The transversal section (or cross-section) is the section perpendicular to the longitudinal direction and thus, to the longitudinally oriented fibres. Therefore, annual rings and cross-sections of wood fibres are visible in the transversal section.

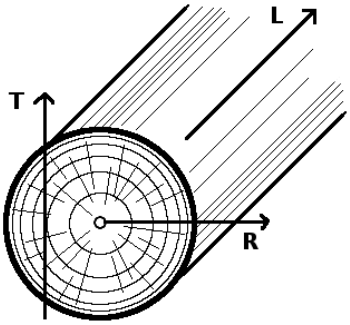

Figure 1.2: Main directions in a wood stem. L: longitudinal axis, R: radial axis, T: tangential axis

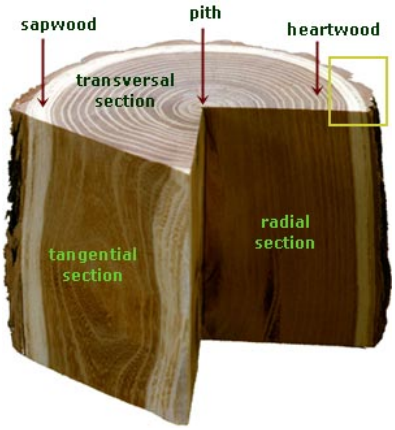

Figure 1.3: Main cutting planes in a wood stem (from [20])

[1]From Personal Webpage of Prof. Emeritus D. Patterson of University of Arkansas at Monticello `http://www.afrc.uamont.edu/pattersond/`

Softwood and hardwood

Before going further into the description of the wood microstructure, it is important to mention that wood species can be divided into two categories: hardwood and softwood. If these names seem to be related to mechanical properties of wood, they are only vaguely related to the ease of cutting or sawing wood.

Also called gymnosperms or conifers, softwoods are mostly needle-leaved evergreen trees. Their basic structure is comparably simple with only two different cell types. Hardwoods are also called angiosperms or flowering plants. They are broadleaved, deciduous trees. They are the most evolved wood species, i.e. they have a great number of basic cell types for a greater degree of variability within the hardwood species and within a tree. As an example of cell types which are not to be found in softwoods, vessel elements are present in hardwoods. Vessels are big cylindrical cells running in stem direction. The vessels may also be called pores, as they appear as cavities within a cross-section under a microscope. Within hardwoods, a further distinction can be made between diffuse porous and ring porous hardwood. This is related to the distribution of vessels within annual rings.

One of the aims of this study is to investigate the variability of mechanical properties among different wood species. Therefore, softwood and hardwood species were chosen for mechanical and microstructural characterization. In particular, Norway spruce, Scots pine and Common yew were selected to represent the group of softwood, while Common beech and European oak were chosen to represent diffuse porous and ring porous hardwood species, respectively.

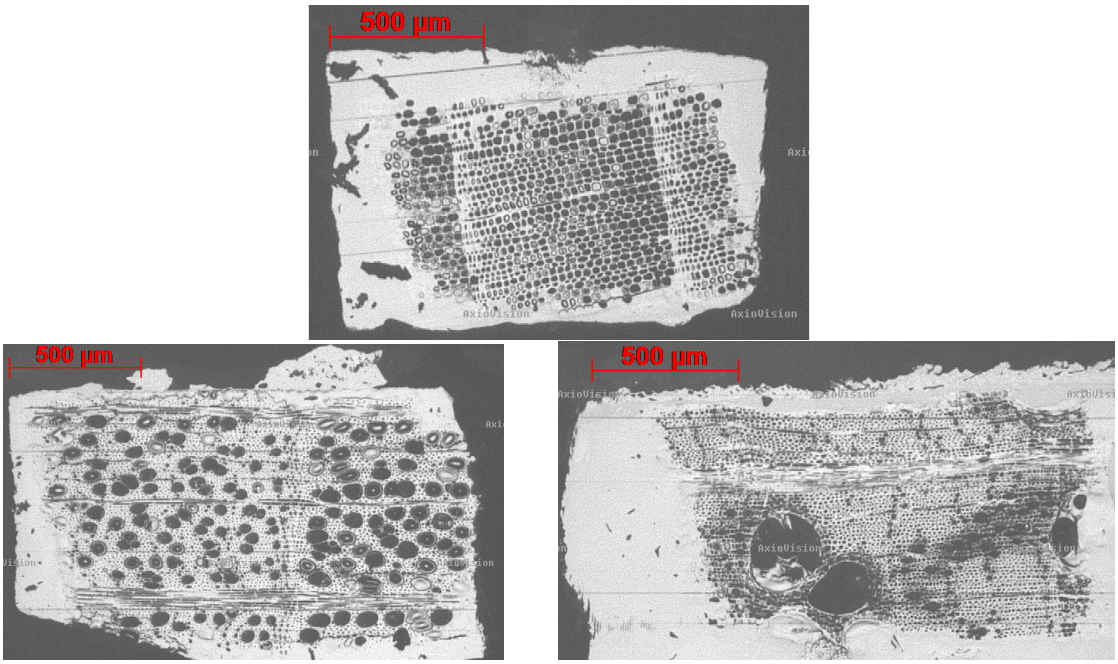

Figure 1.4: Top: microstructure of yew, a softwood, Bottom left: microstructure of beech, a diffuse-porous hardwood, Bottom right: microstructure of oak, a ring porous hardwood.

1.1.2 Microscopic structure of wood

Cells, regardless of their type, are the smallest living units within a tree. They are mostly considerably longer than wide and organized in two interpenetrated and interconnected systems. In the first system, the axial system, cells have their longitudinal axis parallel to the stem, in the longitudinal direction. They are, hence, responsible for the long-distance water transport and are building the bulk of the material, which makes up the mechanical strength of the tree. In the second system, the radial one, cells have their longitudinal axis perpendicular to the stem, i.e. in the radial direction, directed from the pith to the bark. They act as elements for the lateral transport of biochemicals and also have a storage function.

However, not all kinds of cells can be found everywhere within a tree: within the heartwood and the sapwood, we can distinguish growth rings, composed of a layer of earlywood, built during the spring, and of a layer of latewood, composed of summer cells. Earlywood cells are mostly bigger and have thinner cell walls, while latewood cells are more densely packed and have thicker walls.

Different patterns for the transition between the earlywood and the latewood are possible, going from no distinction between these two layers, e.g. in diffuse porous hardwood species, to a sudden and distinct decrease of the inner cell diameter or to the formation of a distinct transition wood layer, as e.g. in ring porous or semi ring porous hardwood species. The pattern depends of the species and of the suddenness of the weather transition between the wet and the dry seasons, as earlywood is mainly produced in wet weather conditions and latewood during the drier season. In ring porous hardwood, large vessels are to be found in the earlywood, while the tissue is denser and more fibrous in the latewood. Figure 1.4A shows the structure of softwood. Figure 1.4B shows a diffuse porous hardwood, Figure 1.4C shows a ring porous hardwood.

Only latewood cells were experimentally investigated in this study.

Microstructure of softwood

As explained in [20], only two kinds of cells make up the biggest part of softwood, namely tracheids and ray cells.

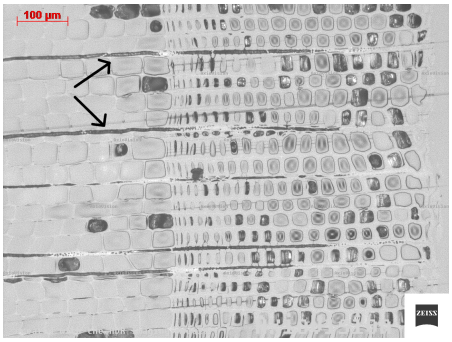

Figure 1.5: Transversal section of spruce. The arrows indicate two uniseriate rays.

Tracheids

Oriented in the longitudinal direction, the tracheids are long cells, measuring from one to ten millimeters in length and 10 to 100 micrometers in width. They make up 97% of the volume of the wood. Therefore, they are responsible for the conductive as well as the mechanical characteristics of the tree. Their cross-sectional shape is square or slightly rectangular and they are organized in radial rows. To ensure the water conduction, the light weight of the structure and possibly the extractives storage, they have hollow cells, with a pore space also called lumina (in sg. lumen). Walls of these cells are thin in earlywood and thick in latewood. Water flow takes place between adjacent tracheid cells within one stack through circular bordered pits concentrated in the long, tapered ends of the cells. The water path seems then slightly zigzagging. Moreover, as the pit membrane offers a resistance to the flow, the water flow in softwoods seems relatively inefficient in comparison to this phenomenon in hardwoods.

Ray parenchyma cells

Ray parenchyma cells are rather radially oriented. They look like rectangular prisms or brick-shaped cells (see Figure 1.5). They typically measure 15 µm in height by 10 µm in width and 150 to 250 µm in length in the radial direction (from [20]). Assembled one after the other, they form ray cell bundles, which have the function to synthetize, transport and store biochemicals and, in a much lower amount, water. Ray cells in softwoods are typically only one cell wide, therefore, they are called uniseriate rays.

Other cells

Other cell types, as e.g. axial parenchyma cells, resin canal complexes (in white in Figure 1.6(left) and ray tracheids can also be found in some softwood species.

As a reason of their importance for the overall behaviour of softwood, tracheids are investigated in this work.

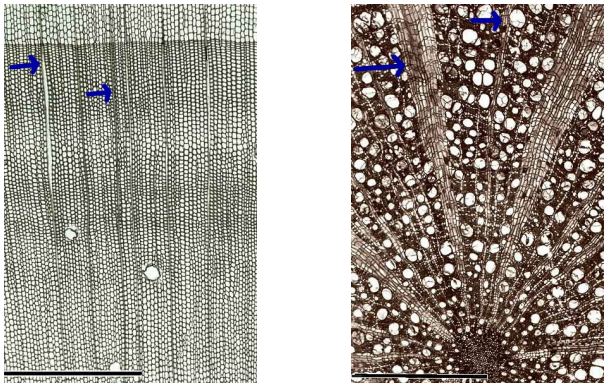

Figure 1.6: Left: transversal section of pine with thin uniseriate rays. Right: transversal section of beech with arrows indicating multiseriate ray bundles. Scale bars: 1 mm (from [47])

Microstructure of hardwood

In contrary to softwood, hardwood shows a greater variety in cell types, shapes and sizes.

Vessels

As illustrated in white in Figure 1.4B, vessels are responsible for the vertical water conduction. Vessel elements are stacked one above the other and perforated on the top. In the transversal direction, they look like large openings, therefore, they are also referred to as pores. Their typical diameter is 50 to 200 µm, for a length that is smaller as for tracheids: 0.1 to 1.2 mm. In diffuse-porous wood, all vessels are more or less regularly scattered throughout the growth ring. In ring-porous wood, earlywood vessels are much bigger than the latewood ones. Intervessel pits however, are present in all species.

Due to the stacking of the vessel elements one above the other, as well as due to the absence of barriers between two following elements, hardwood can easier conduct water than softwood.

Fibres

Fibres are the load supporting cells in hardwood. They are slightly longer than vessels. They are half as wide as softwood tracheids and shorter: their length is about 0.2 to 1.2 mm, but fibres are two to ten times longer than vessels. The thickness of the fibre cell wall is related to the density and mechanical strength of hardwood.

Other cells

There is a higher content in axial parenchyma cells in hardwood than in softwood, see the right image in Figure 1.6. Axial parenchyma cells have a similar shape and size as in softwood.
Rays are structurally more diverse than in softwood. Ray bundles are mostly wider than one cell, with a width of several millimetres and a length from one cell to several centimetres. Therefore, rays can be called multiseriate rays. The types of ray bundles found in a wood is used, in particular, for species identification.

Considering the function of each type of hardwood cells, the focus in this work is laid on the characterization of fibres in hardwood experiments.

1.1.3 Wood cell wall ultrastructure

Cells themselves have a highly regular structure (within all wood species and within one tree) and, at the same time, they are heterogeneous and are composed of:

- the lumen - the void space within the cell,
- the secondary wall,
- the primary wall, and
- the middle lamella between the cells.

Each layer is composed of cellulose microfibrils as reinforcement, of hemicelluloses and of a matrix made of lignin or pectin. These chemical components are described in the following Section 1.1.3.

Figure 1.7 illustrates the location of each wood cell wall layer and sub-layer, with their associate microfibril angle (MFA). The MFA represents the orientation of the stiff cellulose microfibrils with respect to the cell axis.

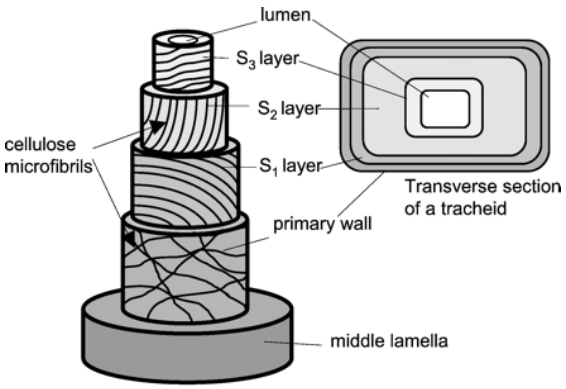

Figure 1.7: Right: Transversal schematical representation of the wood cell wall layers in a tracheid. Left: cellulose microfibril angle in each layer (from [41]).

Different layers within the cell wall

The middle lamella

In order to ensure the global tree cohesion, cells adhere one to each other with the help of the middle lamella (ML). Its thickness is around one micrometer, but is varying with its location and the number of adjacent cells. It is mainly composed of lignin.

The cell wall itself is divided into a primary and a secondary layer, which are very different from each other. Located near the ML, the primary cell wall is very thin and composed of randomly oriented cellulose microfibrils (with an angle of 0° to 90° with respect to the cell axis) and hemicelluloses and pectin as matrix. Since it is often impossible to distinguish it from the ML and since it has got low mechanical properties, the primary cell wall was not investigated in this thesis.

The second layer of the cell wall before the central lumen is the secondary cell wall, which is itself composed of three sub-layers. The most important sub-layer, due to its thickness as well as due to its mechanical properties, is the secondary-2 (S2[2]) layer. The S2-layer is made of a low percentage of lignin and high percentages of cellulose microfibrils and hemicelluloses. The S3-layer, relatively thin, cares for the water adhesion in the lumen and the transpiration of the cell, which has to be related to its very low content of lignin. The S1-layer is thin, quite blended with the primary cell wall layer and the ML. It is mainly composed of hemicelluloses.

Within the secondary wall, the cellulose microfibrils present various angles with respect to the cell axis: around 5° to 30° in the S2-layer, but around 50° to 70° in the S1 and S3-layers. As in every composite, the angle of the microfibril reinforcements with the longitudinal axis is of big importance for the mechanical properties of the layer.

Hence, in the following, cell wall investigations focus on the S2-layer and the middle lamella.

Chemical components

All the cell wall layers consist of the same basic wood components: cellulose micro-fibrils, hemicelluloses and a matrix composed of pectin in the primary wall and lignin in the

[2]similarly secondary-1 is abbreviated by S1 and secondary-3 by S3

secondary wall and in the middle lamella.

Cellulose is a long, string-like polysaccharide molecule with high tensile strength. It is composed of crystalline and amorphous parts. It assembles itself to form long, crystalline, thread-like macro-molecules called microfibrils, which are then even stronger as the sum of all separated cellulose fibres. Within one wood layer, the microfibrils may be oriented with the same angle with respect to the cell axis, the microfibril angle (MFA) of cellulose. Figure 1.8 represents schematically the path of the cellulose microfibrils in the S2-layer of a wood cell wall.

The cellulose can be divided into amorphous and crystalline parts.

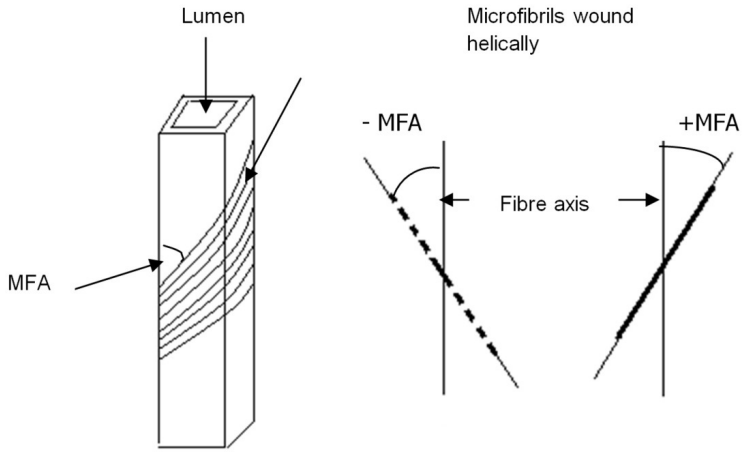

Figure 1.8: Schematic diagram representing the rectangular cross section of wood fibres and the orientation of the cellulose microfibrils in both front, +MFA and back, -MFA around the fibre axis (from [51]).

Hemicelluloses, however, are polysaccharides with a smaller and branched structure. Thus, they are assumed to be amorphous and consequently weaker than cellulose in the longitudinal direction. Hemicelluloses link cellulose and lignin one with each other. The lignin is a quite brittle and soft matrix.

Finally, minor contents of extractives are also embedded inside the layers. Named after their property of being solubilized by organic solvents, they are considered as biotoxic. Their presence in wood finds its justification in their ability to defend the wood against pathogens.

The influence of species-specific chemical compositions on the mechanical behaviour of wood will be considered herein.

1.2 Wood-water interactions

Water has a strong effect on the wood properties, in particular on the density at the macroscopic level and on the mechanical properties. The University of Cambridge in its article of the Dissemination of IT for the Promotion of Materials Science (DoITPoMS) project [8], briefly summarizes about water effects on wood: "water's presence dramatically softens the cell walls". Figure 1.12 shows for example the wood compressive stress

dependency towards wood moisture content under and beyond the wood Fibre Saturation Point (at a moisture content around 30%).

The reason for this lies in the hygroscopic behaviour of wood components.

1.2.1 Chemical interaction of water with the cell wall

In 1962, Sakurada et al. [45] determined the non-dependency of the mechanical properties of a single crystalline cellulose fibre to water.

In 1976, Cousins [10] isolated lignin powder from the wood cell walls of a pine, mould it into a cylindrical shape and performed mechanical tests on it. It showed a linear increase in the Young's Modulus from 3.1 GPa up to 6.7 GPa as the lignin moisture content decreased from 12% to 3,6%. This indicates lignin to be moisture-sensitive.

However, in 1978, Cousins again [11] tested hemicelluloses extracted from pine under several moisture contents, from 10% RH to 90 to 100% RH with an indentation method, the ball indentation. He found that the Young's Modulus decreased from 8 GPa in the nearly dry state to 0.07 GPa in the nearly saturated state. He concluded that hemicelluloses are very moisture-sensitive, especially in comparison with lignin.

It is also supposed that the amorphous cellulose absorbs moisture, based e.g on Salmeǹ [46] and Skaar [49]. Salmeǹ summarized in 1982 his research on softening of the paper components. He described the plasticizing of the amorphous cellulose due to water through the decrease of its glass transition temperature T_g with increasing moisture content. He calculated the decrease of T_g with some polymer-plasticizing equations.

To summarize, hemicelluloses and amorphous cellulose are the most moisture-sensistive wood components of the wood cell walls.

1.2.2 Definitions related to moisture

Moisture

It refers to the free water, which is present in liquid or vapor state in the cell lumina and in the cavities, as well as to the bound water, held by intermolecular attractions within the cell walls.

Moisture content [3]

The moisture content (MC) is the ratio of the mass of water present in the wood under given environmental conditions and of the mass of the oven-dry wood, see Equation (1.1). For the determination of the mass of an oven-dry wood sample, it is dried inside an oven at 103℃until its mass does not vary any more. This indicates that all water naturally present inside the wood has evaporated from the sample.

$$MC = \frac{m_{water}}{m_{wood}}.100 \text{ in } \% = \frac{m_{wetwood} - m_{drywood}}{m_{drywood}}.100 \text{ in } \% \tag{1.1}$$

The MC range for green wood, i.e. the freshly sawn wood, can reach 30 to 200%, the upper limit occurring when the cell walls are completely saturated with water and the lumina as well. A MC above 100% is not impossible at all and only means that there

[3] from EN 13183-1-2002 "Moisture content of a piece of sawn timber - Part 1: Determination by the oven dry method"

is more water than dry wood, in mass, in the sample. It gives an idea of how porous a piece of wood is.

Equilibrium Moisture content

The equilibrium moisture content (EMC) is the moisture content at which the piece of wood is not gaining nor loosing moisture. It is characterized by a constant mass under constant humidity and temperature conditions.

Fibre Saturation Point

According to "The Wood Handbook" [20], the Fibre Saturation Point (FSP) refers to the moisture content at which all cell walls are saturated and no free water is located in the lumina. Furthermore, for moisture contents above the saturation point, physical and mechanical properties of wood do not vary any more. The FSP is usually reached for a moisture content of around 30% [20]. However, there is no unique transition point, but a gradual transition between unsaturated and saturated wood [25, 50]. Therefore, in this thesis, if the FSP will refer to the measurements at 100% RH, no MC is assigned to the FSP, and in the graphs, a FSP between 30 and 40% will be considered.

1.2.3 Diffusion mechanisms of water in wood

There are three states in which water can be found in wood [6, 7, 16, 36]:

- free water is capillary water present mostly within the cell lumina,
- freezing bound water is water loosely bound in the larger water clusters,
- non-freezing bound water is bound water in the cell walls which interacts strongly through hydrogen bonds formed with the hydroxyl and carboxylic acid groups of the wood polymeric components, mostly hemicelluloses and cellulose.

Bound water is water molecules which form a hydrogen bond with the available hydroxyl groups on hemicelluloses or on cellulose.

Water absorption in wood

The moisture content in wood is related to the relative humidity (RH) of its environment and to the temperature. Typically, wood has to go through long-term (or seasonal) changes and short-term (or daily) humidity changes. The second kind of changes affect only the surface of the piece of wood.

The sorption isotherm describing the relationship between the EMC and the RH at a given temperature shows a hysteresis, because the pits and the tracheids stacks are not symmetric for moisture adsorption and desorption. The EMC for adsorption is lower than the EMC for desorption (see Figure 1.9).

This means that at given temperature and relative humidity, a range of different moisture contents are possible in wood. Figure 1.10 shows the MC variation for a given relative humidity. It may reach up to 3% MC.

In the experiments made in this thesis, the wood samples could not be investigated following one sorption hysteresis. They were stored at a relative humidity of 40%, then measured a first time at 10% RH and, subsequently, at 40% RH. Then, they were stored

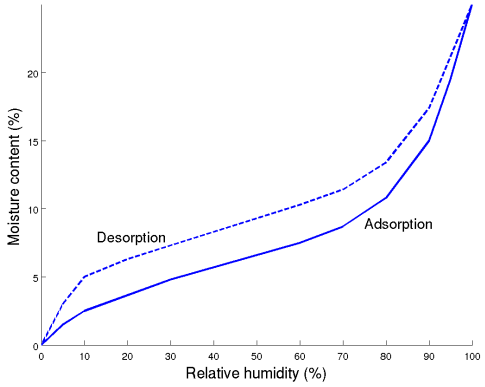

Figure 1.9: Water vapour sorption diagram of a wood sample

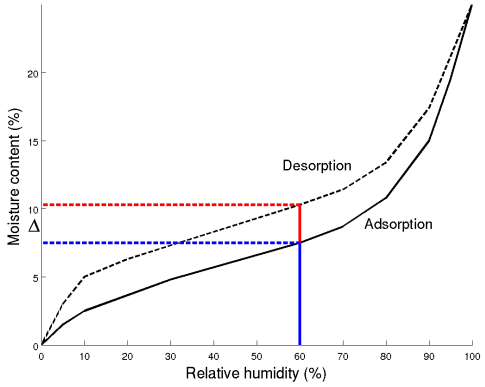

Figure 1.10: Range of possible moisture contents for a given relative humidity and given temperature

at 50% RH, measured at 60% RH and 80% RH and then stored again, at 60% RH. Finally, they were put two times under water (100% RH), while stored in the meanwhile at 60% RH.

Besides that, both absorption and desorption processes encompass a change in temperature and volume within the piece of wood. In other words, work and heat are thermodynamically related to the moisture adsorption and desorption of water in wood. In order to consider only the influence of the moisture content on the wood (see Figure 1.11), the temperature was kept constant around the piece of wood and the possible swelling or shrinkage of wood was not prevented.

Therefore, during the experiments realized for this thesis and when the samples were unused, their surrounding temperature was always kept constant between 20 and 23°.

1.3 Wood mechanics

Wood is an anisotropic, in fact even orthotropic material at all level of hierarchy, according to [20]. This means that the direction of load affects the way the material responds to

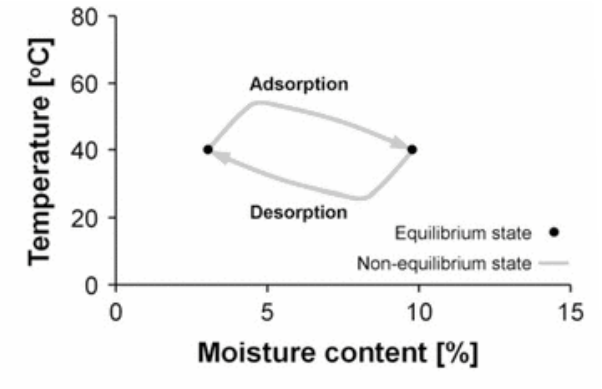

Figure 1.11: Relationship between temperature and moisture content of a wood sample (from [17])

the load. In general, the longitudinal stiffness, parallel to the fibres or to the tracheids, is higher than the radial one, normal to the growth rings, which is itself higher than the tangential one. An anisotropic material requires twelve constants to describe the elastic properties of wood from a macro-mechanical point of view: three moduli of elasticity E, three moduli of rigidity G, and six Poisson's ratios ν. Due to its orthotropy, nine of the wood elastic constants are independent and sufficient for a full mechanical description in (orthotropic) elasticity.

In the cell walls, each layer has its own mechanical properties. The S2-layer has strong cylindrical cellulose microfibrils aligned with an angle corresponding to the microfibril angle (MFA) and embedded in a softer isotropic matrix. Therefore, the S2-layer has a transversely isotropic behaviour in the cellulose microfibrils direction, which is oriented with the MFA with respect to the stem axis.

The middle lamella consists of cellulose microfibrils randomly oriented in the space. No direction is privileged and the middle lamella has an isotropic material behaviour.

1.3.1 Natural characteristics affecting mechanical properties

As explained in [20], the density of wood is directly related to the number of tracheids or fibrils into the wood, to the relative proportion of latewood and earlywood as well as to the proportion of cells with thick walls. Thus, these natural characteristics are playing a big role in the mechanical properties of a piece of wood. Some other parameters from the wood structure that influence its mechanical properties are the number, the size, the location and the soundness of knots or the following parameters:

- fibre directions with regard to the edges of a piece, if the sample is not perpendicularly cut,
- annual ring orientation and other radial density variations,
- presence of reaction wood,
- presence of juvenile wood,

- presence of extractives,
- presence of pitch pockets,
- presence of bird pecks.

Therefore, only clear wood was tested and modeled in this thesis, i.e. wood without growth irregularities like the one cited above.

1.3.2 Effect of the environment

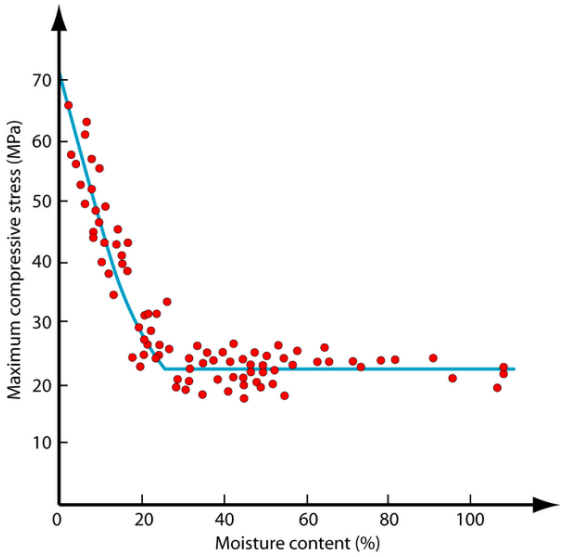

Figure 1.12: Compressive strength of Scots pine under various wood moisture contents (from [13])

Like every biomaterial, wood is more sensitive to its environment than common industrial materials. For example, as already explained in Section 1.2.1, some wood components are very moisture-sensitive. This naturally affects the wood mechanical properties by lowering the stiffness [1] and increasing the creep behavior [31]. But also changes of temperature can lead to softening of wood: changes in mechanical properties are reversible in case of quick temperature changes under 100 °C, while they are irreversible in case of higher temperatures or long impact durations of elevated temperatures.

Moreover, the growth environment of the tree modified its structure and then its properties. Since, for example the climate, i.e. the growth surrounding temperature and humidity are varying constantly around the tree, even the clearwood latewood quality varies from one annual ring to the other and from one cell to the other. Therefore, always cells from the same annual ring were investigated and a certain dispersion in the results was expected.

In this work, the influence of surrounding relative humidity in a range of 10 to 80% will be tested, as well as the mechanical behaviour of wood cell walls when they are fully saturated, i.e. under water.

1.3.3 Effects of time

Moreover, under loading, the duration of load is an important factor for the determination of the resistance of a piece of wood. Wood is prone to creep as soon as it is under loading. The creep phenomenon is defined as the additional deformations which occur under a constant load. Creep deformations can be up to equal to the initial elastic deformations. Associated together, the initial elastic deformation and the creep deformation can even lead to a premature rupture of the beam. For safety reasons, a creep related factor was defined: the duration of load is the maximum load duration that can safely be carried by a wood structure for a specific load level.

Polymers are known for their creep properties. Since the wood components are mostly polymers, the ability of the cell wall layers to creep was investigated and confirmed for sugi by Kojima et al. in 2005 [31] and for different pine species by Meng in 2010 [35]. The dependency of the cell wall creep towards moisture was even modeled by Meng [35] with use of the Burger's model and fitted with the experiments of Kojima.

In this work, the creep properties of five different wood species are investigated, covering a range of relative humidity from 10 to 100%. However, since the creep properties determined by means of nanoindentation are no material properties in a strict sense, the results of this thesis may not be directly comparable with the above cited articles.

Chapter 2

Experimental investigations

In this chapter, first details of the investigated wood specimen are presented, followed by the experimental investigation of their individual behaviour to water and the determination of equilibrium moisture contents. Then, the nanoindentation experiments will be detailed, beginning with the technical presentation of the nanoindentation testing, followed by the experimental protocol. Results from the experimental investigation on five different wood species under various climatic conditions will be presented and discussed.

2.1 Materials

2.1.1 Wood samples

Nanoindentation tests were performed on five different European wood species and one deteriorated wood. They were chosen for their frequent use in the European market and, thus, for their well known microstructures and macroscopic mechanical properties. Three of them are softwoods: pine, spruce and yew, while the two others are hardwoods: beech and oak. Besides these fresh wood specimens, one deteriorated wood was investigated: a sample cut from the Vasa ship which sank in the *Stockholms ström*, the bay of the baltic sea near Stockholm, just after its production in 1628. The wood had been conserved due to the salted sea water and its particular location in the bay, because the pollution of the *Stockholms ström* caused unfavourable conditions for shipworms, which normally devour and destroy wooden ships. The ship was salvaged in 1961 and is now on display at the Vasa museum in Stockholm. However, pollution damaged and is still damaging the wood of the ship, because the sulphides in the water impregnated the wood and are now reacting with the oxygen in the ambient air. This is an ongoing process, even if the ship is protected by a layer of polyethylene glycol (PEG) since its extraction from the ocean.

Table 2.1 summarizes the overall chemical composition in weight fractions of cellulose, hemicelluloses, lignin and extractives for each investigated sample. The MFA of the S2-

Table 2.1: Chemical composition of investigated wood samples, with their microfibril angles and the method used for its determination. C: cellulose, HC: hemicelluloses, L: lignin, Ext: extractives. Methods: a: thin section, b: Wide Angle X-ray Scattering (WAXS), c: Silviscan-3^{TM}

				Chemical composition (%)				
Common name	Scientific name	MFA (°)	Method	C	HC	L	Ext	Ref.
Norway spruce	*Picea abies*	12.5	a	49.1	24.4	23.7	2.8	[4]
Scots pine	*Pinus sylvestris*	12.7	b	46.9	27.1	23.5	2.5	[55]
Common yew	*Taxus baccata*	27	a	44.7	20.8	23.9	10.6	[5]
Common beech	*Fagus sylvatica*	7	a	49.1	25	23.2	2.7	[12]
European oak	*Quercus robur*	3	a	40.8	32.2	21	6	[12]
Vasa oak	*Quercus robur*	17.1	c					

layer of a wood specimen can be determined in a quick way through some techniques:

First, the thin section method consists in cutting samples with 15 µm thickness from the radial section using a microtome. Then, the samples must be water saturated and harsh dried slightly over 100 °C, which produces cracks in parallel orientations with regards to the microfibrils. If the marks are not observable after the first drying cycle, an additional step may be added, consisting of immersing the samples in a iodine solution and add nitric acid on the surface. The microfibril angle is then to be seen "as elongated, dark crystals of iodine filling the cracks in parallel lines" (from [48]). Finally, the MFA can be measured with use of a light microscope.

The second method used for MFA characterization is the Wide Angle X-ray Scattering (WAXS). Again, thin sections of 50 to 70 µm are cut near to the NI specimen. This technique, based on the X-ray diffraction on the crystalline microfibrils and described in [9], was applied by L. Wagner to the wood specimens of this thesis, as documented in [55].

The third technique used for the determination of the MFA is Silviscan. This efficient machine is able to quickly determine many different wood characteristics from a unique sample without destroying it, since it integrates many tools like an image analyser, a X-ray diffraction and a X-ray absorption system.

Chemical composition of wood cell wall layers

As an assumption, Fengel and Wengener [18] divided the global chemical composition of the wood into S2-layer, Middle Lamella and S1-layer specific compositions. Ratios are presented in Table 2.2. However, since the S1-layer is less important for the mechanical properties of the wood cell wall than the two others (see 1.1.3), this distribution was re-calculated for the S2 and the ML layers. Table 2.3 contains the final composition for both layers of spruce as used in this work.

Microstructures of wood samples

Figures 2.1 and 2.2 show the investigated wood specimens at differents scales. On the left sides, the NI sample overview, where one to two annual rings (AR) are observable. The corresponding image on the right shows the latewood and the region selected for nanoindentation tests.

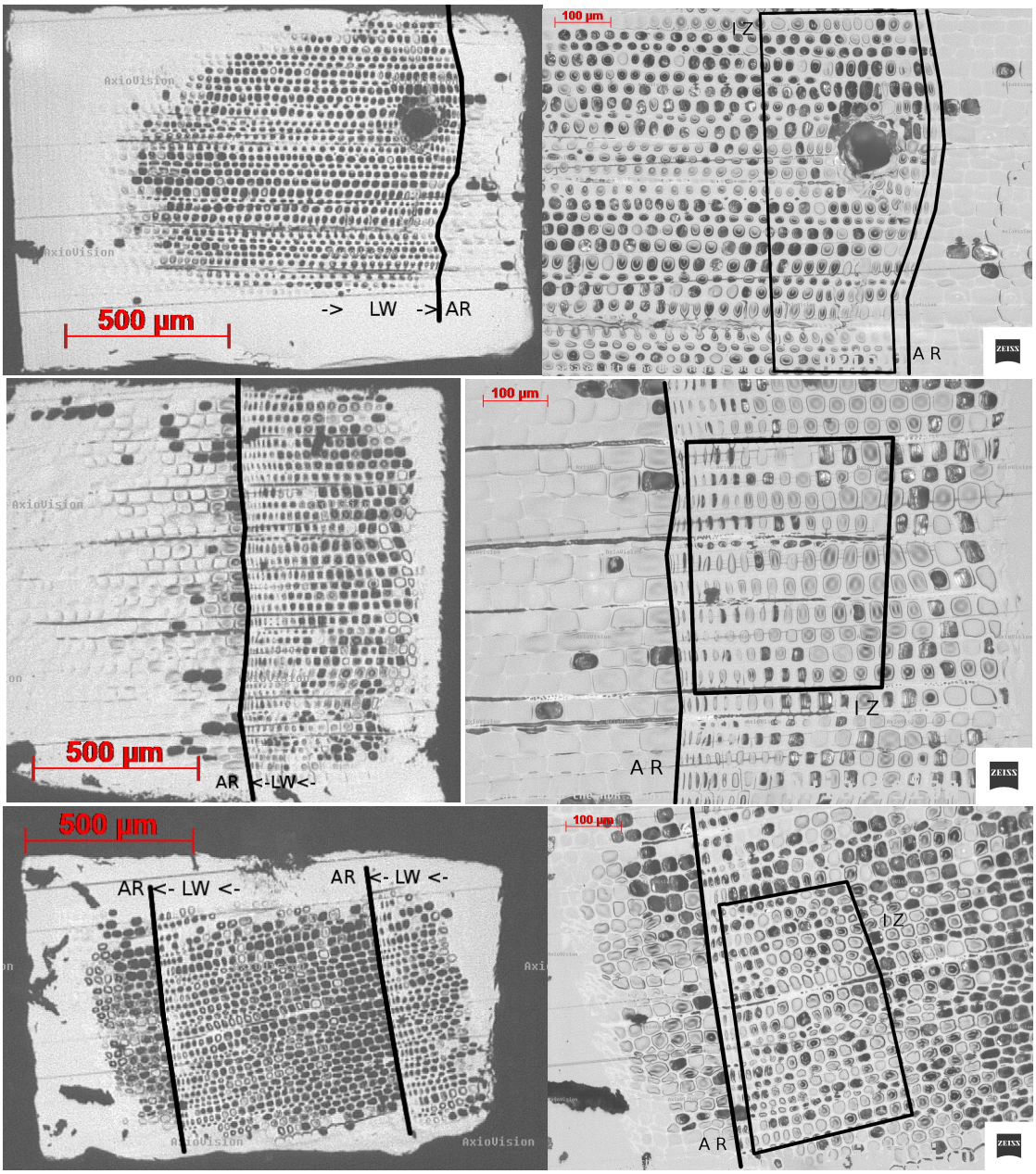

Figure 2.1: Overview and detailed light microscope pictures of the investigated softwood species. On the top: (left) pine sample with a 25x-magnification, (right) pine sample with a 100x-magnification. In the middle line: (Left) spruce sample with a 25x-magnification, (right) spruce sample with a 100x-magnification. On the bottom: (left) yew sample with a 25x-magnification, (right) yew sample with a 100x-magnification. AR: annual ring, LW: latewood, IZ: indentation zone.

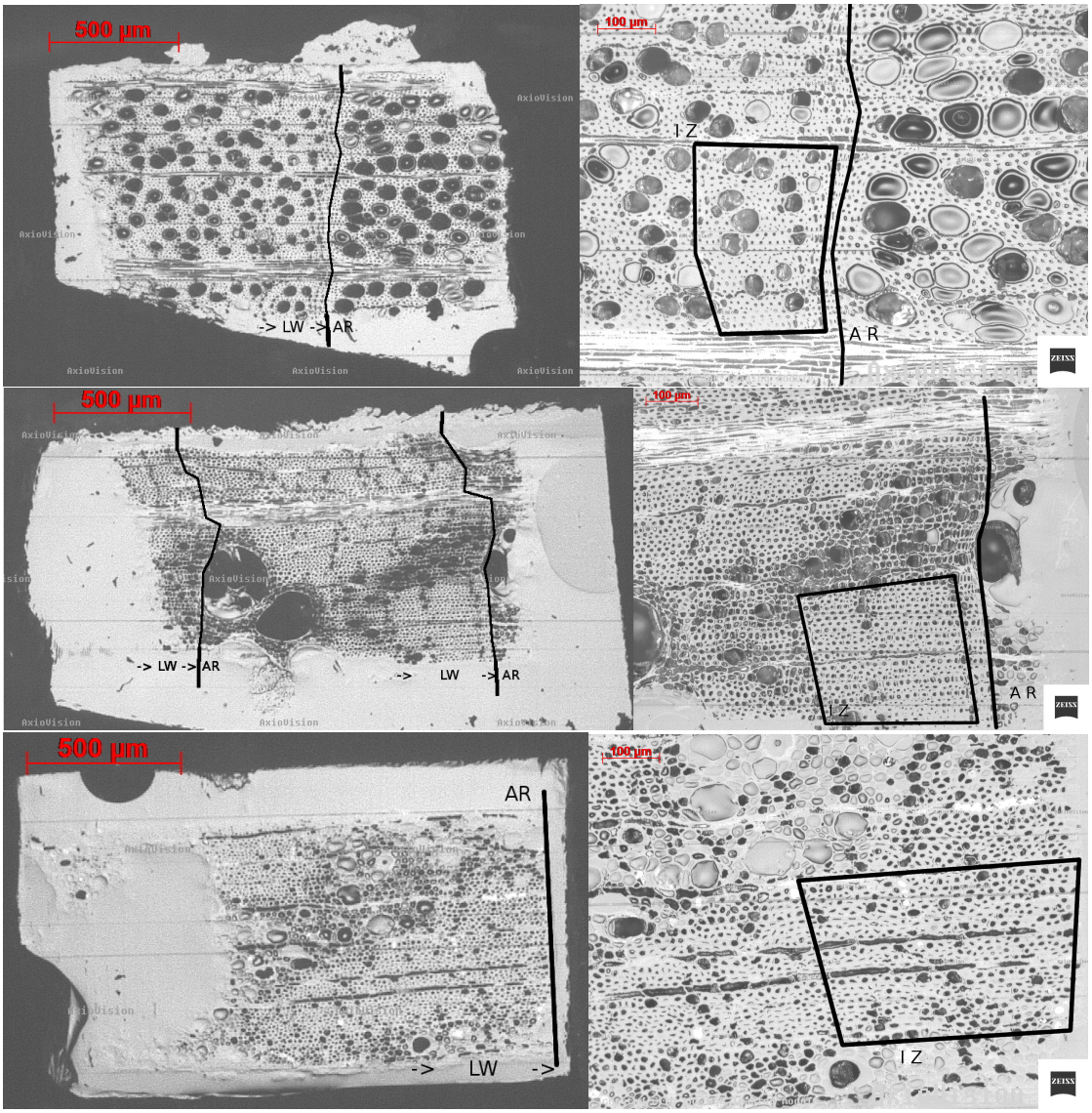

Figure 2.2: Overview and detailed light microscope pictures of the investigated hardwood species. On the top: (left) beech sample with a 25x-magnification, (right) beech sample with a 100x-magnification.
In the middle line: (Left) oak sample with a 25x-magnification, (right) oak sample with a 100x-magnification.
On the bottom: (left) vasa sample with a 25x-magnification, (right) vasa sample with a 100x-magnification. AR: annual ring, LW: latewood, IZ: indentation zone.

Table 2.2: Assumed distribution of components in the cell wall layers for Spruce tracheids in the latewood (in w.%). C: cellulose, HC: hemicelluloses, L: lignin. From [18]

	C	HC	L
Middle Lamella	4.1	20.6	26.8
Secondary wall 2	87	56.1	62.8
Secondary wall 1	8.9	23.2	10.4

Table 2.3: Composition of the spruce cell wall layers (in LW, in w.%) in C: cellulose, HC: hemicelluloses, L: lignin, Ext: extractives

	C	HC	L	Ext
Middle Lamella	14.4	36.1	45.5	4
Secondary wall 2	58.1	18.6	20.2	3

Since softwood is composed of only one type of cells in the longitudinal direction, the tracheids, the difference between latewood and earlywood is easily observable: in the latewood, the cells are thinner, but with thicker cell walls, while the earlywood cells are big with very thin cell walls.

In hardwood however, fibres and vessels are observable in the longitudinal cut, where the vessels are the big often dark openings under a light microscope and the fibres the smaller cells in between. If the fibres can be compared to the tracheids in the softwood, they have less variability in their size and shape within one wood specimen. In addition, the annual ring borders are indicated in Figures 2.1 and 2.2. For example, in beech (on the right top of Figure 2.2), the annual ring is located at the sudden transition between the vessels in the latewood and the twice as big vessels in the earlywood. Here is also a certain fibre discontinuity to be recognized. In oak, the very big vessels on the right or on the left of the investigated sample (left picture in the middle row of Figure 2.2) are always located near the annual ring, but in the earlywood. Then, with a closer look, the size difference of the fibres left and right from the annual ring marks the distinction between latewood and earlywood.

2.1.2 Relation between moisture content and relative humidity

Experimental investigations

Since wood specimens have highly variable properties, no clear relation between the relative humidity of the wood surrounding environment and the specimen equilibrium moisture content (EMC) is described in the literature for a given wood species. With Equation (1.1), the moisture content in the investigated wood species at relative humidities from 10 to 80% RH were determined.

For this purpose, specimens of the different investigated wood species were placed in climate chamber with constant temperature of 21 ℃, first at a RH of 80%. They were regularly weighted, until their mass did not vary any more. The final samples weight was recorded and the process repeated for RH of 60%, 40% and 10%. Finally, all samples were placed in an oven at 103 ℃, until their mass did not vary any more, i.e. their dried masses are reached. This allowed the calculation of equilibrium moisture contents at the

Table 2.4: EMC (%) of the investigated wood species for various relative humidities.

RH (%)	80	60	40	10
Oak	14.2	12.1	9.6	5.5
Yew	13.8	11.9	9.7	5.4
Spruce	17.1	13.5	10.5	5.6
Beech	16.1	12.7	9.7	5.0
Pine	18.1	13.4	11.0	6.0

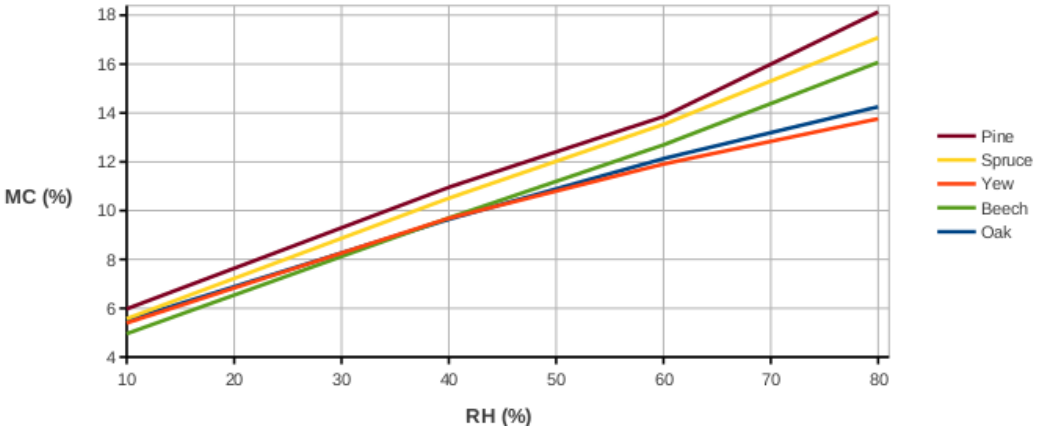

Figure 2.3: Desorption curve of the investigated wood species over a RH-range of 10% to 80% at a temperature of 21 °C.

investigated relative humidities.

Results and discussion

The moisture contents of all wood samples are presented in Table 2.4 for differente relative humidities.

Figure 2.3 shows the desorption curves at 21 °C for the investigated wood species.

Compared to the other softwoods, yew seems to absorb less moisture: at 10% RH, yew absorbs already 10% less moisture than pine, which had the highest moisture content. At 80% RH, the difference in moisture content reaches up to 27%. Generally, the hardwoods have lower MC than the softwoods, except yew.

The particular behaviour of yew may be explained through its chemical composition. It actually has a high extractives content, which do not absorb moisture, and a low hemicelluloses content, which absorb a lot of moisture. This could be the reason why yew absorbs less moisture than pine or spruce, since both (spruce and pine) have higher hemicelluloses and lower extractives contents.

2.2 Nanoindentation experiments

In micro-heterogeneous materials, macroscopic properties depend on microstructural and micromechanical characteristics. Therefore, the determination of mechanical properties

at lower length scales is desired. This is also the case for wood, where macroscopic properties depend on cell wall characteristics. Therefore, research efforts were directed towards the assessment of mechanical properties of wood fibres. Tensile tests of single wood fibres were performed by Page et al. in 1971 [40]. Problems with this method of mechanical characterization may arise from the fibre cross-section variability coming from the natural structure of wood (pits, fibre ends), as well as from the fact that a single fibre is prone to twist and buckle, because of the absence of a lateral reinforcement provided by the other tissue cells on its sides. Last but not least, the isolation process could lead to damages and kinks of the fibre. Recently, Eder and Arnould [14] were affirming that no comprehensive experimental data set on single tensile stiffness of a fibre as a function of moisture content and microfibril angle exists.

Since the aim of this study is to determine the elastic properties of the wood cell wall as well as its viscoelastic properties, attention is then rather paid to another method. Nanoindentation, also called instrumented indentation testing was originally introduced in 1948 and developed in the mid 1970s, according to Poon [42]. Oliver and Pharr [38] presented in 1992 a new evaluation method for nanoindentation data of metal films. Soon, the calculation method was first adapted for homogeneous, hard, thin and isotropic materials, but also for wood by Wimmer et al. in 1997 [56]. In this thesis, calculations are based on the work of Oliver and Pharr [38] and Jäger et al. [30] for indentation of anisotropic materials.

2.2.1 Basics of nanoindentation measurements

Nanoindentation enables the direct characterization of mechanical properties of the wood cell wall. Its principle derives from the macro-indentation tests performed on all kinds of materials to determine their hardness, but transferred to a microscopic or nanoscopic scale. Therefore, the test consists in penetrating a sample with an indenter[1], while the applied load and the penetration depth in the sample are recorded with a high precision. The load range goes indeed theoretically from 100 nN to 30 mN whereas the sample deformation range is 1 nm to 20 µm. These high precision levels were only made possible due to the technological progress in the last twenty years. This explains the relative recentness of this investigation method at this length scale. From the recorded data, the curve of loading and unloading of the sample can be drawn, see Figure 2.4b.

The unloading part of the load displacement curve enables the calculation of the hardness and of the reduced modulus of the material at the indented location, as

$$E_r = \frac{\sqrt{\pi}}{2} \cdot \frac{\mathrm{d}P}{\mathrm{d}h}|_{h=h_{max}} \cdot \frac{1}{\sqrt{A_c}} = \frac{\sqrt{\pi}}{2} \cdot \frac{S}{\sqrt{A_c}}, \tag{2.1}$$

$$H = \frac{P_{max}}{A_c}, \tag{2.2}$$

with P as the applied load (µN), h as the contact depth (nm), A as the projected area of the tip (nm^2) and h_c as the extrapolated indentation depth, which enables to calculate the contact area A_c (according to [56]).
For the mostly used indentation tip, namely the Berkovich tip, a three-sided pyramid

[1] a spike made from a hard, well-known material, with a geometry that is very precisely known

with an semi-angle of 65.27°, the formulae for the calculation of the hardness of the material is approximated by

$$H = \frac{P_{max}}{24.5 \cdot h_c^2}. \tag{2.3}$$

The hardness H is indeed a mean of the contact pressure of the indenter on the material, or, for wood, a measure of the resistance of the material to combined plastic and elastic deformations [19]. It is measured in Pascal (Pa), or more commonly, in GPa.

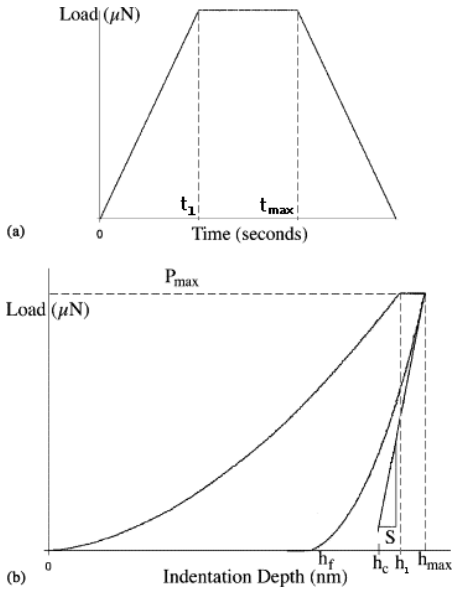

Figure 2.4: Typical load function (a) and load-displacement (b) curves for a nanoindentation test of an elastic material, showing the unloading slope $S = \frac{\mathrm{d}P}{\mathrm{d}h}|_{h=h_{max}}$; the maximum indentation depth at maximum load h_{max}; the final indentation depth at zero load h_f; and the extrapolated indentation depth $h_c = h_{max} - \varepsilon.\frac{P_{max}}{S}$ [38], with $\varepsilon = 0.75$ for a Berkovich tip (from [39]).

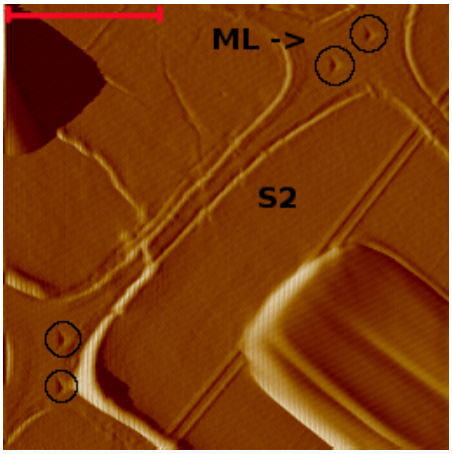

Figure 2.5: Indents in the middle lamella of a spruce sample at 40% RH.
SPM picture. Scale bar: 5 µm

The reduced modulus E_r, also called indentation modulus, can be calculated from the initial slope S of the unloading part of the load-displacement curve, see Figure 2.4b. S is assumed to be purely elastic. As an asumption, the initial unloading behaviour is considered as elastic in the calculation of the indentation modulus.

Based on the horizontal plateau of the indentation curve (constant load at the maximum load P_{max} and increasing indentation depth between h_1 and h_{max}), a creep parameter is calculated. With t_1 and t_{max} as the time at which the indentation depth reaches h_1 and h_{max} respectively, the creep parameter C, indicating the relative amplitude of creep deformation under a constant load, for a duration of $t_{max} - t_1$ is given as

$$C = \frac{h_{max} - h_1}{h_1}. \tag{2.4}$$

Since the remaining imprint has a diameter smaller than one micrometer (µm), indents can be placed within the wood cell wall. Two adjacent indents should be performed at a distance of at least two times the dimension of the remaining imprint. This minimum distance is necessary to avoid influences from the plastic deformation of the wood around a previous indent. This plastic deformation locally changes the mechanical properties of the wood. As an example, the cell wall thickness for pine latewood cells is about 9 to 13 µm. Indents can also be performed within the middle lamella, on the places where it is thicker, i.e. at the intersection of three to four cells, on the cell corner. In order to get informations about the surface of the sample an in order to specify a location for an indent, a Scanning Probe Microscope (SPM) can be used. It is based on AFM (Atomic Force Microscopy) technology and uses the same tips for surface imaging as for indentation.

Since a decade, many studies used nanoindentation (NI) to determine for example the dependency of the indentation modulus and hardness on the MFA [53] or the relationship between the microstructure and the stiffness of wood cell walls [4, 12]. Some research was even done to understand the moisture-dependency of the nanoindentation properties of pine cell walls [35, 57]. In the last two studies, first attempts were made to exploit the moisture-mechanics relationships at the cell wall scale. For this purpose, pine (latewood) cells were investigated. In both studies, NI tests were performed between 18 and 70% RH. Additionally, NI tests using a fluid cell were performed. Moreover, Yu [57] studied the variation of the viscoelastic properties of wood with the humidity and explained the decreasing creep resistance with increase of moisture content by the plasticizing effect of water on the hemicelluloses.

In this thesis, the indentation modulus, the hardness and the creep ability of two cell wall layers of five different wood species and of one deteriorated wood are investigated at different relative humidities from 10 to 80% and under water.

2.2.2 Difficulties of nanoindentation studies

In general, the variability in indentation moduli of wood cell walls as measured by nanoindentation tests is high, due to several reasons. First, as explained in [32], "the very high variability in the measurement of micromechanical wood cell wall properties can be caused by unintentional small fibre misalignment by few degrees with regard to the indentation direction caused by sub-optimal sample preparation". Hence, the specimen preparation plays a decisive role for this kind of study.

Some more factors possibly influencing the parameters measured by nanoindentation can be (from [19]):

the variation in the wood structure. Caused by climatic changes the tree encouters when it grows, local variations of the cell wall structure generates local variations in the mechanical properties of the tree.

the thermal drift. It is different from creep, which is a mechanical drift coming from the plastic flow of the material. Here, as we consider the material at a very small scale, the probe is highly sensitive to thermal expansion or contraction. Therefore, if the wood temperature-sensitivity is also considered, it clearly appears that the laboratory room where the indents are done should be thermally regulated. This is to avoid these effects and increase the measurement precision. All investigated specimens in this study were stored and measured at a constant temperature of 21 ℃±1.5℃.

the initial penetration depth. Although high-performance equipments and electronic components are used, it is still impossible for the indenter to come in contact with the probe without having a contact load P_i and a non-zero contact indentation depth. Therefore, the applied load is always a function of the indentation depth h, but also of two unknown constants according to the following equation: $P = (h + h_i)^m$, where h_i and m are constants depending on the quality of the contact and of the type of indenter.

the indenter geometry. An indenter tip never has a perfect shape, due to the shape complexity (three edges crossing at the exact same location) and of its wear (even if indenter are always made from very hard materials, like quartz or diamond). Therefore, a correction factor $A : A_{ideal}$ for the projected area of the tip should be calculated. It can either be done from a regression analysis for the projected area A as a function of h_{max}, the maximum indentation depth, or by performing a series of indentation at varying peak loads on standard test specimens whose E and ν are known. However, it can also be considered that the conditions for which this effect is highest are not fulfilled, because the tip defects are actually quite only located at the very end of the indenter, this is to say, for small indentation depths or small sample thicknesses.

the surface roughness. This important issue, coming from the unequal height of the sample surface at the nanoscopic scale, causes errors in the determination of the contact area between the indenter and the specimen and then in the hardness values. Indeed, if the tip comes into contact with a peak, it follows a stress concentration within the tested material and then higher deformations for relatively low loads and, thus, a lower hardness. In the contrary, if the tip comes into contact with a valley, the true contact area is underestimated and it follows a higher hardness. In order to avoid these effects, the polishing of the sample should be done particularly carefully and it is advised to use a Berkovich indenter, which is the sharpest one. Figure 2.6 illustrates the induced variability of the results due to the surface roughness. Thus, the surface has been cut with a diamond blade, as explained in Section 2.2.3.

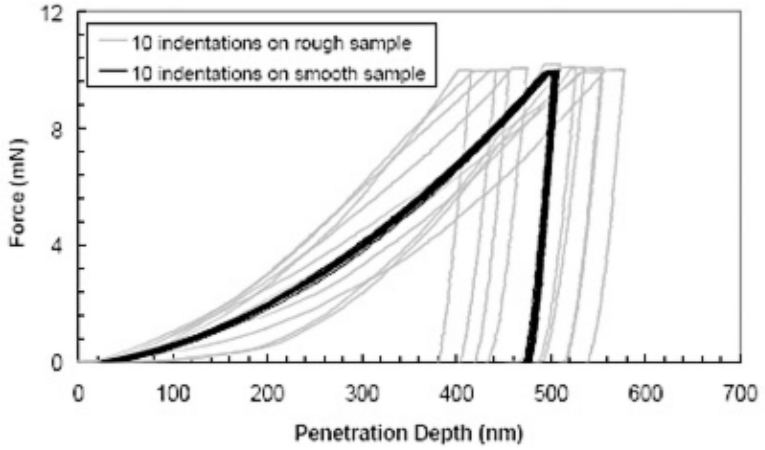

Figure 2.6: Force-penetration depth curves performed at a 10 mN-load on smooth and rough copper surfaces. Ten indentation tests have been performed on each surface showing that the curves are more scattered on the rough surface than on the smooth surface (from CSM Instruments [29]).

2.2.3 Preparation of nanoindentation samples

The first step of the sample preparation is to cut with a saw a thin section of wood with a cross-section of 1.5 x 0.9 mm^2, which corresponds to one or two annual rings. The samples used for this study were cut far from any reaction wood, juvenile wood, from pitch pockets or from knots in order to avoid special wood cells configurations. The rectangular cross-section includes at least one annual ring, so that the latewood, where the measurements will be done, can be easily distinguished from the earlywood. The second step in the nanoindentation sample preparation is to embed the wood specimen into a resin called Agar Low Viscosity Resin Kit from Agar Scientific in Essex, UK. The resin reduced modulus E_r is around 3 to 4 GPa, measured by nanoindentation. For the hardening, the embedded sample is put into a vacuum generator in order to ensure in the best possible way the resin penetration into the wood cell lumina. Then the resin is cured in an oven at 70 ℃ for 24 hours. Particular attention has been given to the sample orientation, so that the fibre orientation can always be identified by simple observation of the sample. It enables the operator in the next steps to orientate in the next steps the sample along the longitudinal axis of the fibres, which reduces the strong and partially inevitable variability of the results [32].
As the manual positioning is suboptimal for the requirements of the indentation tests, the angle between the fibre orientation and the length direction of the embedded sample is measured and compensated by an additional cut in the perpendicular fibre plane after resin hardening. The final precision in the fibre alignment perpendicular to the indentation direction is around 0.5°.
Then, the embedded sample is glued on a stainless still disc, which enables the sample to be magnetically fixed in the moving plate in the nanoindenter chamber.

The last step consists of the sample surface preparation, using a ultramicrotome. The aim is to prepare, as far as possible, a flat surface by cutting away extremely thin slices

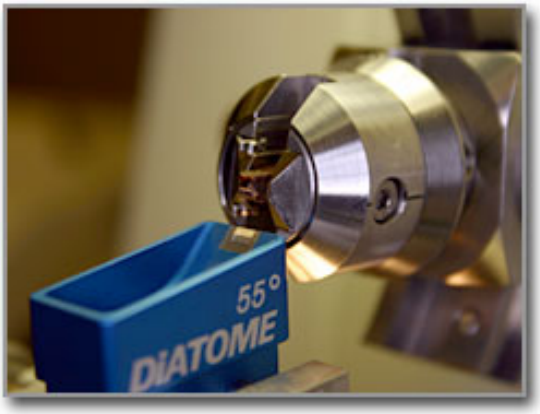

Figure 2.7: Ultramicrotome with diamond knife. Knife width around four mm. From [37]

of material (i.e. with a thickness in a range of 10 to 500 nm) with the help of a sharp glass splinter or a diamond knife. The latter enables to produce a flat surface suitable for nanoindentation tests (see Figure 2.7).

Environmental Scanning Electron Microscop (ESEM) measurements were caried out, the swelling of the cell walls with increasing moisture content was investigated. It enables to affirm the capacity of the embedded wood cell walls to absorb moisture as well as the ability to deform, also in case of embedded cell walls. However, the quantification of the results is beyond the scope of this thesis.

2.2.4 Equipment

The instrument used for the nanoindentation tests is a Triboindenter TI 900 (Hysitron, Minneapolis, USA), see Figure 2.8. The tip used for all measurements in this work is a three-sided pyramidal Berkovitch tip, specify "flat". For measurements under water, a fluid cell tip with Berkovich geometry was used. The longer tip enables to reach the sample even when it is placed in a fluid cell with high walls. In order to maintain a constant humidity in the indenter, a humidity generator RH200 (L&C Science and Technology, Hialeah, Florida, USA) was used, see Figure 2.9. This instrument regulates the humidity inside the indenter chamber by mixing in the right proportions the ambient air with either vapour or nitrogen gas, which contains no water. Adding moisture to the ambient air enables to reach a relative humidity of up to 80%, while adding nitrogen gas was used for relative humidities down to 10%. Since also temperature influences the relationship between relative humidity and wood moisture content, the temperature of the samples should be controlled. For this reason, the nanoindentation instruments is placed in an air-conditioned room at a temperature varying between 20 and 23 ℃.

2.2.5 Order of the experiments

The majority of the measurements at the driest humidity (10% RH) was realized in winter, when the air is already quite dry (down to 30% RH). Less nitrogen was then necessary to air-condition the quite big chamber. Naturally, the high humidity measurements have been done during the summer, when the ambient average humidity can reach

Figure 2.8: Left: Triboindenter TI 900 from Hysitron. Right: Triboindenter stage. Light microscope, capacitive transducer and stage [28].

Figure 2.9: Humidity Generator RH 200, from L&C [33]

up to 70% RH. It was then much easier and quicker to reach the requested high humidity percentages inside the chamber, starting from the ambient humidity.

Before and during the measurements, all unused samples were stored in the air-conditioned room, i.e. at 20 to 23 ℃ and 30 to 60% RH. For the measurements, all samples are put into the nanoindenter chamber and conditioned, the first time at 10% RH, the second at 40% RH, the third at 60% RH and the fourth at 80% RH. Between each experiment, the samples are stored in the air-conditioned room. The fluid cell experiments were realized at the end. Between each measurement series under water, the samples were let dry naturally at room temperature and relative humidity for at least 18 hours.

2.2.6 Measurements course

Once the humidity generator is started, it takes up to 24 hours before the desired humidity inside the measure chamber and the sample dimensions are reached. In the meanwhile, the indenter and its software are started and calibrated. Then the samples, glued at a previous step on some steel disc and already fixed on the supporting plate in the chamber by magnets, are localized with the light microscope and a "Quick approach" is executed. This process consists of moving very slowly the tip towards the surface until a load of two µN is registered. This enables a precise localisation of the sample surface.

The first step is to localize the latewood to be measured in the sample using a light microscope with a magnification of 10 to 150. This can quite easily be done for every species because of the visually big differences between the thin cells in the earlywood and the thick cells in the latewood (already observable at a bigger scale, as they build the annual rings). Then, a place to be indented is chosen and the tip is moved slowly over the sample. Indents at different relative humidities were performed within the same region of latewood cells, as documented in Figures 2.1 and 2.2.

The second step is to use the Scanning Probe Microscopy (SPM) imaging tool provided by the instrument in order to get a topography of the sample surface with a side length of 15 µm and a resolution of a few hundred nanometers (see Figure 2.10). As on the lower part of Figure 2.10, it frequently happens that the picture is partially or totally blurred and not accurate enough to enable the wood cells to be recognized. It was noticed that this phenomenon seems to happen more often at higher humidity percentages.

Then, the next step is to define the load function that should be applied by the tip on the sample. Its choice depends on the mechanical properties of the indent, the measured layer, the relative humidity of the air and the global measuring duration. A load function duration of around one minute was in these experiments a good compromise between the global measurements duration, the drift of the piezo actuator and the creep properties accuracy. The applied load functions is shown in Figure 2.11. The maximum load varied from 90 to 200 µN to pay heed to the layer and its expected stiffness.

The measurement course depends if the sample is in the fluid cell or not.

Nanoindentation measurements from 10% to 80% RH

The last step consists in positioning the points to be indented, launch the measurements and post-process the obtained data (for each time, the applied load and the resulting indentation depth are saved) to get the indentation modulus E_r and the hardness H at this position (see Equations (2.1) and (2.2)). As the applied load function (see Figure 2.11) consists of two unloading parts, two E_r and H-values are obtained

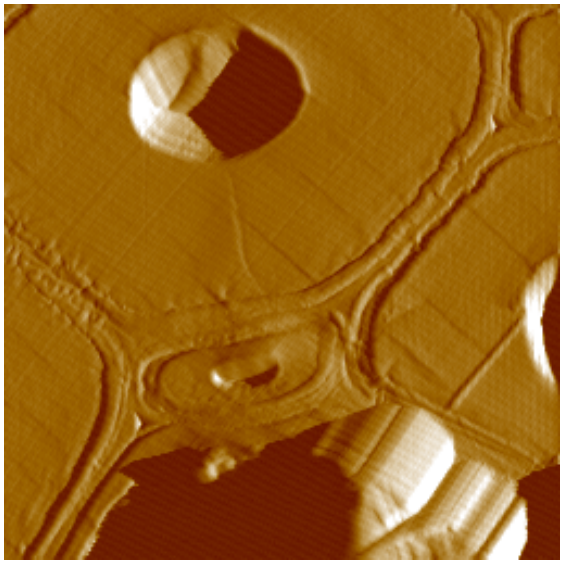

Figure 2.10: SPM-picture of beech wood cells at 10% RH. Side length: 15 µm

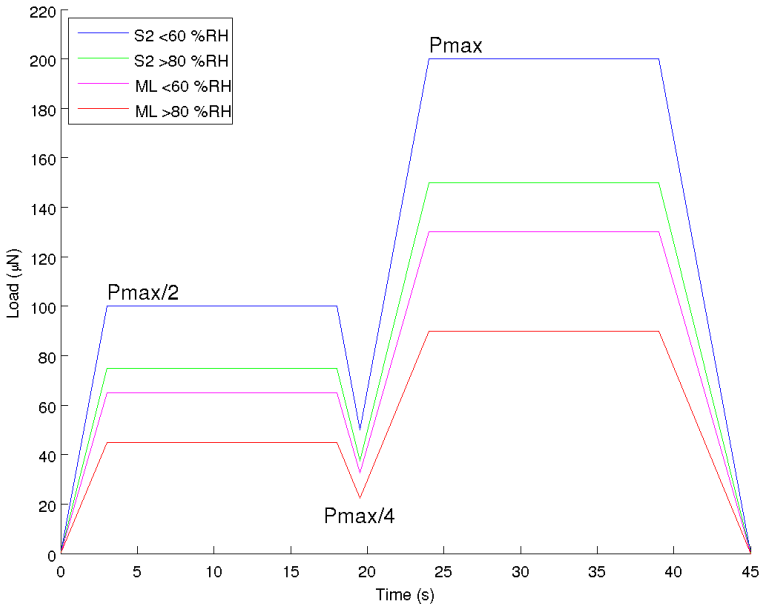

Figure 2.11: Load functions used in the nanoindentation experiments

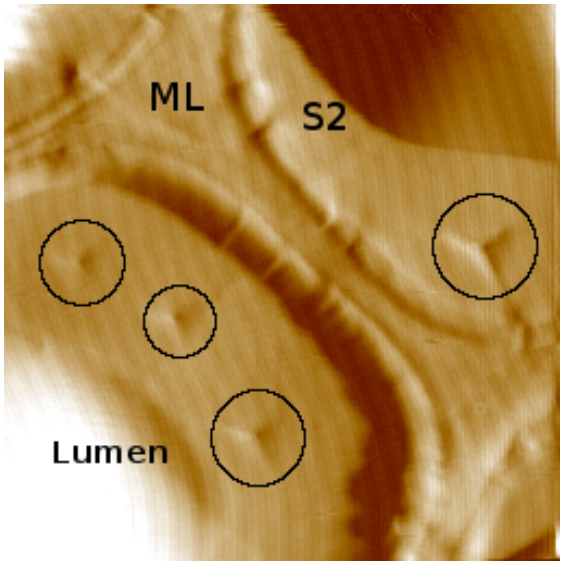

Figure 2.12: SPM-Image of a spruce sample under water. Four indents are marked in the S2-layer.

per indentation point, as well as two creep parameters. The two creep parameters are the relative augmentation of the indentation depth during the first and second constant loadings at $P_{max}/2$ and P_{max} respectively. This way, at least twelve indents were made for each specimen in the middle lamella and eighteen in the S2-layer for the four tested relative humidities between 10 and 80% RH. In the S2-layer, up to two indents could be made in the cell wall thickness and up to seven lengthwise.

Particularities of the fluid cell experiments

In this case, the nanoindentation sample is lying in a small dish. The first steps are similar to the procedure outlined above:

- observe the dry sample with the light microscope,
- choose a reasonably convenient place to indent and
- take a picture of the surface with the SPM tool.

Then, the tip is lifted away from the sample in order to allow free deformations of the NI-specimen. Distilled water is very carefully poured into the dish, so that none of the surrounding objects like the dish, the sample, the tip or the controller are moved during the operation. As soon as the sample is under water, the measurement course is stopped for at least 20 minutes, the necessary time for the sample to absorb the water and to swell. Then, the tip is placed again in contact with the sample and a new SPM picture is done. Generally, since the measurements last longer, less indents are done under water as in the air. So, at least five and eleven indents were made in the ML and the S2-layer of each sample, respectively .

Figure 2.12 shows the surface of a spruce sample under water. Four indents are visible in the S2-layer.

For both procedures, the number of data is considered as statistically representative. Pictures were taken to control the shape and the location of each indent.

2.2.7 Results and discussion

Figures 2.13 to 2.31 show the results of the nanoindentation test performed in this project. Some conclusions can already be done considering the elastic and time-dependent mechanical properties of wood at the cell wall material.

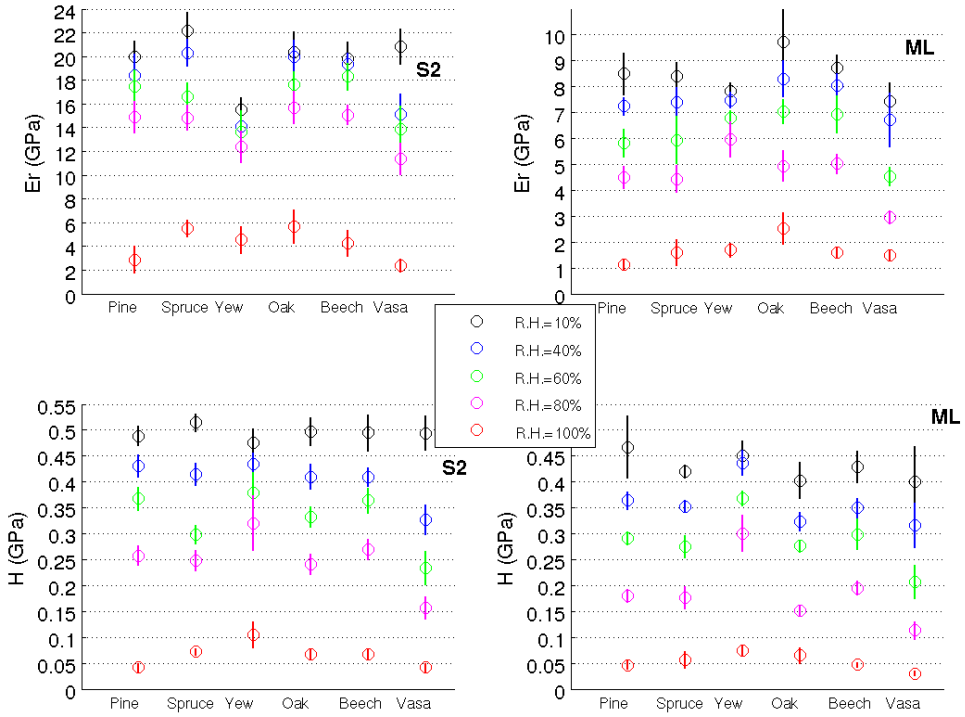

Figure 2.13: Indentation modulus and hardness of the wood cell walls of different wood species (layers S2 and ML) under varying relative humidity of the environment.

Nanoindentation modulus and hardness

Numerical values

Table 2.5 presents the mean values and the standard deviation of the indentation moduli (in GPa) for indents made in the S2-layer of different wood species under various humidity conditions.

Table 2.6 presents the mean values and the standard deviation of the indentation moduli (in GPa) for indents made in the middle lamella of different wood species under various humidity conditions.

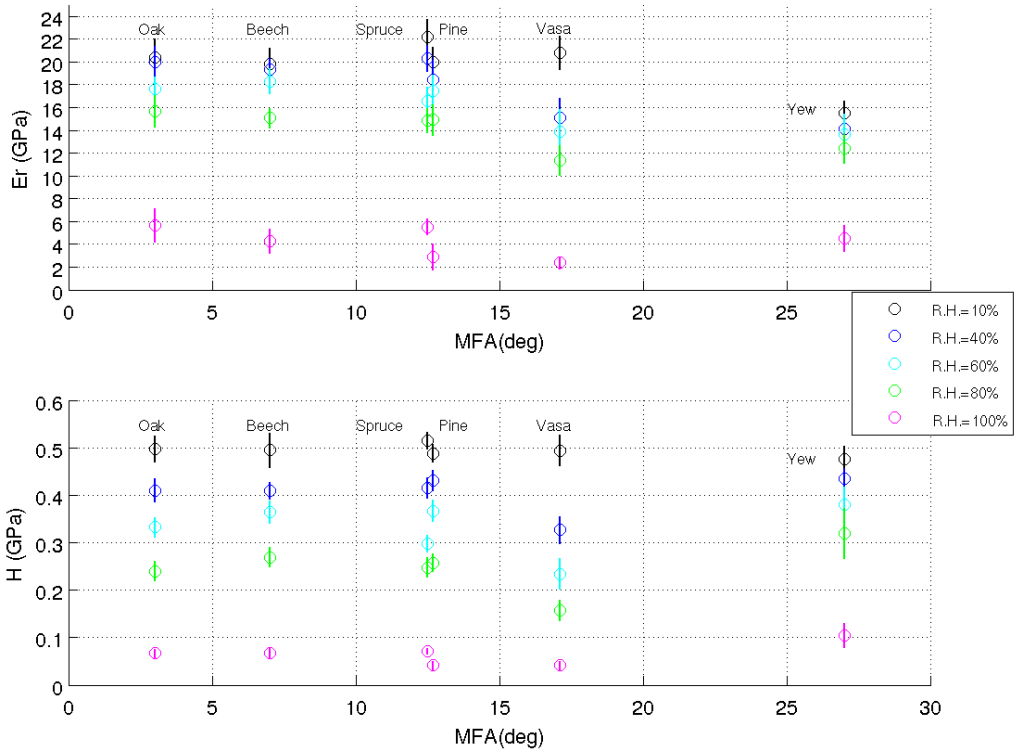

Figure 2.14: Indentation modulus and hardness of the wood cell walls of different wood species under varying relative humidity of the environment compared to the microfibril-angle of the S2-layer.

Table 2.5: Average values and standard deviation of indentation modulus measured in the S2-layer by nanoindentation in different wood species under various humidity conditions

E_r (GPa)	10% RH	40% RH	60% RH	80% RH	FSP
Pine	20.00 ± 1.31	18.42 ± 1.77	17.45 ± 1.41	14.91 ± 1.32	2.86 ± 1.14
Spruce	22.19 ± 1.51	20.32 ± 1.15	16.61 ± 1.15	14.84 ± 1.06	5.53 ± 0.7
Yew	15.53 ± 1.03	14.13 ± 0.94	13.66 ± 1.77	12.41 ± 1.32	4.56 ± 1.14
Oak	20.36 ± 1.70	19.95 ± 1.46	17.67 ± 1.05	15.69 ± 1.38	5.67 ± 1.44
Beech	19.84 ± 1.34	19.35 ± 0.96	18.32 ± 1.14	15.09 ± 1.84	4.29 ± 1.07
Vasa	20.84 ± 1.47	15.12 ± 1.73	13.91 ± 1.89	11.37 ± 1.33	2.39 ± 0.52

Table 2.6: Average values and standard deviation of indentation modulus measured in the middle lamella by nanoindentation in different wood species under various humidity conditions

E_r (GPa)	10% RH	40% RH	60% RH	80% RH	FSP
Pine	8.50 ± 0.80	7.24 ± 0.33	5.82 ± 0.53	4.49 ± 0.43	1.26 ± 0.21
Spruce	8.4 ± 0.53	7.39 ± 0.58	5.94 ± 0.90	4.44 ± 0.51	1.59 ± 0.51
Yew	7.82 ± 0.35	7.48 ± 0.31	6.78 ± 0.30	5.96 ± 0.69	1.68 ± 0.25
Oak	9.73 ± 1.26	8.31 ± 0.69	7.05 ± 0.46	4.94 ± 0.58	2.52 ± 0.60
Beech	8.72 ± 0.51	8.04 ± 0.45	6.93 ± 0.73	5.02 ± 0.38	1.58 ± 0.20
Vasa	7.44 ± 0.69	6.71 ± 1.04	4.54 ± 0.37	2.94 ± 0.25	1.48 ± 0.17

Table 2.7 presents the mean values and the standard deviation of hardness (in GPa) for indents made in the S2-layer of different wood species under various humidity conditions.

Table 2.7: Average values and standard deviation of hardness measured in the S2-layer by nanoindentation in different wood species under various humidity conditions

H (GPa)	10% RH	40% RH	60% RH	80% RH	FSP
Pine	0.49 ± 0.019	0.43 ± 0.022	0.37 ± 0.022	0.26 ± 0.019	0.042 ± 0.009
Spruce	0.51 ± 0.017	0.41 ± 0.022	0.30 ± 0.017	0.25 ± 0.020	0.072 ± 0.006
Yew	0.48 ± 0.028	0.43 ± 0.022	0.38 ± 0.038	0.32 ± 0.053	0.100 ± 0.025
Oak	0.50 ± 0.027	0.41 ± 0.024	0.33 ± 0.020	0.24 ± 0.020	0.067 ± 0.009
Beech	0.49 ± 0.036	0.41 ± 0.017	0.36 ± 0.024	0.27 ± 0.020	0.067 ± 0.010
Vasa	0.49 ± 0.033	0.33 ± 0.028	0.23 ± 0.032	0.16 ± 0.021	0.041 ± 0.009

Finally, Table 2.8 presents the mean values and the standard deviation of hardness (in GPa) for indents made in the middle lamella of different wood species under various humidity conditions.

Graphical presentation

Plotted either over the surrounding relative humidity or the wood moisture content, nanoindentation moduli and hardness of the investigated wood are presented in Figures 2.15 to 2.24. When plotted over the wood MC, the FSP was separated from the other values and plotted over a MC-range between 30% and 40% in order to highlight the

Table 2.8: Average values and standard deviation of hardness measured in the middle lamella by nanoindentation in different wood species under various humidity conditions

H (GPa)	10% RH	40% RH	60% RH	80% RH	FSP
Pine	0.47 ± 0.061	0.36 ± 0.018	0.29 ± 0.012	0.18 ± 0.013	0.046 ± 0.008
Spruce	0.42 ± 0.013	0.35 ± 0.011	0.27 ± 0.021	0.18 ± 0.021	0.057 ± 0.016
Yew	0.45 ± 0.028	0.44 ± 0.024	0.37 ± 0.015	0.30 ± 0.035	0.075 ± 0.010
Oak	0.40 ± 0.036	0.32 ± 0.019	0.28 ± 0.012	0.15 ± 0.010	0.065 ± 0.015
Beech	0.43 ± 0.031	0.35 ± 0.019	0.30 ± 0.029	0.19 ± 0.014	0.047 ± 0.004
Vasa	0.40 ± 0.068	0.32 ± 0.043	0.21 ± 0.032	0.11 ± 0.018	0.03 ± 0.004

fact that the exact MC of the cell wall is not known. For the same reason, the regression curves of the mean values were only drawn for a RH-range between 10 and 80%.

Figures 2.13 and 2.14 illustrate the results of nanoindentation modulus and hardness for all investigated wood species. As expected from the literature review, by increasing the relative humidity around the wood samples from 10% RH up to full saturation (corresponding to 100% RH), the wood cell walls encounter a clear degradation in all their mechanical properties. This stiffness and hardness losses happen for all wood species and every investigated layers, see in particular Figures 2.15 to 2.22.

The loss seems to be non linear with the relative humidity and also with the MC. The linear fitting curve over the four lowest MC seems to fit the original points quite well, but with a closer look, the second or third points are nearly always above the linear regression curve. In other words, all wood species follow the same trend: a smaller variation of the mechanical properties between 10 and 40% RH than between 40 and 80% RH, followed by a stronger decrease above 80% RH (Figures 2.15, 2.17, 2.19 and 2.21). For example for yew, the decrease of the indentation modulus reaches about 20% between 10% RH and 80% RH, while it accounts to 63% between 80% RH and 100% RH in the S2-layer. The entire decrease of the indentation modulus of yew in the S2-layer (Figure 2.15) reaches about 70%, while it reaches for example more than 85% for pine and 75% for spruce in the same layer. This value means that yew has lost about 70% of its original stiffness at 10% RH when the relative humidity increases to 100% RH. Yew is therefore the investigated softwood with the highest moisture-resistivity. This result is similar as the one obtained in Section 2.1.2. Since yew stores less moisture under the same surrounding conditions, its mechanical properties are less affected. On the contrary, since pine stores a lot of moisture (see Section 2.1.2), the loss in its mechanical properties is also higher.

As regards hardwoods, beech and oak have similar behaviours for stiffness and hardness, with a global loss of their indentation moduli in the S2-layer of 78 and 72%, respectively. Similar to softwoods, a smaller decrease of their mechanical properties under 60% RH than above 60% RH is observed.

At 10% RH, the Vasa wood is as stiff as and as hard as the other investigated hardwoods. But it looses much sooner its stiffness and hardness: between 10 and 40% RH. While oak encounters a stiffness loss in the S2-layer of around 2%, the Vasa wood encounters a loss of around 27%. Its entire softening from 10 to 100% RH is the highest among all investigated wood species with 88%.

The loss between two successive measure points is always smaller than the loss be-

tween 80% RH and the Fibre Saturation Point (FSP = 100% RH). Indeed, when taking a closer look at Figures 2.16, 2.18, 2.20 and 2.22, the reason appears clearly: the difference in the wood MC for RH between 80 and 100% is bigger than for RH under 80%. In consequence, the wood fibres or tracheids absorb much more water (around twice the MC at 80% RH) and then soften much more above 80% RH than under 80% RH (around three to five times in the S2-layer and two to three times in the middle lamella for both the hardness and the stiffness).

Considering the upper graphic in Figure 2.14, it can be noticed that yew is the weakest wood in the S2-layer for the indentation modulus. However, yew is also, as mentioned before, the most resistant wood against humidity. And its hardness is the highest of all investigated wood species in both layers between 40 and 100% RH (and even at 10% RH for the ML). This is most likely a consequence of its very high MFA of 27° as well as of its low moisture-absorbency, due to its high extractives content.

Last but not least, considering the lower graphic in Figure 2.14, the hardness in both layers seems to be independent of the MFA in the S2-layer. All values are indeed quite on a horizontal line in the S2-layer, except for the Vasa wood and for yew. The Vasa, through its particular history, clearly has different properties. In contrary, it remains unclear why yew has such a different behaviour compared to the other wood species.

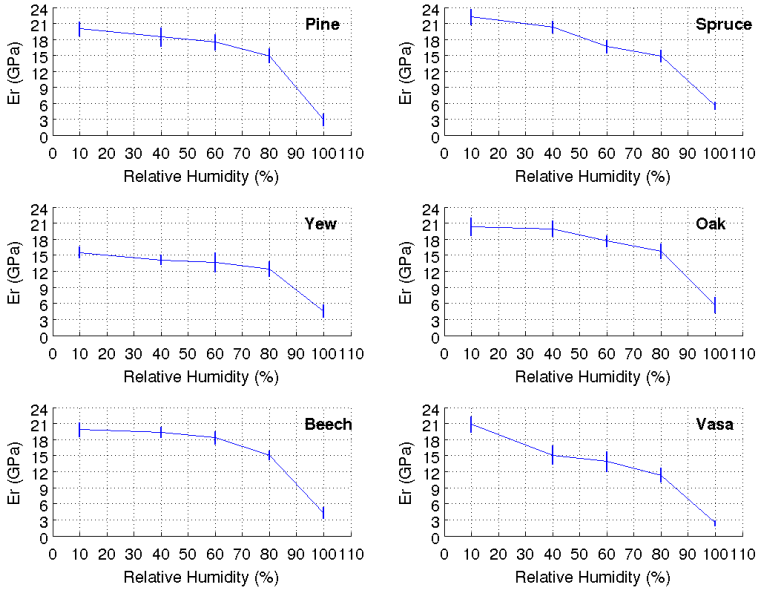

Figure 2.15: Indentation modulus in the S2-layer of different wood species under varying relative humidity

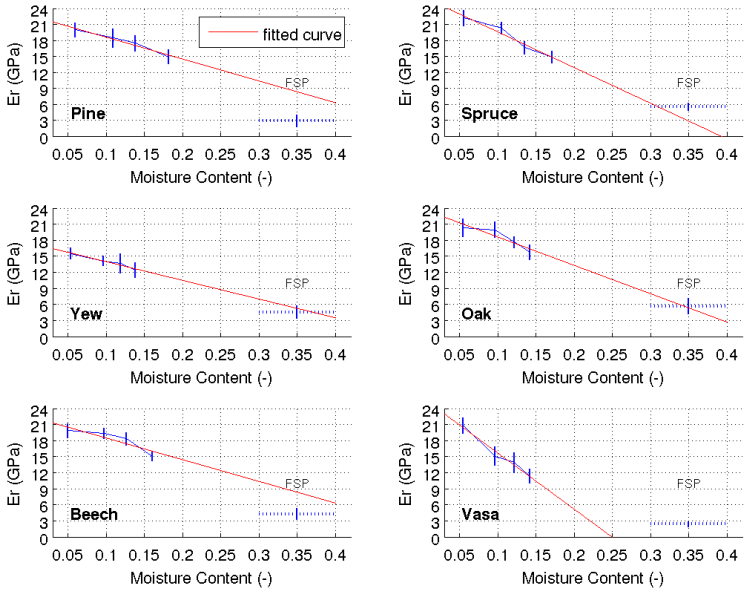

Figure 2.16: Indentation modulus in the S2-layer of different wood species with various MC

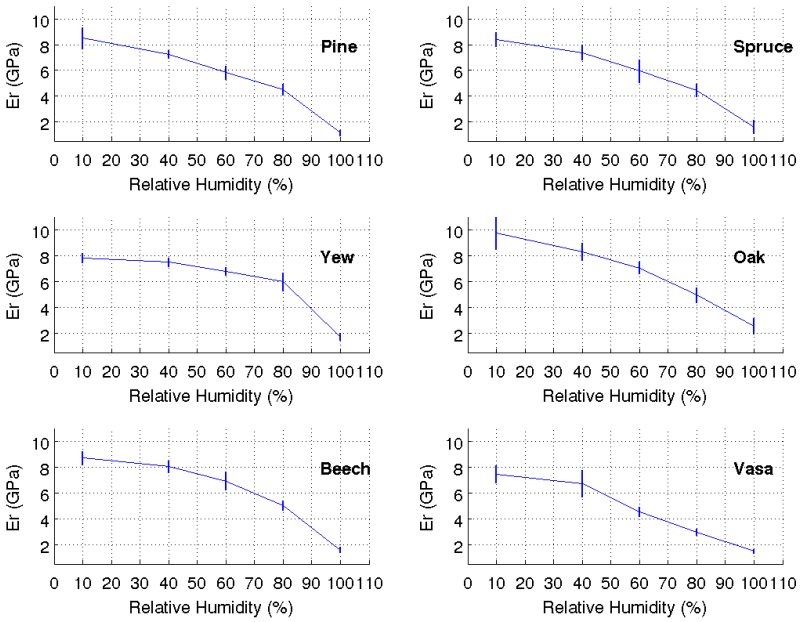

Figure 2.17: Indentation modulus in the middle lamella of different wood species under varying relative humidity

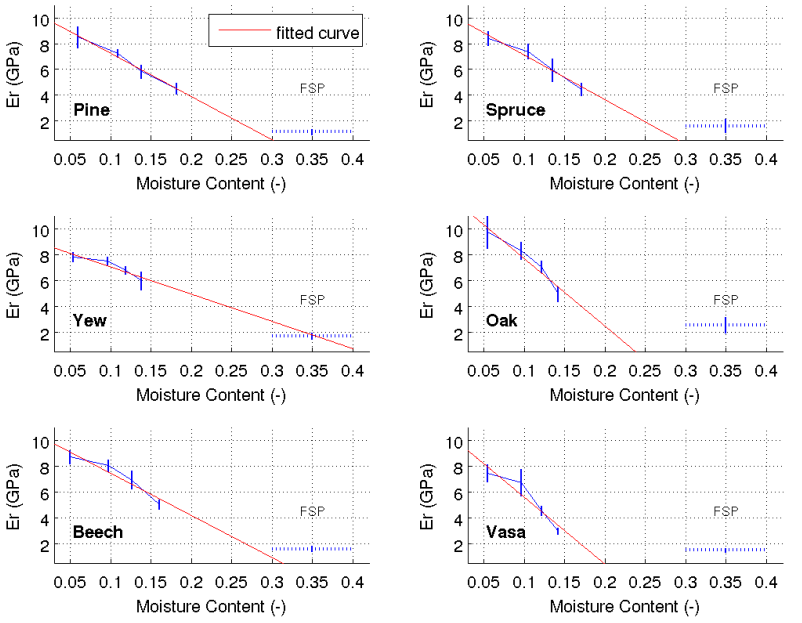

Figure 2.18: Indentation modulus in the middle lamella of different wood species with various MC

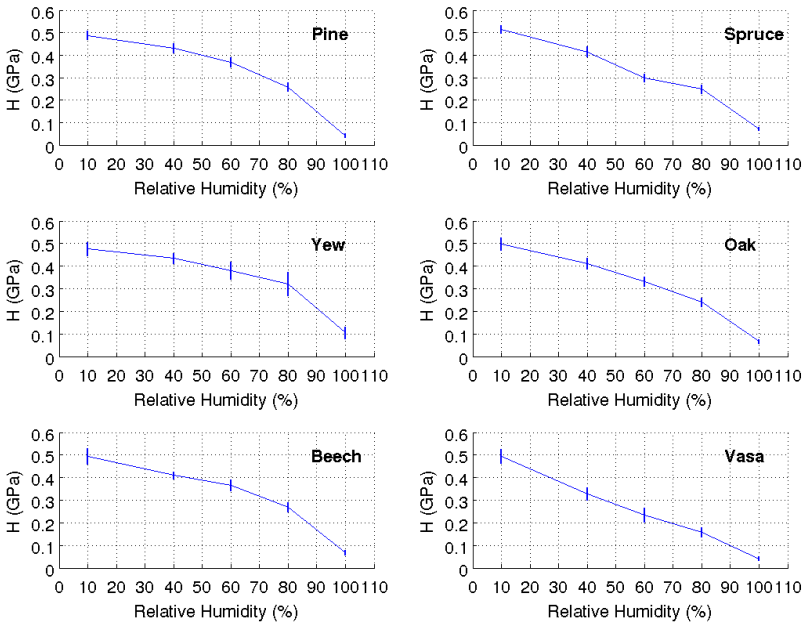

Figure 2.19: Hardness in the S2-layer of different wood species under varying relative humidity

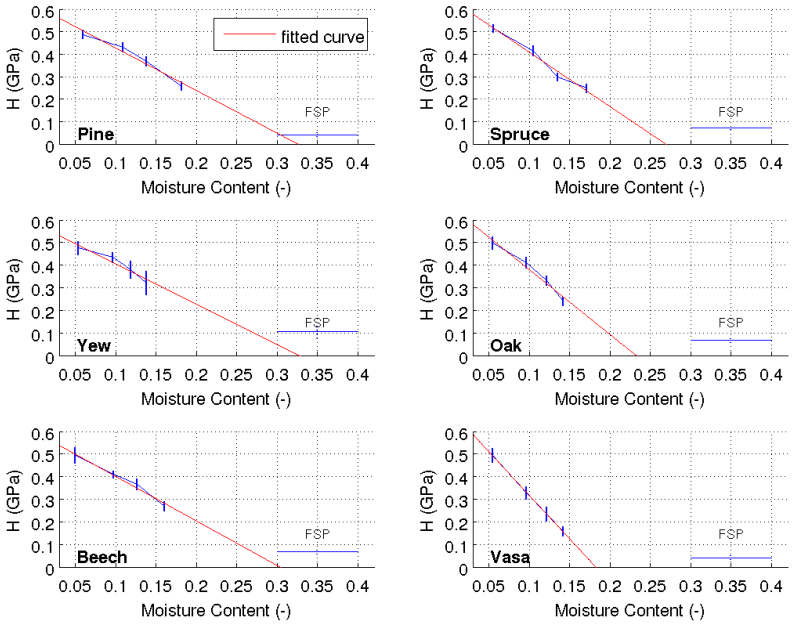

Figure 2.20: Hardness in the S2-layer of different wood species with various MC

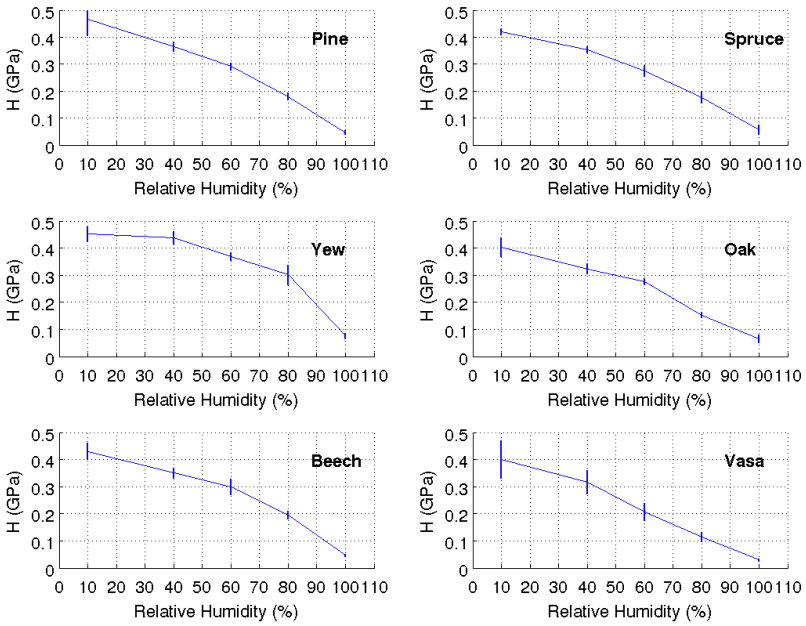

Figure 2.21: Hardness in the middle lamella of different wood species under varying relative humidity

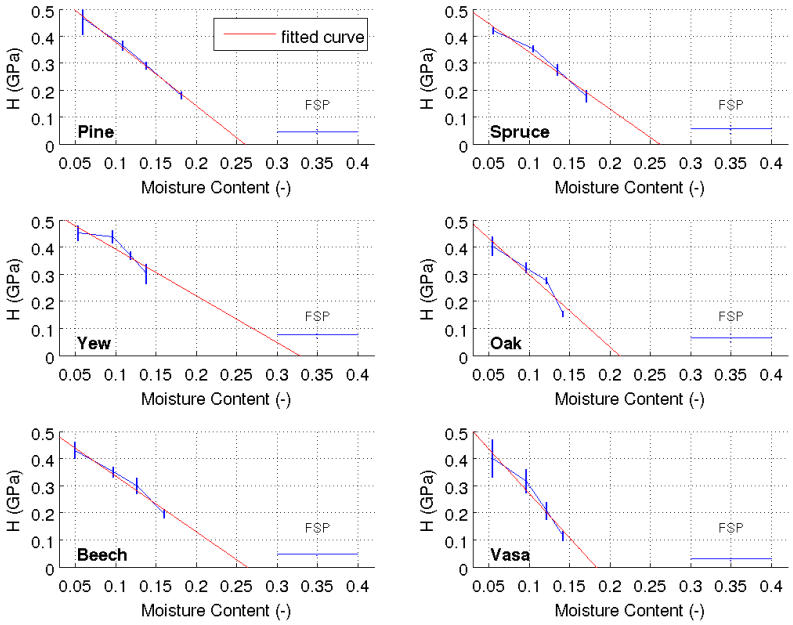

Figure 2.22: Hardness in the middle lamella of different wood species with various MC

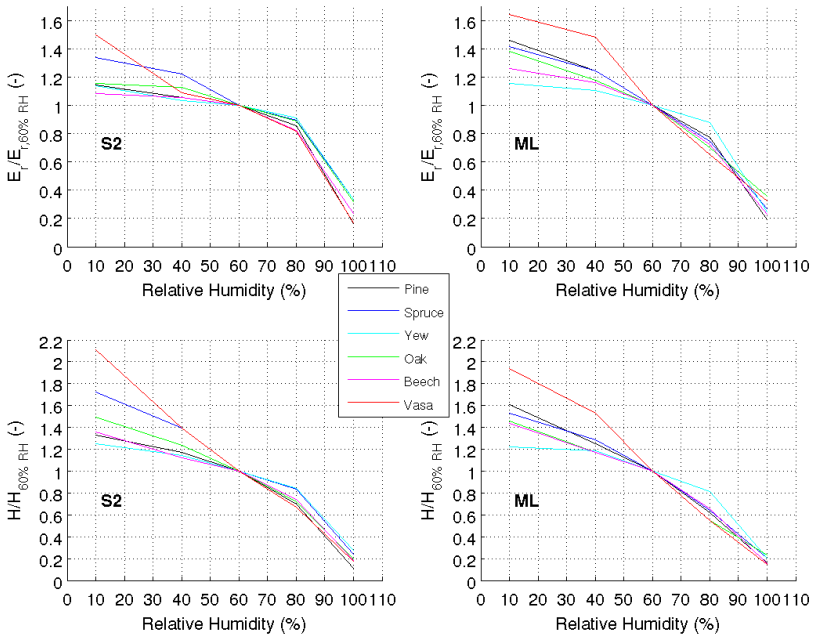

Figure 2.23: Comparison of relative stiffness and hardness of different wood species under varying relative humidity with respect to the stiffness or the hardness at 60% RH

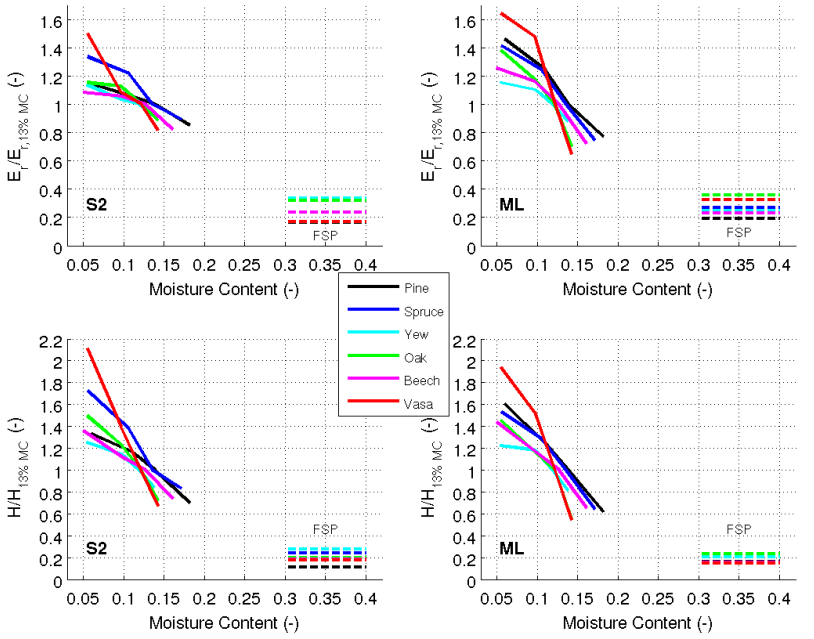

Figure 2.24: Comparison of relative stiffness and hardness of different wood species with various MC with respect to the stiffness or the hardness at 60% RH (around 13% MC)

Creep properties

Numerical values

Table 2.9 to 2.12 present the mean values and the standard deviation of the creep parameters (in %) for indents made in the S2-layer or in the middle lamella of different wood species under various humidity conditions.

Table 2.9: Average and standard deviation of first creep parameter (%) measured in the S2-layer by nanoindentation in different wood species under various humidity conditions

$Creep1$ (%)	10% RH	40% RH	60% RH	80% RH	FSP
Pine	13.58 ± 1.56	14.12 ± 2.36	14.84 ± 1.20	19.32 ± 2.43	24.44 ± 8.35
Spruce	14.63 ± 2.35	14.25 ± 1.36	17.27 ± 1.45	19.15 ± 2.63	21.35 ± 2.52
Yew	12.85 ± 1.50	12.47 ± 1.23	13.28 ± 1.94	21.96 ± 5.03	21.14 ± 7.14
Oak	13.83 ± 0.94	14.25 ± 0.94	15.92 ± 1.42	18.81 ± 1.67	23.61 ± 3.66
Beech	14.22 ± 1.62	14.29 ± 1.51	15.91 ± 0.99	20.86 ± 2.01	25.48 ± 7.09
Vasa	15.20 ± 1.77	19.21 ± 1.51	22.22 ± 1.17	24.61 ± 2.53	27.20 ± 4.23

Table 2.10: Average and standard deviation of first creep parameter (%) measured in the middle lamella by nanoindentation in different wood species under various humidity conditions

$Creep1$ (%)	10% RH	40% RH	60% RH	80% RH	FSP
Pine	14.94 ± 2.25	13.63 ± 0.51	14.48 ± 0.46	19.87 ± 1.39	21.66 ± 5.04
Spruce	13.70 ± 0.87	13.84 ± 0.98	15.12 ± 0.88	20.86 ± 1.08	22.07 ± 2.84
Yew	12.48 ± 1.86	12.06 ± 0.58	13.17 ± 0.36	28.27 ± 9.9	23.1 ± 3.45
Oak	15.42 ± 1.36	16.21 ± 2.04	16.25 ± 1.14	21.64 ± 1.68	25.80 ± 8.48
Beech	14.52 ± 1.45	14.38 ± 0.79	15.99 ± 1.15	25.18 ± 3.35	18.09 ± 3.00
Vasa	14.38 ± 2.86	15.94 ± 1.25	21.14 ± 1.44	28.35 ± 2.14	25.78 ± 3.80

Table 2.11: Average and standard deviation of second creep parameter (%) measured in the S2-layer by nanoindentation in different wood species under various humidity conditions

$Creep2$ (%)	10% RH	40% RH	60% RH	80% RH	FSP
Pine	10.16 ± 1.38	10.00 ± 0.72	10.90 ± 1.74	14.29 ± 3.21	14.42 ± 4.28
Spruce	8.95 ± 0.94	10.20 ± 0.83	12.82 ± 1.38	13.61 ± 1.41	16.06 ± 1.09
Yew	10.28 ± 1.80	9.51 ± 0.72	9.54 ± 1.54	14.55 ± 2.04	15.9 ± 2.86
Oak	10.37 ± 1.3	10.43 ± 1.07	11.93 ± 0.95	13.50 ± 0.90	15.64 ± 1.18
Beech	10.13 ± 0.74	10.61 ± 0.67	12.04 ± 1.05	14.71 ± 1.37	16.39 ± 2.48
Vasa	11.39 ± 1.77	13.75 ± 1.14	16.09 ± 1.71	17.99 ± 1.99	19.32 ± 2.9

Graphical presentation

Figures 2.25 to 2.31 show creep properties as measured by nanoindentation at various humidity conditions.

Table 2.12: Average and standard deviation of second creep parameter (%) measured in the middle lamella by nanoindentation in different wood species under various humidity conditions

*Creep*2 (%)	10% RH	40% RH	60% RH	80% RH	FSP
Pine	10.74 ± 0.50	11.13 ± 0.61	12.69 ± 1.01	15.27 ± 0.67	16.48 ± 3.75
Spruce	10.73 ± 0.72	10.92 ± 0.77	11.61 ± 0.70	14.85 ± 0.51	16.49 ± 2.23
Yew	9.59 ± 0.90	9.28 ± 0.39	10.37 ± 0.43	17.62 ± 5.20	15.36 ± 3.17
Oak	12.20 ± 1.06	12.35 ± 0.95	12.58 ± 0.64	15.84 ± 1.76	19.96 ± 3.66
Beech	11.21 ± 0.89	11.64 ± 0.80	12.40 ± 0.67	17.19 ± 2.04	14.06 ± 3.04
Vasa	10.83 ± 2.16	12.37 ± 0.64	14.57 ± 0.87	17.86 ± 2.04	18.04 ± 1.05

In contrary to the two other investigated mechanical properties, creep properties of the wood cell wall remarkably increase due to an increase of the relative humidity of the environment. This effect is particularly pronounced for a RH over 60%. This is clearly visible for example for oak in both layers or for pine in the S2-layer in Figures 2.26 and 2.28. However, considering Figures 2.27 and 2.29, the expected high increase in the creep properties over 80% RH is not visible for every investigated wood species. Also, for yew and beech, the 100% RH-creep values are lower than the ones at 80% RH. These results should then be put into perspective. For example, it is possible that the duration of the holding phase is too short to let the material creep as much as it could or that the small amount of indents realized under water led to non-representative values.

The parameter $Creep2$, corresponding to the holding phase at the highest load $Pmax$ seems to have the same behaviour than the parameter $Creep1$, calculated at the load $Pmax/2$. $Creep1$ and $Creep2$ follow the same trend between 10 and 80% RH with a factor of around 1.5. The fact that $Creep2$ is lower than $Creep1$ is most likely due to the higher load applied on the wood at this time. Since the plastic deformation of the wood cell wall under the indent is at the beginning much higher, the wood cell wall can less easily deform under constant loading.

A linear regression over the 10 to 80% RH creep properties plotted over the wood MC of the species seems to fit particularly good with the experimental results. Only in the cases of yew (in both layers) and beech (in the ML), the linear regression also fits quite well the 100% RH measurements, even if the fitting curve is always located above the experiments.

About the deteriorated wood of the Vasa, it seems to creep easier than the fresh oak, in particular for RH over 40% in the S2 and over 60% in the ML. The experimental values coming from the measurements under water, however, do not fit with a linear regression on the experimental values under 80% RH.

As a short conclusion, as explained in Chapter 1, the water bound in the wood cell wall layers softens the wood polymers and, in consequence, lowers the stiffness of the cell walls. The higher the moisture content in wood, the bigger the loss in the wood stiffness and hardness and the higher the increase of the creep phenomenon, in particular above 60% RH. With an average global decrease of the indentation modulus in the S2-layer of the investigated wood species of around 75% between 10 and 100% RH, the wood moisture content seems to be a relevant parameter to take into consideration in the determination of the wood mechanical properties at a microscopical level.

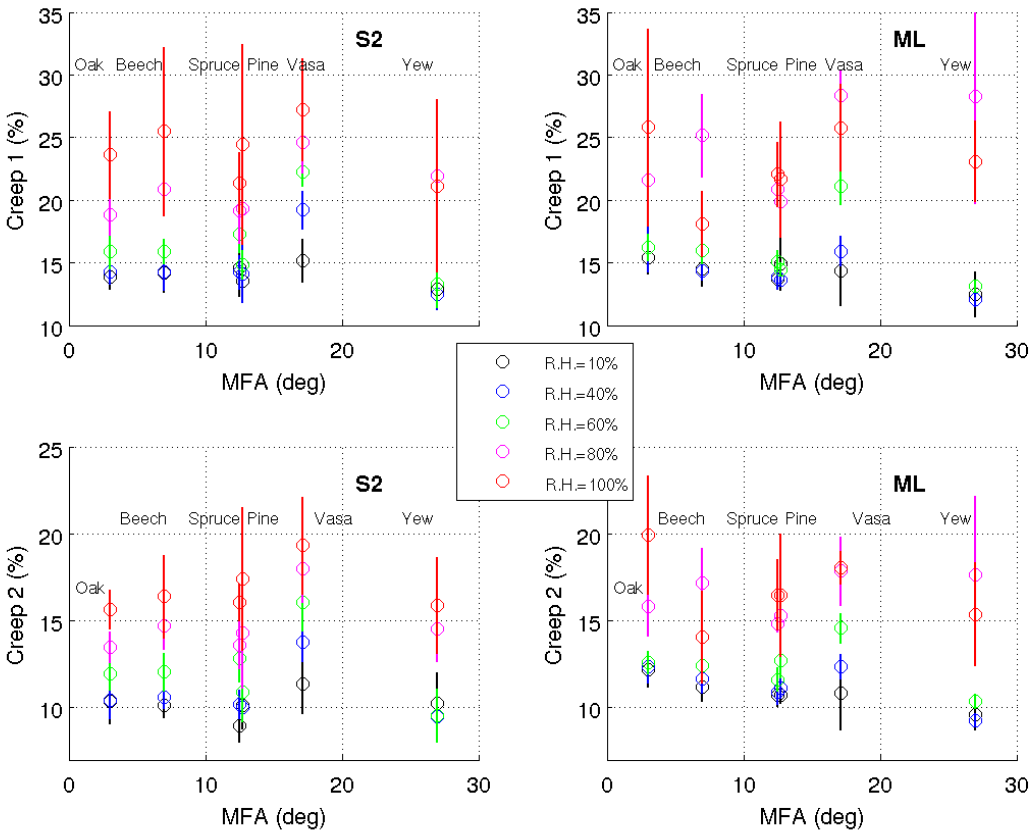

Figure 2.25: Creep parameters of cell wall layers of different wood species under varying relative humidity compared to their microfibril-angle

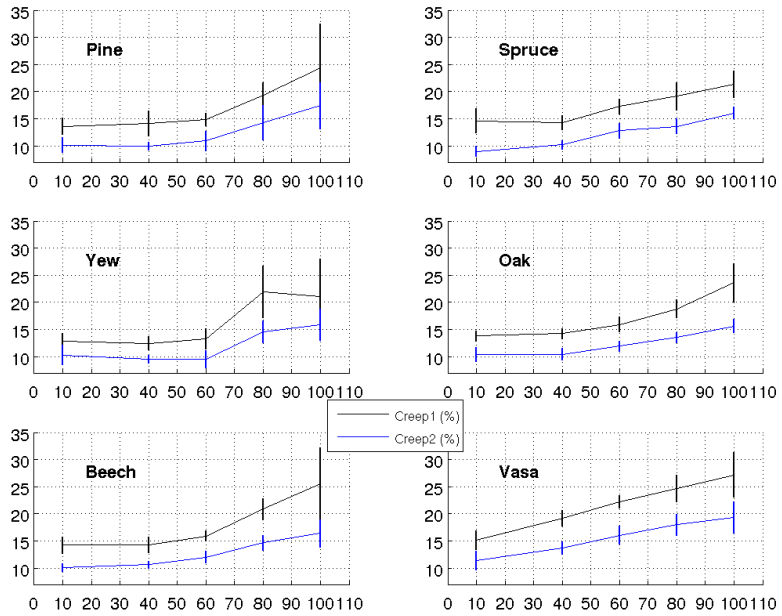

Figure 2.26: Creep parameters of the S2-layer of different wood species under varying relative humidity

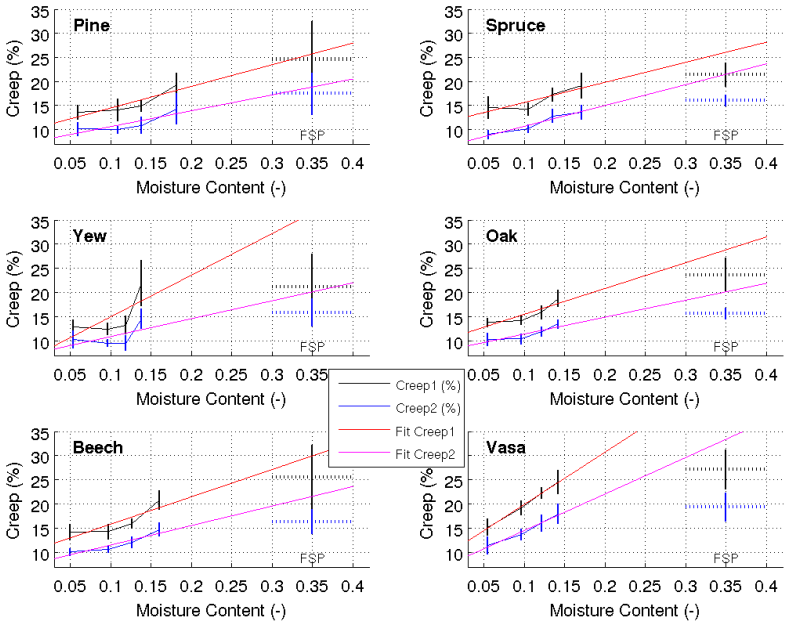

Figure 2.27: Creep parameters of the S2-layer of different wood species with various MC

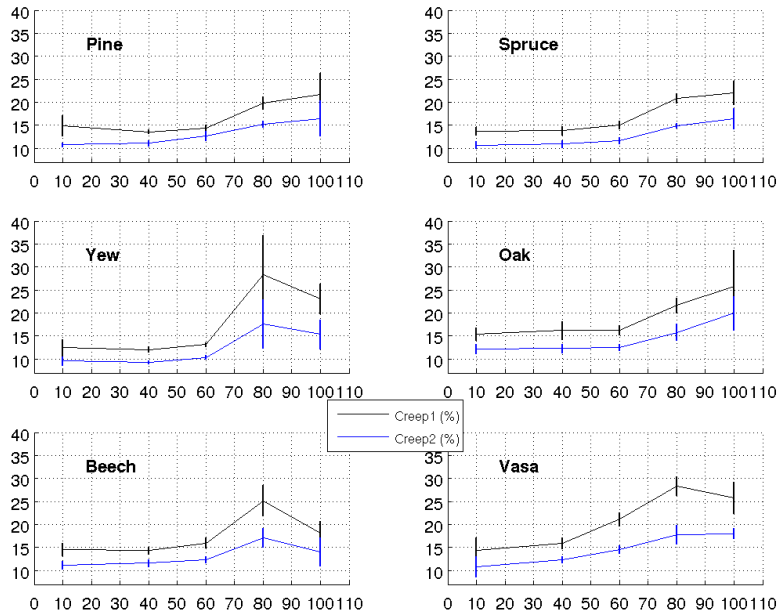

Figure 2.28: Creep parameters of the middle lamella of different wood species under varying relative humidity

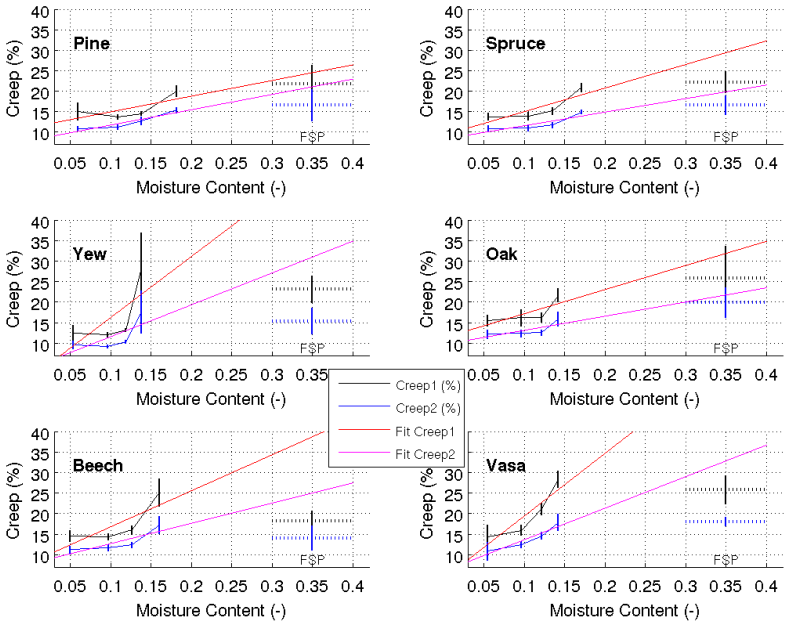

Figure 2.29: Creep parameters of the middle lamella of different wood species with various MC

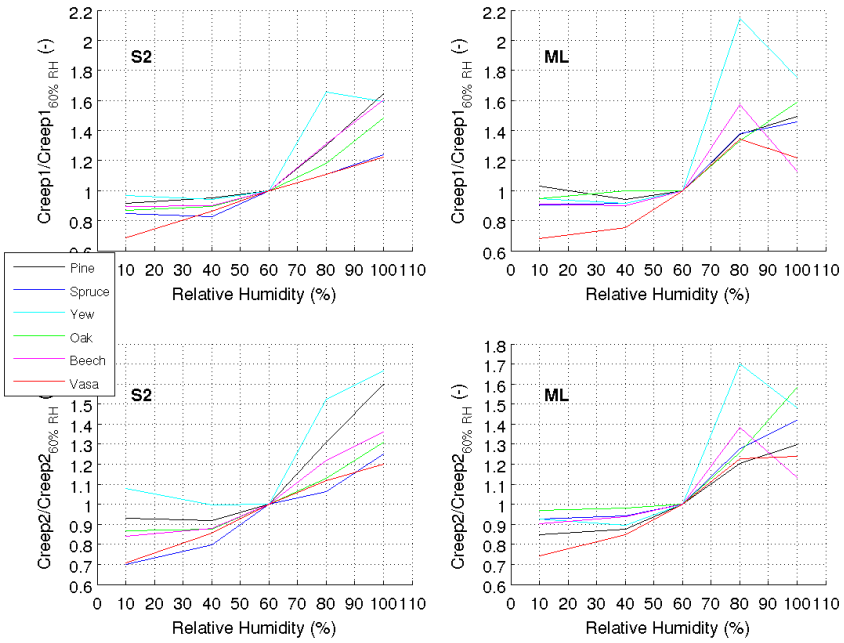

Figure 2.30: Comparison of relative creep parameters of different wood species under varying relative humidity with respect to the creep parameter at 60% RH

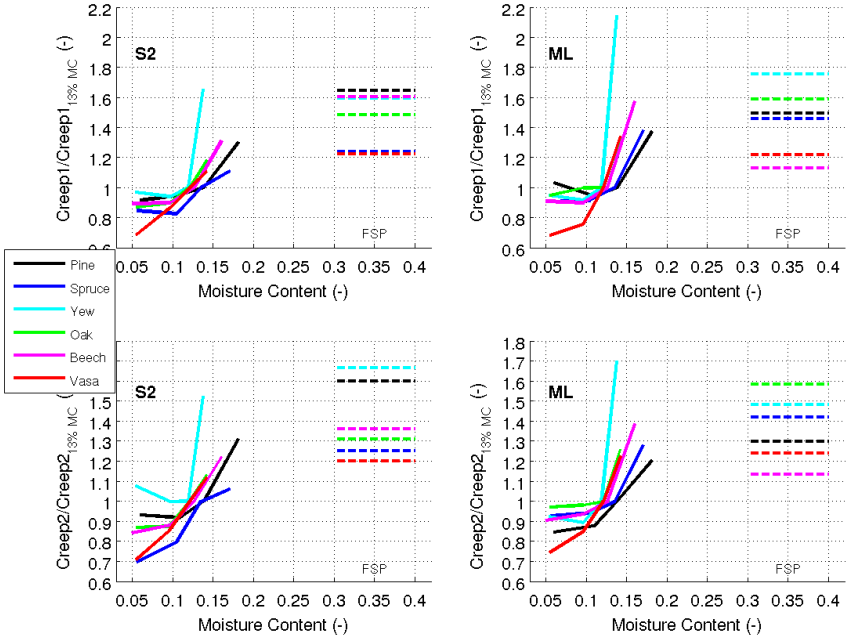

Figure 2.31: Comparison of relative creep parameters of different wood species with various MC with respect to the creep parameter at 60% RH (around 13% MC)

Chapter 3

Micromechanical modeling

3.1 Micromechanical modeling of micro-heterogeneous materials

In all technological fields, microheterogeneous materials are used: composites in transport industry, concrete and wood in civil engineering or bones in bioengineering. However, due to their complexity, microheterogeneous materials are difficult to investigate at a macroscopical scale. Therefore, for material optimization or for the prediction of their macroscopic mechanical constitutive behaviour, models had to be developed.

First models for composites were proposed in 1887 by Voigt [54] and in 1929 by Reuth [44], with the first "laws of mixtures". It is only for about fifty years that the first methods of continuum micromechanics were developed, shortly after the basic characteristics of "representative volume element" (RVE) and "homogeneous equivalent medium" were defined. For example, Hill [24] modeled in 1965 the elastoplasticity of polycrystals with a self-consistent scheme, an incremental method. These methods are not limited to elastic material properties, since some extensions were done to encompass e.g. linear elasticity with eigenstrains and poroelasticity.

As regards modeling approaches for wood, Astley and Harrigton et al. combined in 1996 and 1998 [2, 22, 3] finite element models with continuum mechanics at the wood cell scale, while Hofstetter et al. developed in 2005 and 2007 [26, 27] continuum micromechanical models. Bader et al [5] used a poromechanical approach in order to model softwood. Water was described as a fluid filling pore spaces.

As explained in Sections 1.1.3 and 1.2.1, water from the surrounding environment interacts with the wood structure at the molecular level, with consequences at all hierarchical levels of the material. At the scale we are interested in, the scale of the wood cell wall, the rather small water molecules, in comparison with the polymer chains, are penetrating the amorphous phases and are reacting with these media. The chemical reactions induced by water in the media are not heeded, since water is modeled as an inert incompressible fluid, i.e. it is modeled with a given bulk modulus and no shear modulus,

following [23].

3.1.1 Principles of linear elastic continuum micromechanics [1]

In continuum mechanics, the concept of continuity of a material implies that adjacent elements remain connected while a global deformation is applied. Considering a characteristic length of inhomogeneities d within a micro-heterogeneous material and a RVE with a characteristic length l, the condition $l \gg d$ must be fulfilled. With L the characteristic length of the structure or of the loading at the boundaries of the RVE, the second inequation describing the necessary separation of the length scales in continuum micromechanics is $L \gg l$. This "separation of scales" allows the homogenization of the material over the RVE.

Actually, modeling a RVE with its exact composition and components is mostly far too complicated. Therefore, quasi-homogeneous sub-regions with known quantitative properties, namely stiffness, volume fraction or eigenstresses, are suitably chosen to build up the RVE: they are the so-called material phases. Also, some qualitative properties are specified for each phase, namely a phase shape (e.g. cylinder, sphere, ellipsoid) and the interaction with the other phases. Then, the homogenized material behaviour can be derived from the characteristics of the RVE, the method used in this thesis is the Eshelby-Laws matrix-inclusion problem.

In linear elasticity, the Eshelby-tensor $\mathbb{P}_r^0$ of the inclusion r with given shape and stiffness $\mathbb{C}_r$ in a matrix (0) with stiffness $\mathbb{C}^0$ allows to link the average strains within the inhomogeneity (or phase) r, $\boldsymbol{\varepsilon_r}$, to the far-field strain $\mathbf{E^0}$ acting on the boundaries of an infinitely large matrix by:

$$\boldsymbol{\varepsilon_r} = [\mathbb{I} + \mathbb{P}_r^0 : (\mathbb{C}_r - \mathbb{C}^0)]^{-1} : \mathbf{E^0}, \tag{3.1}$$

with $\mathbb{I}$ as the fourth-order identity tensor.

Then, with the mathematical background of the Hill's Lemma, of the superposition principle and of the formulation of the linear concentration problem (i.e. with linear elasticity and linearised strains), the following relations are derived

$$\text{(a)} \quad \mathbf{E} = \sum_r f_r \boldsymbol{\varepsilon_r}, \qquad \text{(b)} \quad \boldsymbol{\Sigma} = \sum_r f_r \boldsymbol{\sigma_r}, \tag{3.2}$$

$$\text{(a)} \quad \boldsymbol{\varepsilon_r} = \mathbb{A}_r^{est} : \mathbf{E}, \qquad \text{(b)} \quad \boldsymbol{\sigma_r} = \mathbb{B}_r^{est} : \boldsymbol{\Sigma}, \tag{3.3}$$

with f_r as the volume fraction of phase r, $\boldsymbol{\sigma_r}$ as the stress in phase r and with $\mathbb{A}_r^{est}$ and $\mathbb{B}_r^{est}$ as the estimated strain and stress concentration tensors relative to the phase r, respectively.

Using $\mathbb{A}_r^{est}$ and $\mathbb{B}_r^{est}$, the stiffness $\mathbb{C}^{est}$ and compliance $\mathbb{D}^{est}$ of the homogenized material can be estimated as

$$\mathbb{C}^{est} = \sum_r f_r \mathbb{C}_r : \mathbb{A}_r^{est}, \tag{3.4}$$

$$\mathbb{D}^{est} = \sum_r f_r \mathbb{D}_r : \mathbb{B}_r^{est}. \tag{3.5}$$

[1] from course on "Advanced micro- and macromodeling of materials" Christian Hellmich, LVA 202.051 and 202.052, TU Wien and from Bader in 2010 [5]

By combining for each phase the strain average Equation (3.2(a)) with Equations (3.1), a relation between $\mathbf{E}^0$, the fictitious strain at the boundary of an infinitely large matrix, and $\mathbf{E}$, the strain at the boundary of the RVE, is obtained. Inserted back into Equation (3.1) for each phase, it enables the elimination of $\mathbf{E}^0$ from the calculation and the strain concentration tensor for each phase can be estimated from Equation (3.3(a)). For linear elasticity, the estimated strain concentration tensor reads as

$$\mathbb{A}_r^{est} = [\mathbb{I} + \mathbb{P}_r^0 : (\mathbb{C}_r - \mathbb{C}^0)]^{-1} : \left\{ \sum_s f_s [\mathbb{I} + \mathbb{P}_s^0 : (\mathbb{C}_s - \mathbb{C}^0)]^{-1} \right\}^{-1}. \tag{3.6}$$

Inserting Equation (3.6) into Equation (3.4) gives the estimated stiffness $\mathbb{C}^{est}$ as

$$\mathbb{C}^{est} = \sum_r f_r \mathbb{C}_r : [\mathbb{I} + \mathbb{P}_r^0 : (\mathbb{C}_r - \mathbb{C}^0)]^{-1} : \left\{ \sum_s f_s [\mathbb{I} + \mathbb{P}_s^0 : (\mathbb{C}_s - \mathbb{C}^0)]^{-1} \right\}^{-1}. \tag{3.7}$$

$\mathbb{C}^0$ must be reasonably chosen.

- For a composite with a continuous matrix (i.e. e.g. fibres embedded into a matrix), a Mori-Tanaka scheme is used. In this case, $\mathbb{C}^0 = \mathbb{C}_{Matrix}$.
- For a polycrystalline material (i.e. many inhomogeneities in more or less equal proportions), a self-consistent scheme is applied. In this case, $\mathbb{C}^0 = \mathbb{C}^{est}$. Therefore, an iterative calculation of $\mathbb{C}^{est}$ is required.

3.1.2 Principles of linear poro-elastic continuum micromechanics (from [23, 58, 43])

In linear poroelasticity, pore spaces are considered as an additional material phase, with no stiffness, but possibly filled with a fluid. Therefore, eigenstresses in water are $\boldsymbol{\sigma_r} = -\mathbf{1}.p$, with p as the fluid pressure in the pores. Then, the porous material can be considered in the framework of continuum micromechanics with eigenstresses. According to [58], the poroelastic problem can be formulated similar to

$$\boldsymbol{\varepsilon_r} = [\mathbb{I} + \mathbb{P}_r^0 : (\mathbb{C}_r - \mathbb{C}^0)]^{-1} : [\mathbf{E}^0 + \mathbb{P}_r^0 : (\boldsymbol{\sigma}^T - \boldsymbol{\Sigma}^T)], \tag{3.8}$$

with σ as the eigenstress within phase r and Σ as the eigenstress within the matrix.

The first state equation of poroelasticity,

$$\boldsymbol{\Sigma} = \mathbb{C} : \mathbf{E} - \boldsymbol{b}p, \tag{3.9}$$

is derived for the poroelastic framework from the basic equation of linear elasticity:

$$\boldsymbol{\Sigma} = \mathbb{C} : \mathbf{E}, \tag{3.10}$$

and extended by the eigenstresses within the RVE. Therefore, also an eigenstress in matrix can be considered.

Moreover, $\boldsymbol{b}_0^{hom}$ and N_0^{hom} for the homogenized poroelastic phase (0) are calculated by identification between the second state equation of poroelasticity (Equation (3.11),

from [23]) and Equation (3.12), where r is the porous phase, in order to determine the global porosity change $\phi - \phi_0$ in the homogenized material.

$$\phi - \phi_0 = \boldsymbol{b}^{hom} : \mathbf{E} + \frac{p}{N^{hom}} \tag{3.11}$$

$$\phi - \phi_0 = f_r \mathbf{1} : \boldsymbol{\varepsilon_r} \tag{3.12}$$

The expressions for the calculation of $\boldsymbol{b}_0^{hom}$ and N_0^{hom} are then

$$\boldsymbol{b}^{hom} = f_r \cdot \mathbb{I} : \mathbb{A}_r^{est}, \tag{3.13}$$

$$\text{and} \quad \frac{1}{N^{hom}} = f_r \cdot \mathbb{I} : \boldsymbol{a}_r^{est}, \tag{3.14}$$

with $\boldsymbol{a}_r^{est}$ as

$$\boldsymbol{\varepsilon}_r = \mathbb{A}_r^{est} : \mathbf{E} + \boldsymbol{a}_r^{est} \cdot p. \tag{3.15}$$

3.1.3 Multistep homogenization

For hierarchically structured materials, a multistep homogenization enables then to determine the homogenized material properties at each length scale (see Figure 3.1), as long as the characteristic length conditions are fulfilled for each step

$$d_3 \ll l_3 \leq d_2 \ll l_2 \leq d \ll l. \tag{3.16}$$

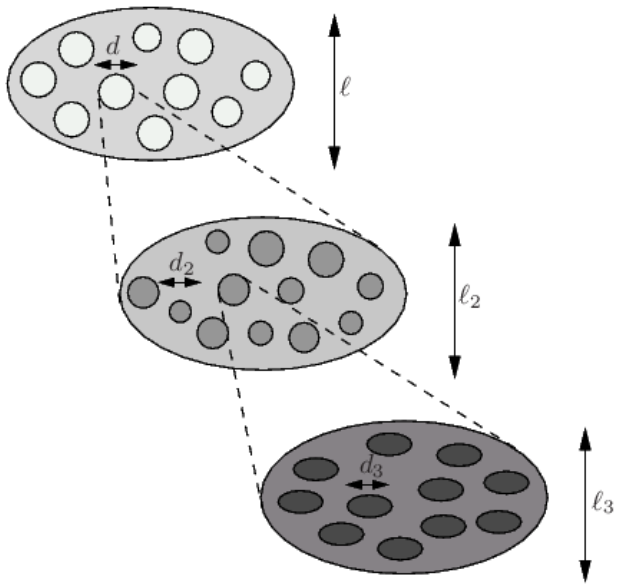

Figure 3.1: Multistep homogenization: properties of upper phase with RVE of characteristic length l are determined from homogenization over smaller RVEs with characteristic lengths of l_2 and l_3 respectively. (from [5])

3.2 Micromechanical modeling of wood cell walls

3.2.1 Poromechanical model for the wood cell wall material

The multiscale homogenization model of the wood cell wall encompasses three steps of homogenization, considering the relative complex structure of the material, which are represented in a 2D-visualization in Figure 3.2.

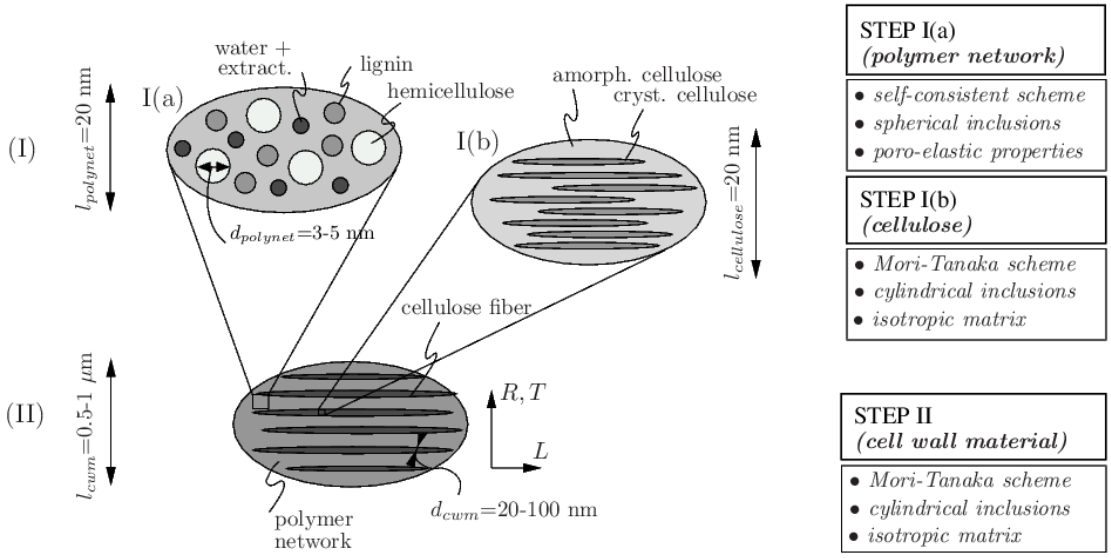

Figure 3.2: Homogenization steps for the cell wall material (from [5]).

Table 3.1 summarizes the elastic constants of each component of the wood cell wall.

Table 3.1: Mechanical properties of basic components of the wood cell wall

Phase	E (GPa)	ν	k (GPa)	μ (GPa)	Reference
Hemicelluloses (Cousins)	6.1	0.39	8.89	2.2	[11]
Amorphous Cellulose	5	0.35	5.56	1.85	[15]
Lignin (Cousins)	5.76	0.31	5	2.2	[10]
Extractives	0.15	0.5	3	0.05	[5]
Water	0	0.5	2.3	0	[5]

Phase	Stiffness components (GPa)	Reference
Crystalline cellulose	$C_{1111} = 34.87$ $C_{1122} = 0$ $C_{2233} = 0$ $C_{3333} = 167.8$ $C_{1313} = 5.81$	[52]

Step Ia: Polymer Network

The first step is the homogenization of the poro-elastic polymer network into which cellulose fibres are embedded in a later homogenization step. As a simplification, only

three elements are considered in this material.

- hemicelluloses
- lignin
- extractives and water mixed in poroelastic pores, with phase stiffness

$$\mathbb{C}_{H20,Ext} = \frac{f_{H2O}\mathbb{C}_{H2O} + f_{Ext}\mathbb{C}_{Ext}}{f_{H2O} + f_{Ext}}. \tag{3.17}$$

A self-consistent scheme is used, as non of the phases has a predominant role in the material, and, in a first approximation, all phases are considered to have a spherical shape. In a second approximation, the water and extractives-spheres are replaced by cylinders with a random orientation in the homogenized phase. Furthermore, in a further approximation, the extractives are separated from the water and are represented as spheres. None of these successive modifications has a great impact on the obtained values, as detailed in Section 3.3.2.

Due to the presence of pores filled with water, the homogenized polymer network has poro-elastic properties. This model gives an isotropic poroelastic polymer network, with drained stiffness $\mathbb{C}_{poly}$, with Biot tensor $\boldsymbol{b}_{poly}$ and with Biot modulus N_{poly}.

Step Ib: Cellulose

In wood, there are two different types of cellulose: crystalline cellulose fibres that are surrounded by an amorphous cellulose matrix. In this model, these two materials are combined and defined under the name *cellulose microfibrils*. A Mori-Tanaka scheme is used, where the crystalline fibres are modeled as transversely isotropic cylinders aligned in the third direction that are embedded into an isotropic amorphous matrix. The result is a transversely isotropic material with elastic stiffness $\mathbb{C}_{cell}$.

Step II: Cell Wall Material

From all layers building up the wood cell wall, the S2-layer and the ML are most important for the mechanical behaviour of the cell wall and accessible by nanoindentation tests. For both layers, a micromechanical model was developed.

S2-layer

The S2-layer is composed of cellulose microfibrils (from step Ib) embedded into a polymer network (from step Ia). The fibrils, however, are oriented within the wall with an angle θ inclined to the cell axis, the so-called microfibril angle (MFA). A Mori-Tanaka scheme is basically used and returns a transversely isotropic material in the third direction, i.e. with the direction of anisotropy parallel to the cellulose fibrils and an isotropic plane perpendicular to it.

In order to account for variations in the orientation of the cellulose microfibrils, an additional small variation $\Delta\theta$ in the MFA within the cell wall is used. This is taken in consideration in the algorithm with the introduction of a new phase, the cross cellulose. It consists in cellulose microfibrils with an orientation $\theta + \Delta\theta$ or $\theta - \Delta\theta$ with regards to the cell axis. The amount of cross cellulose and the value of $\Delta\theta$ are controlled as input

parameters. For this purpose, another homogenization scheme should be used to avoid the weaknesses of the Mori-Tanaka approach for multi-phase composite materials [34]. A Li-approach is used in this work. This model accounts for the fact that not all microfibrils are exactly oriented with an angle θ with respect to the cell axis.

In the micromechanical model, the microfibril angle is set equal to zero. The influence of the MFA is considered in the indentation theory.

Middle lamella

The middle lamella consists of the same components as the S2-layer, but the cellulose fibrils are not oriented in the third direction, but randomly in all space directions, which, by using a Mori-Tanaka scheme, returns an isotropic material.

The undrained elastic stiffness tensor $\mathbb{C}^{undr}$ is a function of the drained elastic stiffness tensor $\mathbb{C}^{dr}$, the initial porosity of the material ϕ_0, the bulk modulus of water k_{H2O} and of the Biot modulus N, as

$$\mathbb{C}^{undr} = \mathbb{C}^{dr} + M\boldsymbol{b} \otimes \boldsymbol{b}, \tag{3.18}$$

with M as

$$M = \frac{\phi_0}{k_{H2O}} + \frac{1}{N^{hom}}. \tag{3.19}$$

3.2.2 Homogenized stiffness and nanoindentation modulus

The calculation of the indentation modulus of an isotropic material from its stiffness is done by

$$E_r = \frac{E}{1-\nu^2}, \tag{3.20}$$

where E is the Young's Modulus, ν the Poisson's ratio and E_r the indentation modulus of the material. Therefore, the results obtained from the nanoindentation measurements in Chapter 2 can be compared with the homogenized stiffness of the ML obtained from the micromechanical model (see for example Figure 3.8).

However, for anisotropic materials as the S2-layer, the calculation is more complicated, as the indentation modulus is depending of the indentation direction. To enable the comparison between NI experimental data and the elastic properties of the S2-layer, Jäger et al. [30] developed in 2010 a model for the study of transversely isotropic materials. With the material undrained elastic stiffness tensor and the indentation direction with respect to the transversal axis as inputs, the model returns the indentation modulus.

3.2.3 Model input parameters

Tables 3.2, 3.3 and 3.4 (see also subsection 2.1.1) summarize the chemical, physical and microstructural input parameters for the micromechanical modeling of the wood cell walls.

The relationship between a RH and a MC has been made possible from the investigations summarized in Section 2.1.2. The MC used in the model represents the average values of the MC obtained experimentally for the investigated wood species.

In addition to these parameters, the chosen shape of the water modeling, the chosen algorithm for the second step of homogenization and the angle and the proportion of cross cellulose are input for the model o the S2 layer.

Table 3.2: Input parameters for the micromechanical model of the S2-layer

			Chemical composition (w.-%)			
Common name	Scientific name	MFA (°)	C	HC	L	Ext
Norway spruce	*Picea abies*	12.5	58.1	18.6	20	3.0
Scots pine	*Pinus sylvestris*	12.7	56.1	20.9	20	2.7
Common yew	*Taxus baccata*	27	53.6	17.6	25.9	2.9
Common beech	*Fagus sylvatica*	7	58.1	19.1	19.8	2.9
European oak	*Quercus robur*	3	49.6	25.2	18.4	6.7

Table 3.3: Input parameters for the micromechanical model of the middle lamella

		Chemical composition (w.-%)			
Common name	Scientific name	C	HC	L	Ext
Norway spruce	*Picea abies*	14.4	36.0	45.5	4.0
Scots pine	*Pinus sylvestris*	13.4	39.0	44.0	3.5
Common yew	*Taxus baccata*	12.5	29.3	43.7	14.5
Common beech	*Fagus sylvatica*	14.5	37.0	44.7	3.9
European oak	*Quercus robur*	11.1	43.8	37.2	7.9

Table 3.4: Moisture contents for micromechanical modeling and their corresponding relative humidity for the comparison with the experimental data

Relative Humidity (%)	10	40	60	80	100
Moisture Content (-)	0.055	0.1	0.13	0.16	0.30

3.2.4 Model predictions

Figures 3.3 and 3.5 show the model predictions for the stiffness components and for the indentation modulus of several wood species (as investigated experimentally in Chapter 2) in the S2-layer and in the middle lamella. The investigated moisture content is between 5.5 to 30% corresponding to relative humidities of 10 (5.5% MC) to 80% (16% MC) and to the FSP (assumed to be around 30% MC). The Vasa wood will not be modeled, due to its specific microstructure and components (because of its particular history). The consideration of the degradation and the modification of wood cell walls in this micromechanical model is beyond the scope of this work.

S2-layer

Subscript 3 indicates the longitudinal direction of the cellulose microfibrils, subscript 1 the radial or tangential directions to the cellulose microfibrils, as the S2-layer material has a transversely isotropic behaviour.

All investigated wood species encounter a loss in their mechanical properties with increasing wood moisture content (which corresponds to a decrease of all moduli and a slight increase in the Poisson's ratio with increasing MC). The influence of the microfibril angle (MFA) is obvious on the last graphic on the left in Figure 3.3, which shows the indentation modulus E_r in the cell longitudinal direction as a function of the moisture

content for different wood species. The indentation modulus was then calculated with the MFA.

Hence, oak, which has the lowest mechanical properties of the four first diagrams (low Young's moduli, low shear modulus and high Poisson's ratios), has a quite high indentation modulus, comparable to most wood species, due to its MFA that is 3°. Similarly, beech, due to its MFA of 7°, the second lowest after oak, and due to its high stiffness properties, encounters the highest indentation modulus among the investigated wood species. On the contrary, yew has similar stiffness properties and Poisson's ratios as the other wood species, except oak. However, dur to its MFA of 27°, its indentation modulus at 5.5% MC is about 27% lower compared to pine.

Oak stiffness properties seem to have the lowest moisture sensitivity. With a loss in its indentation modulus of around 62% starting above 21 GPa, the indentation modulus of beech encounters the highest moisture-dependency.

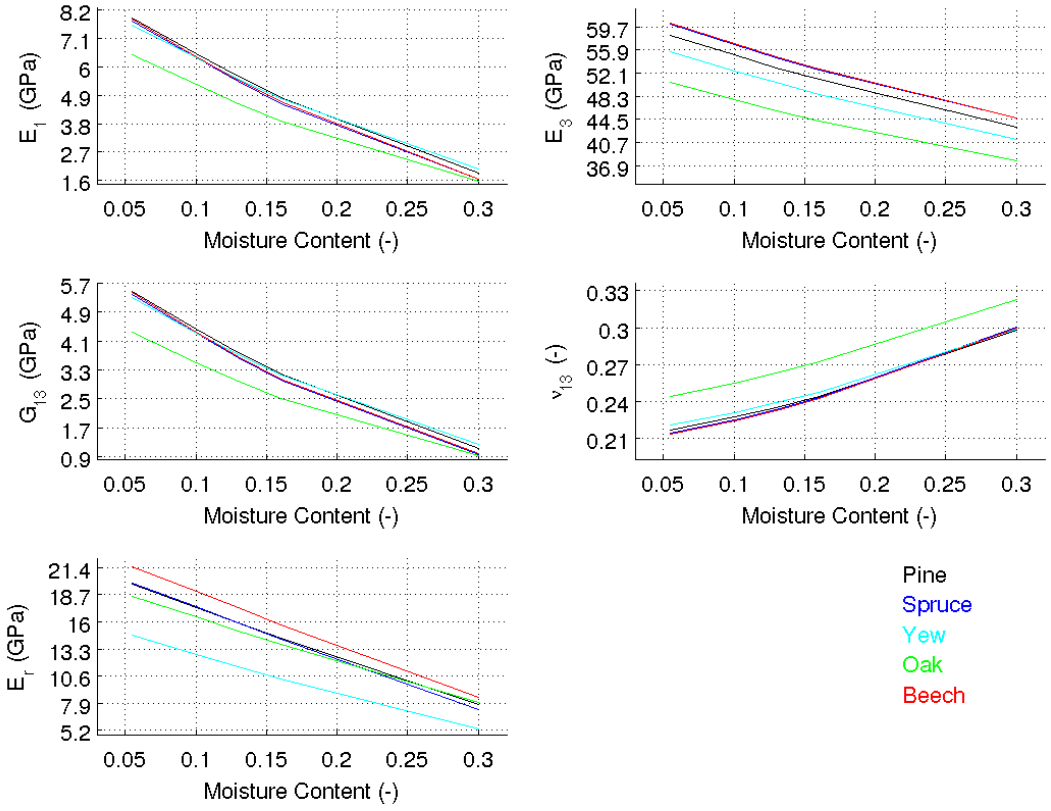

Figure 3.3: Modell predictions (stiffness components E_1, E_3, G_{13} and ν_{13} and indentation modulus E_r) for the S2-layer of different wood species

Figure 3.4 shows the predicted value and experimental values of the indentation modulus of the S2-layer. For a better comparison of the model predicted influence of moisture on elastic properties, relative values are plotted in Figure 3.4. The moisture

dependency of the indentation modulus seems underestimated by the micromechanical model for most wood species.

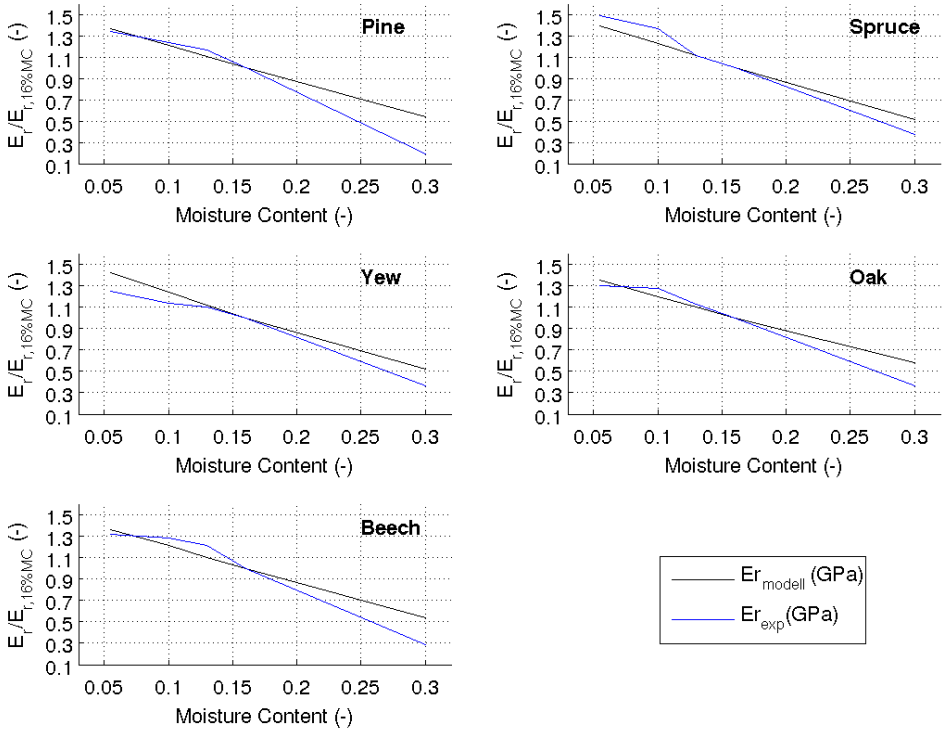

Figure 3.4: Comparison of the predicted and experimental relative indentation moduli of the S2-layer for different wood species with respect to the indentation moduli at 16% MC

Middle Lamella

The middle lamella has isotropic mechanical properties, due to the high dispersion of the cellulose microfibrils directions in the ML. Therefore, E is its Young's modulus in every direction and its indentation modulus E_r does not differ so strong from the elastic modulus. Again, all plotted properties (stiffness properties and indentation modulus) of the wood species are moisture-sensitive. They decrease with increasing moisture content, except the Poisson's ratio, which slightly increases.

More precisely, yew is the wood with the lowest stiffness properties and indentation modulus and the highest Poisson's ratio. Its indentation modulus moisture-dependency reaches around 30%, starting from 5.5% MC up to 30% MC. On the contrary, beech is again the modeled wood species with the highest indentation modulus. Its moisture dependency reaches around 34% in the investigated moisture range.

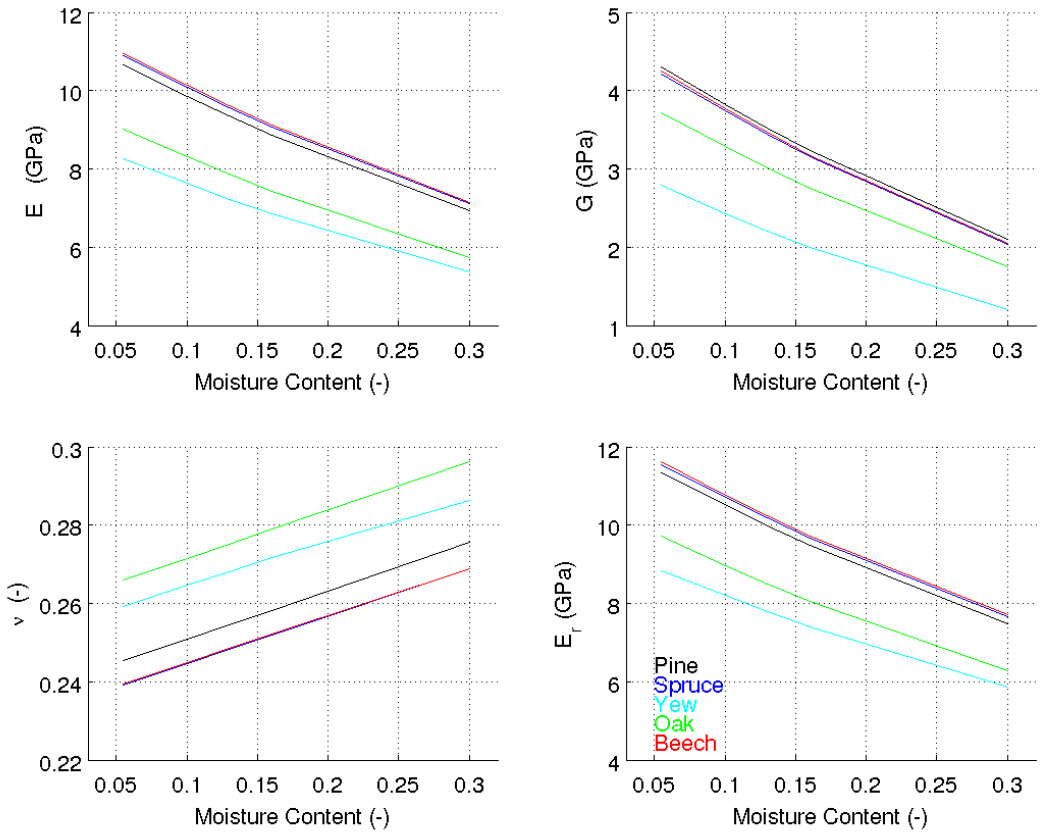

Figure 3.5: Modell predictions (stiffness components E, G and ν and indentation modulus E_r) for the middle lamella of different wood species

Figure 3.6 shows the predicted value and experimental values of the indentation modulus of the middle lamella. For a better comparison of the model predicted influence of moisture on elastic properties, relative values are plotted in Figure 3.6. The moisture dependency of the indentation modulus seems overestimated for most wood species, despite

the fact that the indentation modulus is generally overestimated by the micromechanical model. Possible reasons for this will be discussed in the following sections.

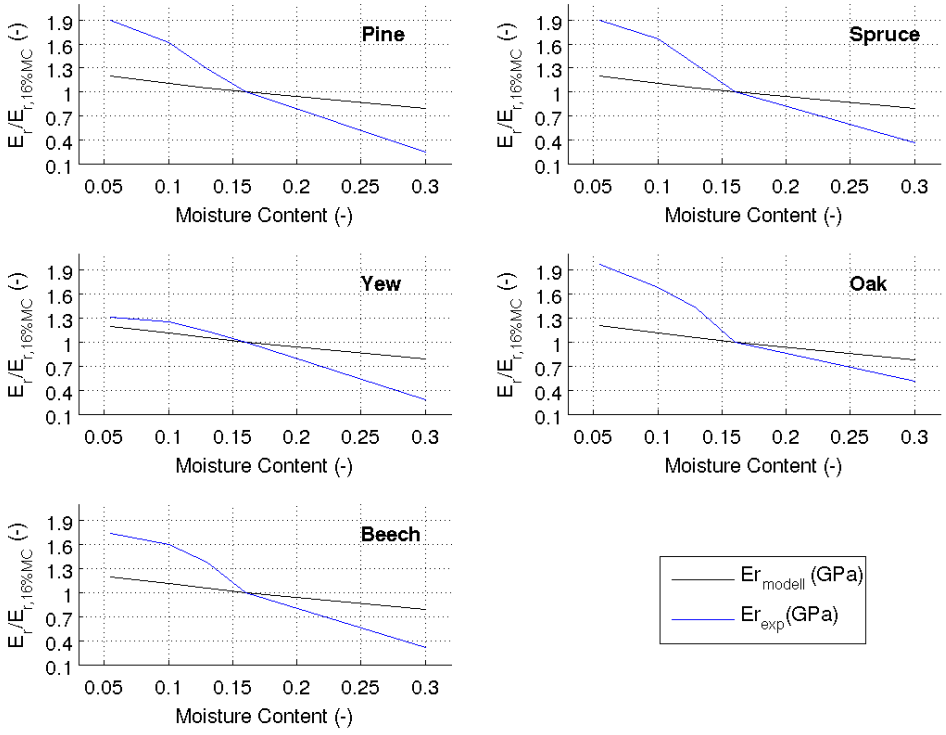

Figure 3.6: Comparison of the predicted and experimental relative indentation moduli of the middle lamella for different wood species with respect to the indentation moduli at 16% MC

3.3 Parameter studies

Parameter studies are discussed for spruce with reference input parameters as discussed in Section 3.2.3.

3.3.1 Variation of the chemical composition

Comparing model predictions with the experimental data enables to characterize the influence of the parameters on the prediction accuracy and to determine if further model improvements are required to enhance the model predictions.

A good agreement between experiments and model predictions is an indication for a suitably represented micro-structure of wood and of moisture uptake. In order to evaluate and quantify the influence of assumptions on micro-structural characteristics on the stiffness of wood cell walls, a parameter study is carried out. In a first step, the influence of the chemical composition of wood cell wall layers is assessed.

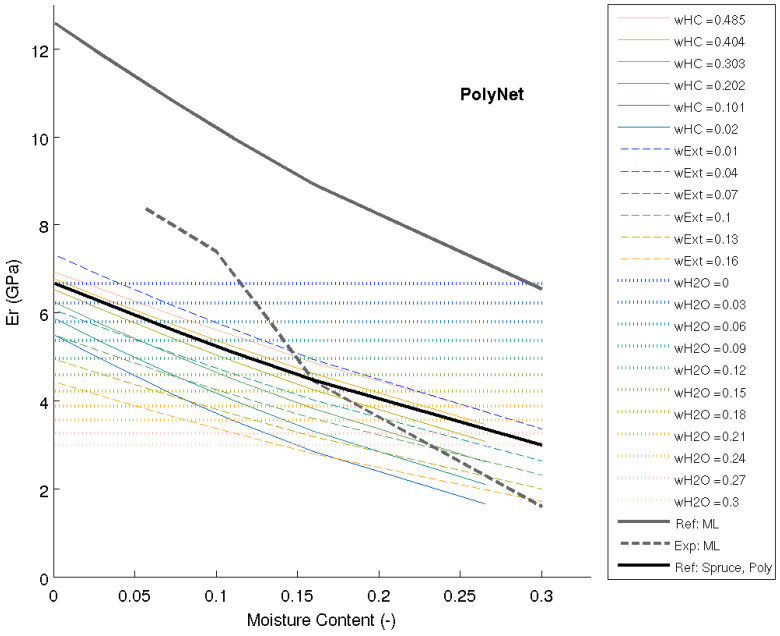

Figure 3.7: Parameter study: influence of chemical composition of the indentation modulus of the polymer network

Chemical composition of the polymer network

The chemical composition of spruce is considered to vary in many ways in order to assess its influence on the indentation modulus.

In a first simulation, the hemicelluloses content of the polymer network is varied from 2% to 48% of the total middle lamella chemical composition. In the same time, the

amount of the other components are proportionally varied to make a total of 1. Then, with the same compensation system, the extractives are also varied from 1% up to 16%.

In Figure 3.7, the predicted values of the ML indentation modulus for different chemical compositions are plotted, but only with the first step of the micromechanical model, i.e. the polymer network as well as the experimental and predicted values for the ML indentation modulus (this time, the values is predicted with the ML model). This enables to get an idea of the influence of the cellulose on the ML material.

From this calculation and comparison, one can conclude that cellulose has obviously a reinforcing effect in the ML, which nearly doubles the indentation modulus in comparison to the matrix alone.

Possible reasons for the deviation between experiments and model could be that there is a lower cellulose content in the ML, which would reduce the model predictions.

The influence of moisture on the indentation modulus is also underestimated by the model. This might be influenced by the assumption of similar moisture contents of the S2-layer and the ML.

Chemical composition of the middle lamella

In the first simulation, the cellulose content of the middle lamella is considered to vary between 1% to 50%, compensated by the hemicelluloses content.

The second simulation is related to the extractives, for contents from 1% up to 16%.

In Figure 3.8, the great influence of the cellulose ratio on the mechanical properties of the middle lamella is easy to observe, while the extractives have less effects on the indentation modulus. More impressive is the big difference between the predicted values, for quite all tested compositions, with the experimental values. The indentation modulus is overestimated in all cases. Therefore, assumptions in this model should be reconsidered so that it better fits with the experiments.

As a reference, the formerly predicted values from Figure 3.3 were also plotted in Figure 3.8, as well as the experimental data. Moreover, two supplementary curves were plotted: they are related to the original spruce composition in the ML, but using the S2-model, with an indentation angle of 0° for the upper one and 90° for the lower one. This enables to compare the influence of the cellulose in the ML mechanical properties, in particular the influence of the MFA, or, in other words, the influence of the fact that all cellulose phases are oriented in a unique direction.

The anisotropy, due to the shear modulus in the S2-prediction, seems to have a great influence on the indentation modulus, even if it is indented in the direction of the microfibrils with a MFA of 0°.

Chemical composition of the S2-layer

In a first simulation, the cellulose content was continuously changed from 1% to 75% of the layer. To compensate this imbalance, the hemicelluloses content decreased from 75% to 1% of the global layer composition. The original values are around 58% for the cellulose and 19% for the hemicelluloses (see Table 3.2). To make the comparison easier, the original predicted values as well as the experimental data are plotted on the same graph (see Figure 3.9). As a conclusion from this variation, the cellulose contents would have to be higher to better fit the experimental results.

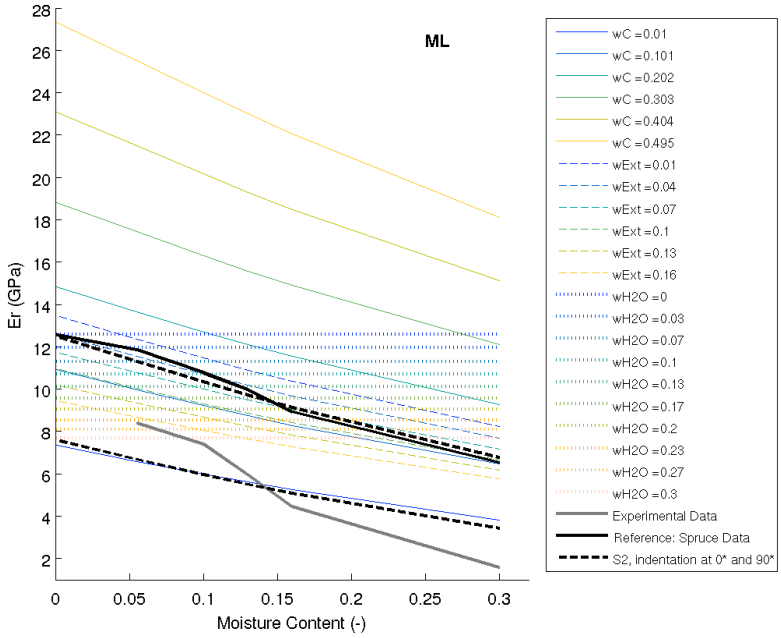

Figure 3.8: Parameter study for the influence of the chemical composition on the indentation modulus E_r of the middle lamella

Additionally, the extractives contents are considered to vary between 1% and 16%, the balance being conserved by a proportional equalization of the other wood chemical components at 1.

In Figure 3.9, both components, the cellulose and the extractives, seem to have a great influence on the mechanical properties of the cell wall, at all wood moisture contents. It also seems to confirm that the S2-layer should be modeled with higher cellulose contents and lower extractives contents than considered in Tab. 3.2. For example, only by varying the moisture content (under 30%) of spruce with its original chemical composition, the experimental indentation modulus measured at 100% RH can not be reached. But it could be reached with a MC of 30% if the cellulose content were higher (yellow solid line) or lower (blue solid line) or the extractives content lower (blue broken line).

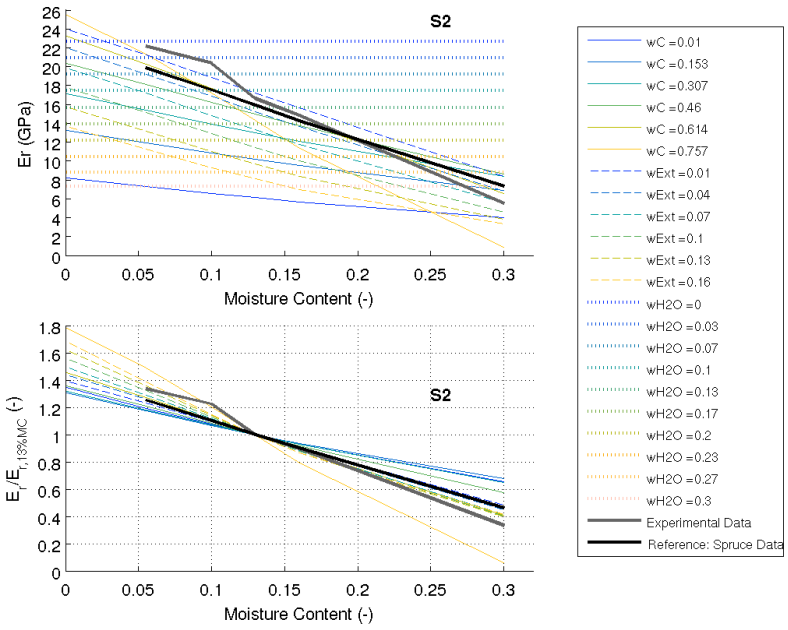

Figure 3.9: Parameter study for the influence of the chemical composition on the indentation modulus E_r of the S2-layer. Lower graphic: relative stiffness with respect to the stiffness at 13% MC

3.3.2 Variations of modeling approaches

The influence of different homogenization methods and of assumptions on microstructural characteristics of wood components will be assessed in the following.

Choice of the homogenization approach for step II

Two algorithms can be chosen for the last homogenization step of the model. The Mori-Tanaka (MT) approach is the classical one for composites made of one matrix phase and one reinforcement phase. But, when some cross-cellulose is added to the cellulose, as Li in 1999 [34] found out, the MT approach in this configuration gives a non-symmetric effective modulus, which contradicts the fundamental principles of mechanics. Thus, he developed a more accurate approach for multi-phase composite materials, named after himself, the so-called Li-approach. The disadvantage of this approach is the much longer computing time, because of the higher complexity of the algorithm. As regards the boundary conditions used in this approach, it can be considered as a mixture of the Mori-Tanaka and the self-consistent scheme (SCS) approaches.

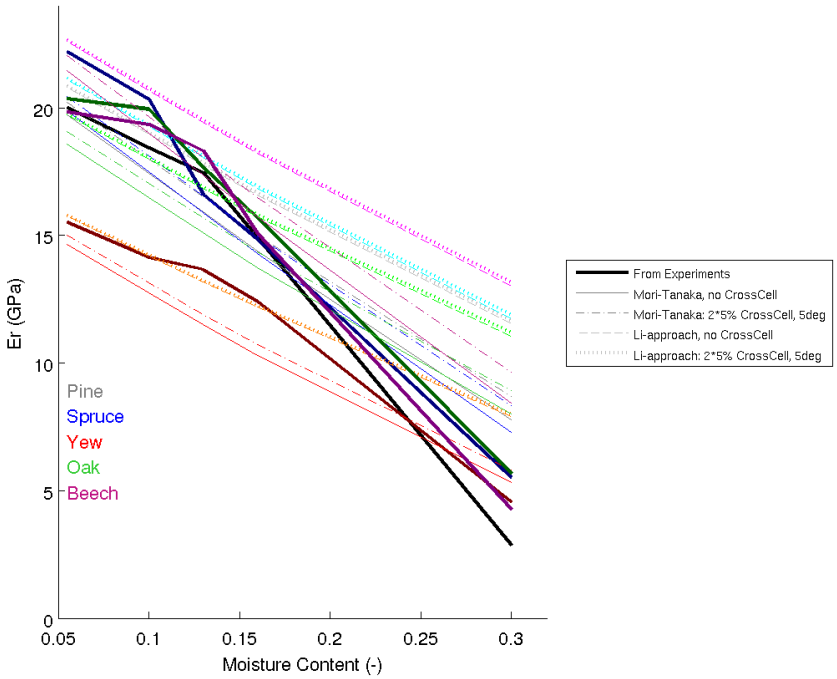

Figure 3.10: Comparison of indentation moduli E_r as predicted by two different approaches in step II (S2-layer model)

In Figure 3.10, as far as the indentation modulus is concerned, the MT approach clearly gives lower (from 1.5 and up to 2 GPa) and more moisture-sensitive results than the Li approach (the difference between the Li and the MT approaches increases up to 1.5 GPa between a MC of 0% and a MC of 30%), in all cellulose configurations. The Li approach, however, only barely takes into account the presence of cross cellulose.

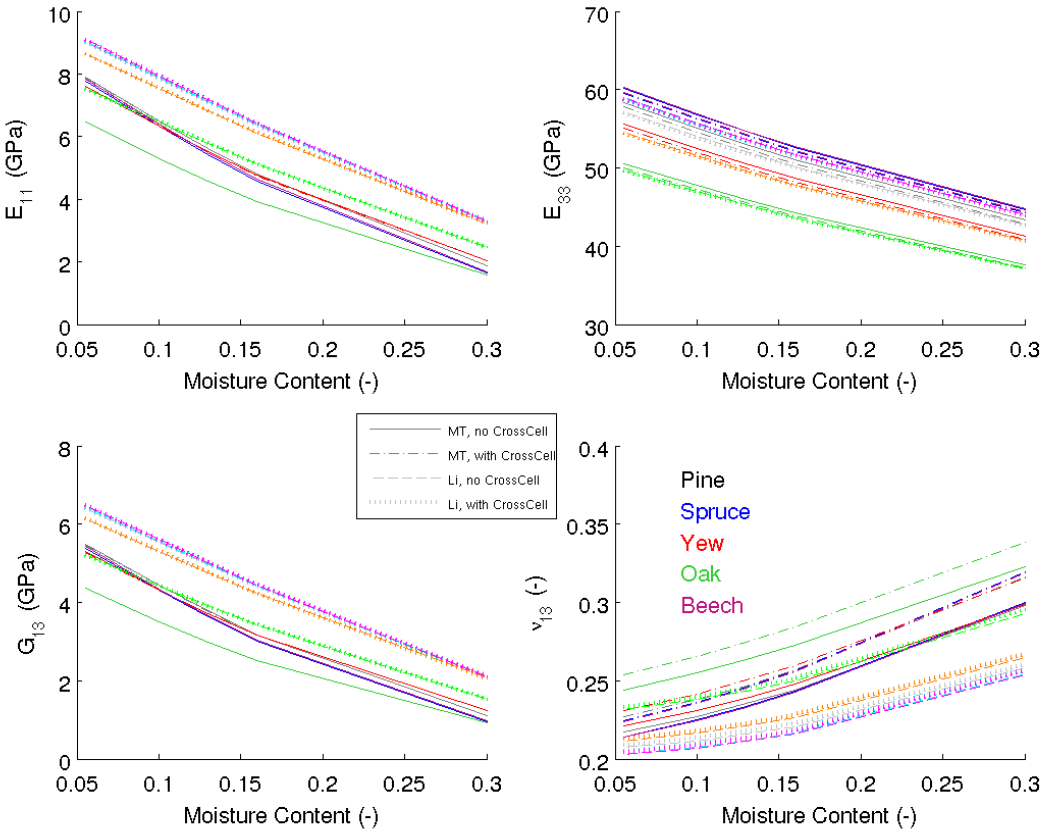

Figure 3.11: Comparison of stiffness components E_1, E_3, G_{13} and ν_{13} as predicted by two different approaches in step II (S2-layer model)

The stiffness components in Figure 3.11 all slightly follow the same trend as for the indentation modulus in Figure 3.10, except the elastic modulus in the longitudinal direction, which is nearly equal for all wood species, whatever approaches or cellulose configurations.

Choice of the modeling of water

By modeling the wood cell walls for different moisture contents, a crucial point of the work is the way the water is considered within the various cell wall layers.

Actually, two shapes for water in the polymer network are studied: spheres, which always lead to an isotropic material in the first step, or cylinders, which only lead to isotropic material behaviour if randomly distributed. Therefore, for cylinders, the water content is divided in three equal parts, which are all oriented in one of the three main directions of the current mathematical frame.

To ensure that no interference between the way the water is modeled and the choice of the algorithm in the final step influences the conclusions of this parameter study, the water model parameter study is combined with both the MT and the Li approaches.

S2-layer model

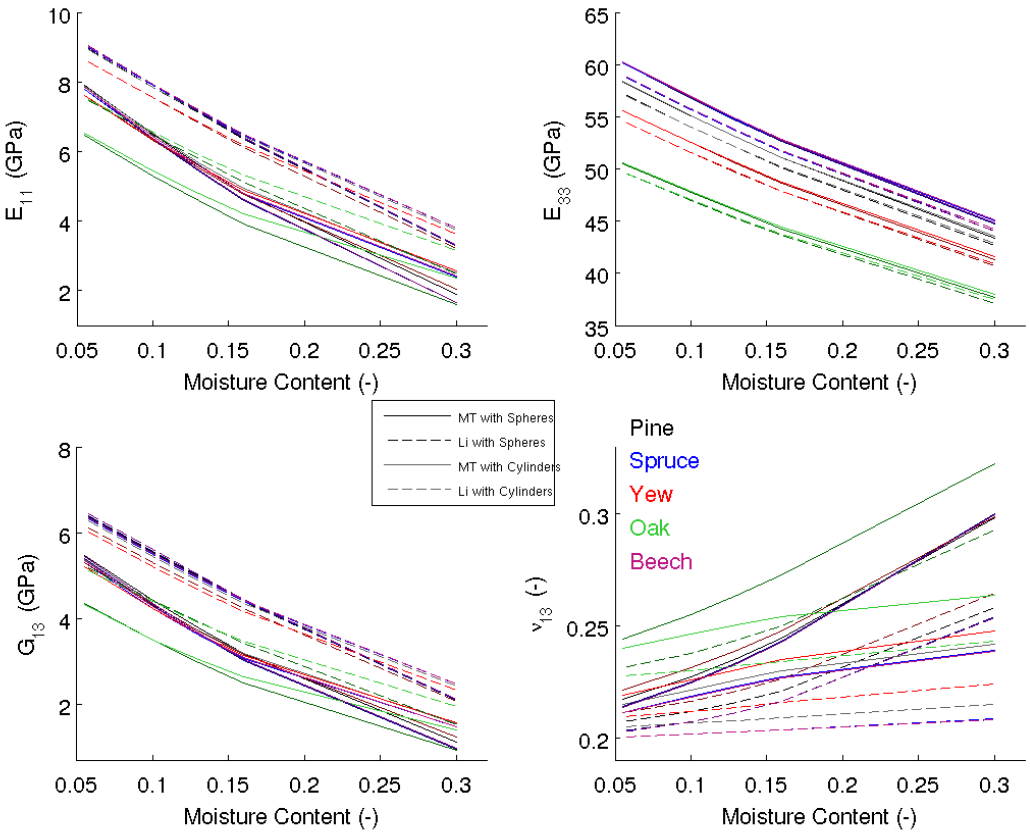

Figure 3.12: Comparison of stiffness components E_1, E_3, G_{13} and ν_{13} of the S2-layer as predicted by using two different models for the shape and orientation of water within the polymer network (step Ia)

For the indentation moduli (see Figure 3.13), the difference between the MT and the Li approaches is here to be found again. This difference is much bigger than the difference

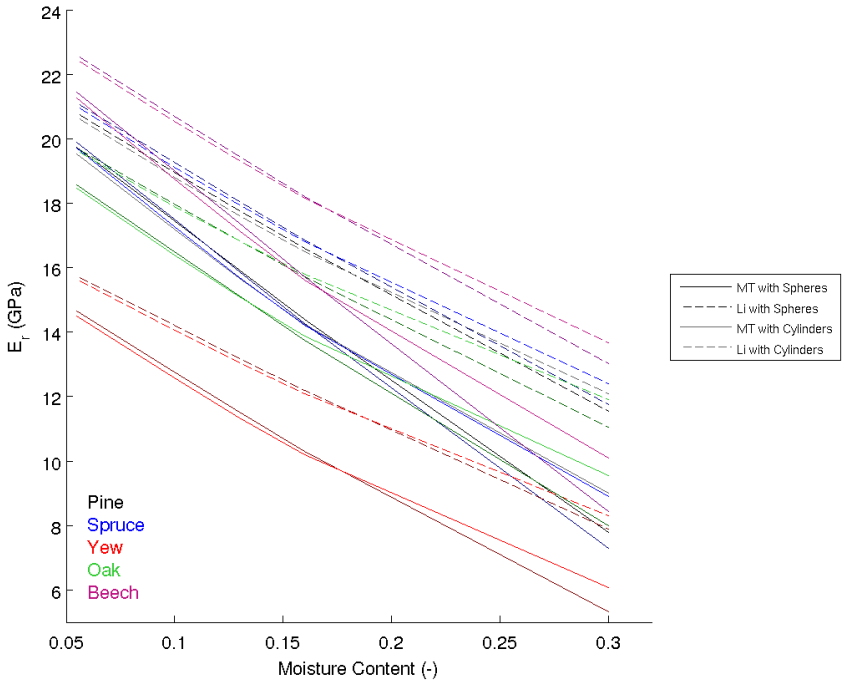

Figure 3.13: Comparison of indentation moduli E_r of the S2-layer as predicted by using two different models for the shape and orientation of water within the polymer network (step Ia)

caused by changing from a spherical shape to a cylindrical shape for the water. So, the highest indentation moduli are obtained for spheres with the Li approach, followed closely by these obtained for cylinders with the Li approach. Then comes the values for spheres with the MT approach and, at last, for cylinders with the MT approach.

For the stiffness components (see Figure 3.12), except for the Poisson's ratio, no clear difference can be seen between spherical and cylindrical shapes. Note that the spheres seem to be a little more moisture-sensitive than the cylinders.

Middle lamella

As shown in Figure 3.14, similar conclusions as for the S2-layer can be drawn for the ML. The only difference between the different ways of modeling is to be seen in the Poisson's ratio of the middle lamella model, which gives a little variation on the indentation modulus. However, this is small compared to the importance of the chosen approach in step II. Regardless of the chosen homogeneous approach, the difference between a water modeling as spheres and as cylinders is restricted to less than 1% over the whole investigated moisture range.

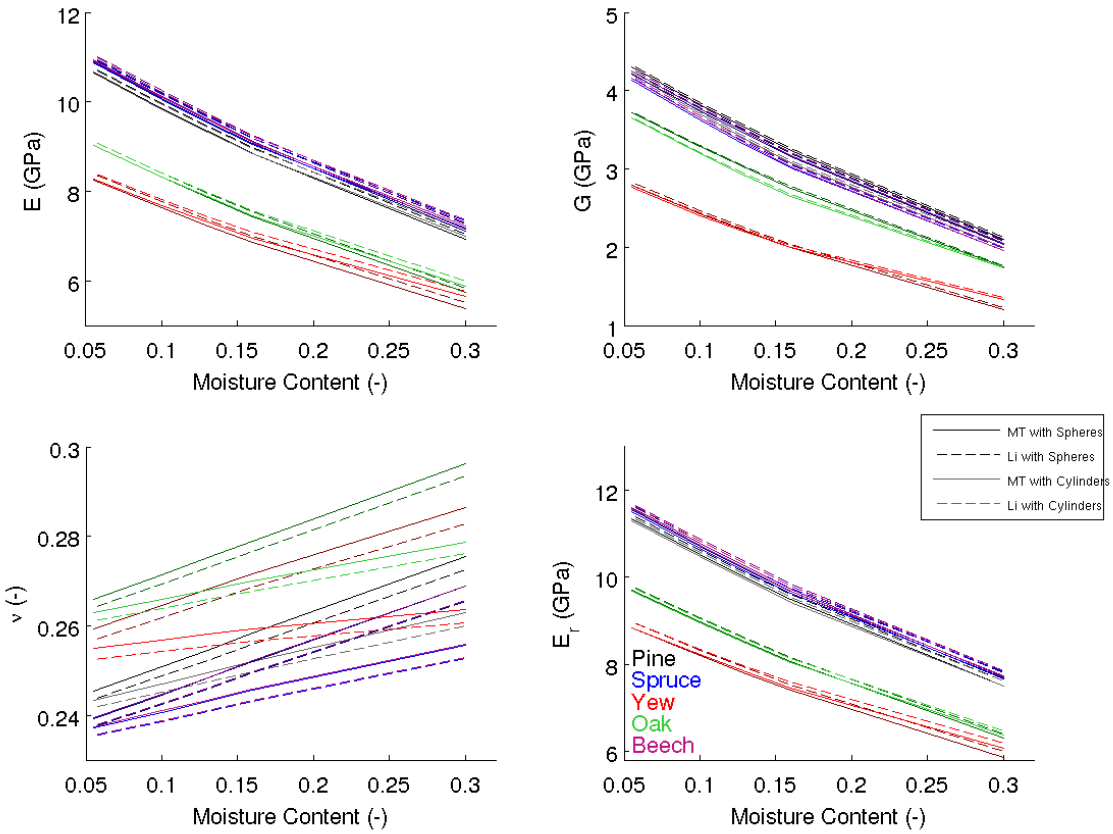

Figure 3.14: Comparison of indentation moduli E_r and of the stiffness components E, G and ν of the middle lamella as predicted by using two different models for the shape and orientation of water within the polymer network (step Ia)

3.4 Improvements of the micromechanical model

In the initial model, water was modeled by pores filled at least with the extractives, and, as the moisture content increases, also with water. There are several problems with this model.

From former studies (compiled in the doctoral thesis of Gloimüller [21]), it is known that water is mostly absorbed by the cellulose at 40% and the hemicelluloses at 43%, which implies some problems in the current model:

- Since only the polymer network is considered to absorb water, the cellulose model in step Ib has no poroelastic, but only linear elastic properties. However, the cellulose absorbs water, in more or less, as high proportions as the hemicelluloses.
- So far, the water was considered to be equally distributed over the middle lamella and the S2-layer. However, considering the affinity of hemicelluloses and cellulose with water as well as the different contents of these constituents within the cell wall layers, it clearly not equally distributed over these layers. Moreover, considering the comparison between model predictions and experiments, Figures 3.4 and 3.6, it seems that the influence of water is underestimated in the S2-layer and overestimated in the middle lamella. The presupposed water repartition between the S2-layer and the middle lamella has to be reconsidered.
- Water should rather be separated from the extractives, as the latest are rather hydrophobic.

Due to these issues, model improvements are proposed in the following.

3.4.1 Proposed adaptation for the simulation of water

As outlined in the paragraph above, the modeling of water has to be reconsidered to yield a better fit with the experimental results.

- First, water is separated from the extractives and considered as a separate phase in step Ia. Therefore, water is modeled in spherical pores, embedded in the polymer network made of hemicelluloses, lignin and extractives. The extractives are also modeled with a spherical shape.
- Then, a part of the total wood layer water is added to the cellulose in step Ib. It is modeled either by cylinders, with their directions spread out in the cellulose phase or aligned with the crystalline cellulose fibres, or by spheres. Hence, cellulose will exhibit poroelastic properties.
- Furthermore, the repartition of water within the cell wall, i.e. between the S2-layer and the middle lamella, as well as within one layer, i.e. between the polymer network in step Ia and the cellulose in step Ib, is calculated. In the PhD thesis of Gloimüller [21], a method for the calculation of water repartition between the S2-layer and the middle lamella was developed. This is reviewed in the following.

First, it is assumed that water is only repartitioned between the S2-layer and the ML, which yields the equation

$$m_{H_2O} = m_{H_2O,S2} + m_{H_2O,ML}. \tag{3.21}$$

Then, dividing this first equation by the dry wood mass m_{dry}, an equation for the total wood moisture content is obtained:

$$MC = \frac{m_{H_2O,S2}}{m_{dry}} + \frac{m_{H_2O,ML}}{m_{dry}}. \tag{3.22}$$

Replacing now $m_{H_2O,S2}$ by $MC_{S2} \cdot m_{dry,S2}$ in the latter equation, with the definitions $f_{S2} = \frac{m_{dry,S2}}{m_{dry}}$ and $f_{ML} = \frac{m_{dry,ML}}{m_{dry}}$, another expression for the global moisture content is obtained

$$MC = MC_{S2} \cdot f_{S2} + MC_{ML} \cdot f_{ML}. \tag{3.23}$$

The difficulty is to obtain an expression for MC_{S2} and MC_{ML}. Therefore, the relative sorptive capacities of the wood chemicals are used. They are summarized in Table 3.5 (from [21]). It is assumed that the sorptive capacity of one layer has a linear dependency on the sorptive capacities of its components, which means that $SC_{S2} = \sum_{i \in I} SC_i f_{S2,i}$ and $SC_{ML} = \sum_{i \in I} SC_i f_{ML,i}$, with I as the ensemble of all chemical components of the corresponding layer.

Table 3.5: Relative sorption capacities of chemical components of wood

Component	Sorption capacity
Cellulose	0.4
Hemicelluloses	0.43
Lignin	0.17
Extractives	0

Furthermore, with the definition of $SC_{j,rel} = \frac{SC_j}{\sum_{k \in S2,ML} SC_k}$ the relative sorptive capacity for the layer j, $j \in S2, ML$, we obtain the following relation

$$\frac{SC_{ML,rel}}{SC_{S2,rel}} = \frac{MC_{ML}}{MC_{S2}}. \tag{3.24}$$

Isolating the variable MC_{ML} (or MC_{S2}) from Equation (3.24) and reinserting it into Equation (3.23), an expression for MC_{ML} can be obtained

$$MC_{ML} = \frac{MC}{f_{S2} \cdot \frac{SC_{S2,rel}}{SC_{ML,rel}} + f_{ML}}. \tag{3.25}$$

The missing paramaters, f_{S2} and $f_{ML} = 1 - f_{S2}$ are obtained from [18]: for the latewood in softwoods, f_{S2} is 95% of the wood microstructure.

Finally, the calculated proportions of water in the ML and in the S2-layer are presented in Table 3.6.

For example, for a wood MC of 10%, the weight-percentage of water among the S2-layer will be of 10.075%, and only of 8.57% in the ML.

Table 3.6: Relative percentage of the wood total moisture content in the middle lamella and in the S2-layer

Wood species	$MC_{H2O,S2}(\%)$	$MC_{H2O,ML}(\%)$
Pine	100.75	85.7
Spruce	100.83	84.3
Yew	101.27	75.9
Oak	100.63	88.0
Beech	100.8	84.7

3.4.2 Improved micromechanical model for wood cell wall material

Step Ia: Polymer Network

Only minor changes compared to the model of Bader et al. [5] were implemented. The main difference is the introduction of a 4th phase for water, separated from the extractives.

Step Ib: Cellulose fibrils

The homogenization step of cellulose is the step that is adapted in this model. Indeed, due to the introduction of pores filled with water, cellulose gets poroelastic properties.

Corresponding phase strains are given in the following, with AC as the amorphous cellulose, CC as the crystalline cellulose and p as the pores filled with water:

$$\epsilon_{AC} = \mathbf{E}^0, \tag{3.26}$$

$$\boldsymbol{\varepsilon}_{CC} = [\mathbb{I} + \mathbb{P}_{CC} : (\mathbb{C}_{CC} - \mathbb{C}_{AC})]^{-1} : \mathbf{E}^0, \tag{3.27}$$

$$\boldsymbol{\varepsilon}_p = [\mathbb{I} - \mathbb{P}_p : \mathbb{C}_{AC}]^{-1} : [\mathbf{E}^0 - \mathbb{P}_p : \mathbf{1}p]. \tag{3.28}$$

Strain average equation gives a relation between $\mathbf{E}^0$ and $\mathbf{E}$, derived from Equations (3.2(a)) and (3.26) to (3.28).

$$\begin{aligned}\mathbf{E} = f_{AC}\mathbf{E}^0 + f_{CC}[\mathbb{I} + \mathbb{P}_{CC} : (\mathbb{C}_{CC} - \mathbb{C}_{AC})]^{-1} : \mathbf{E}^0 \\ + f_p[\mathbb{I} - \mathbb{P}_p : \mathbb{C}_{AC}]^{-1} : [\mathbf{E}^0 - \mathbb{P}_p : \mathbf{1}p]\end{aligned} \tag{3.29}$$

$$\begin{aligned}\mathbf{E}^0 = [f_{AC}\mathbb{I} + f_{CC}[\mathbb{I} + \mathbb{P}_{CC} : (\mathbb{C}_{CC} - \mathbb{C}_{AC})]^{-1} + f_p[\mathbb{I} - \mathbb{P}_p : \mathbb{C}_{AC}]^{-1}]^{-1} : \\ [\mathbf{E} + f_p\mathbb{P}_p : \mathbf{1}p]\end{aligned} \tag{3.30}$$

Then, we can extract the concentration tensors for the three phases with Equation (3.3(a)), reading as

$$\mathbb{A}_{AC} = [f_{AC}\mathbb{I} + f_{CC}[\mathbb{I} + \mathbb{P}_{CC} : (\mathbb{C}_{CC} - \mathbb{C}_{AC})]^{-1} + f_p[\mathbb{I} - \mathbb{P}_p : \mathbb{C}_{AC}]^{-1}]^{-1}, \tag{3.31}$$

$$\mathbb{A}_{CC} = [\mathbb{I} + \mathbb{P}_{CC} : (\mathbb{C}_{CC} - \mathbb{C}_{AC})]^{-1} : \mathbb{A}_{AC}, \tag{3.32}$$

$$\mathbb{A}_p = [\mathbb{I} - \mathbb{P}_p : \mathbb{C}_{AC}]^{-1} : \mathbb{A}_{AC}, \tag{3.33}$$

for amorphous cellulose, crystalline cellulose and the pore space filled with water, respectively.

The next step is to calculate the macroscopic average stress tensor $\boldsymbol{\Sigma}$, with

$$\boldsymbol{\Sigma} = f_{CC} \cdot \mathbb{C}_{CC} : \boldsymbol{\varepsilon}_{CC} + f_{AC} \cdot \mathbb{C}_{AC} : \boldsymbol{\varepsilon}_{AC} - f_p \cdot \mathbf{1} \cdot p, \tag{3.34}$$

which enables to get the homogenized drained stiffness of the material $\mathbb{C}_{cell}^{hom}$ with the poroelastic Equations (3.35) and 3.37.

$$\boldsymbol{\Sigma} = \mathbb{C}_{cell}^{hom} : \mathbf{E} + \boldsymbol{a}_p \cdot p, \tag{3.35}$$

with $\boldsymbol{a}_p$ is the pore pressure-related influence tensor as

$$\boldsymbol{a}_p = [\mathbb{I} - \mathbb{P}_p : \mathbb{C}_{AC}]^{-1} : [f_p \cdot \mathbb{A}_{AC} : [\mathbb{I} - \mathbb{P}_p : \mathbb{C}_{AC}]^{-1} - \mathbb{I}] : \mathbb{P}_p : \mathbf{1}. \tag{3.36}$$

The homogenized drained stiffness is given as

$$\mathbb{C}_{cell}^{hom} = f_{CC} \cdot \mathbb{C}_{CC} : \mathbb{A}_{CC} + f_{AC} \cdot \mathbb{C}_{AC} : \mathbb{A}_{AC}. \tag{3.37}$$

Finally, with the change of porosity

$$\phi - \phi_0 = f_p \cdot \mathbf{1} : \boldsymbol{\varepsilon}_p, \tag{3.38}$$

the Biot tensor $\boldsymbol{b}_{cell}$ and the Biot modulus N_{cell} can be calculated as

$$\boldsymbol{b}_{cell} = f_p \cdot \mathbf{1} : \mathbb{A}_p, \tag{3.39}$$

$$\frac{1}{N_{cell}} = f_p \cdot \mathbf{1} : \boldsymbol{a}_p. \tag{3.40}$$

Step II: In the cell wall

Phase strains of the components of the wood cell wall are given in Equations (3.41) and (3.42), where poly is the polymer network from step Ia and cell the cellulose fibrils from step Ib

$$\boldsymbol{\varepsilon}_{poly} = \mathbf{E}^0, \tag{3.41}$$

$$\boldsymbol{\varepsilon}_{cell} = [\mathbb{I} + \mathbb{P}_{cell} : (\mathbb{C}_{cell} - \mathbb{C}_{poly})]^{-1} : [\mathbf{E}^0 + \mathbb{P}_{cell} : (\boldsymbol{b}_{cell} - \boldsymbol{b}_{poly}) \cdot p]. \tag{3.42}$$

Then, with

$$\mathbf{E} = \sum_r f_r \boldsymbol{\varepsilon}_r, \tag{3.43}$$

$\mathbf{E}^0$ can be calculated as a function of $\mathbf{E}$, giving

$$\begin{aligned} \mathbf{E}^0 = [f_{poly} \cdot \mathbb{I} + f_{cell} \cdot [\mathbb{I} + \mathbb{P}_{cell} : (\mathbb{C}_{cell} - \mathbb{C}_{poly})]^{-1}]^{-1} : \\ [\mathbf{E} - f_{cell} \cdot [\mathbb{I} + \mathbb{P}_{cell} : (\mathbb{C}_{cell} - \mathbb{C}_{poly})]^{-1} : \mathbb{P}_{cell} : (\boldsymbol{b}_{cell} - \boldsymbol{b}_{poly}) \cdot p]. \end{aligned} \tag{3.44}$$

Combining Equation (3.44) with Equations (3.41) and (3.42) enables to get the expression for the phase concentration tensors $\mathbb{A}_{poly}$ and $\mathbb{A}_{cell}$

$$\mathbb{A}_{poly} = [f_{poly} \cdot \mathbb{I} + f_{cell} \cdot [\mathbb{I} + \mathbb{P}_{cell} : (\mathbb{C}_{cell} - \mathbb{C}_{poly})]^{-1}]^{-1}, \tag{3.45}$$

$$\mathbb{A}_{cell} = [\mathbb{I} + \mathbb{P}_{cell} : (\mathbb{C}_{cell} - \mathbb{C}_{poly})]^{-1} : \mathbb{A}_{poly}. \tag{3.46}$$

Then comes the classical equation for the homogenized drained stiffness of the cell wall material

$$\mathbb{C}^{hom} = f_{cell} \cdot \mathbb{C}_{cell} : \mathbb{A}_{cell} + f_{poly} \cdot \mathbb{C}_{poly} : \mathbb{A}_{poly} \tag{3.47}$$

Finally, for the calculation of the Biot tensor and Biot modulus, the porosity of both material phases has to be considered. Therefore, the porosity change $\phi - \phi_0$ is equal to

$$f_{poly} \cdot (\phi - \phi_0)_{poly} + f_{cell} \cdot (\phi - \phi_0)_{cell}. \tag{3.48}$$

Hence, using $\boldsymbol{a}_{cell}$, $\boldsymbol{a}_{poly}$, $\boldsymbol{b}_{cell}$,$\boldsymbol{b}_{poly}$, N_{cell} and N_{poly}, the Biot components of the homogenized cell wall material are given as

$$\boldsymbol{b}^{hom} = f_{cell} \cdot \boldsymbol{b}_{cell} : \mathbb{A}_{cell} + f_{poly} \cdot \boldsymbol{b}_{poly} : \mathbb{A}_{poly}, \tag{3.49}$$

$$\frac{1}{N^{hom}} = f_{cell} \cdot \boldsymbol{b}_{cell} : \boldsymbol{a}_{cell} + f_{poly} \cdot \boldsymbol{b}_{poly} : \boldsymbol{a}_{poly} + \frac{f_{poly}}{N_{poly}} + \frac{f_{cell}}{N_{cell}}. \tag{3.50}$$

Undrainded stiffness is used for comparison of model predictions with experimental data

$$\mathbb{C}_l^{undr} = \mathbb{C}_l^{dr} + M\boldsymbol{b}_l^{hom} \otimes \boldsymbol{b}_l^{hom}, \tag{3.51}$$

where $\mathbb{C}_l^{dr}$ the homogenized drained stiffness of the layer l, $\mathbb{C}_l^{undr}$ the homogenized undrained stiffness of the layer l and M as

$$M = \frac{\phi_0}{k_{H2O}} + \frac{1}{N^{hom}}. \tag{3.52}$$

ϕ_0 is the volume fraction of the pores and k_{H2O} the bulk modulus of water.

3.4.3 Model validation

Figures 3.15 and 3.16 show the corresponding model predictions for the indentation modulus of different wood species.

The proposed adaptation of the model for higher moisture contents does not seem to have improved the agreement between the indentation moduli of the S2-layer from the nanoindentation experiments and from the homogenization. In the following, the example of beech is detailed.

Table 3.7 summarizes the indentation moduli of the S2-layer of beech as determined by experiments, the initial and the improved model. The modified model decreased the indentation modulus of around 1 GPa for a moisture content range of 5.5 to 16%, but increased it for the FSP. The moisture-dependency of the modeled S2-layer has then been reduced with the improvements in the water modeling and it seems to better fit the experiments, especially at very low and very high moisture contents.

Table 3.7: Indentation modulus (GPa) of the S2-layer of beech from experiments, the initial model and the improved model

Relative humidity	10%	40%	60%	80%	100%
Moisture content	5.5%	10%	13%	16%	30%
Experiments	19.8	19.3	18.3	15.1	4.3
Initial model	21.5	19.0	17.4	15.7	8.4
Improved model	20.5	17.9	16.3	14.9	10.2

Table 3.8 summarizes the indentation moduli of the middle lamella of beech as determined by experiments, the initial and the improved model. The modified model decreased the indentation modulus of the modeled middle lamella by 0.3 to 0.7 GPa under 16% MC and 1 GPa for 30% MC. Thus, the moisture-dependency of the modeled middle lamella has been increased with the improvements in the water modeling.

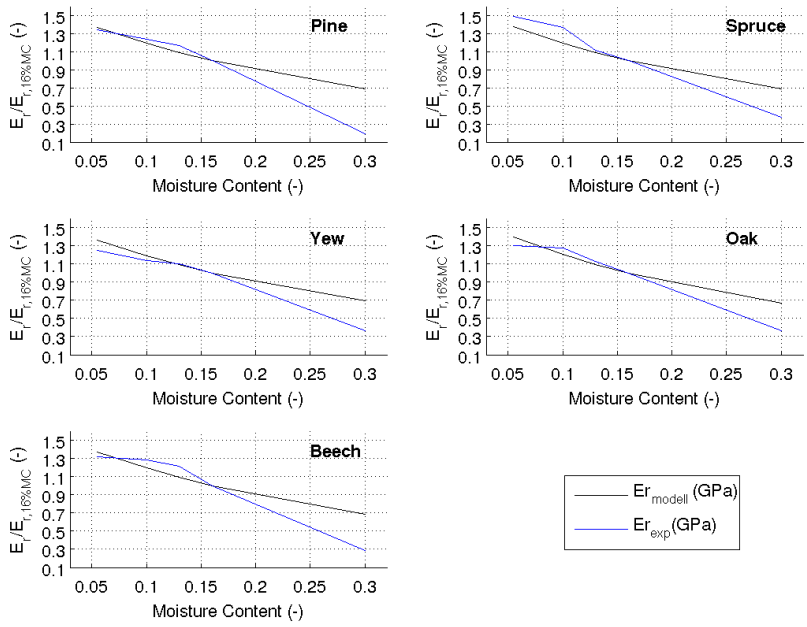

Figure 3.15: Comparison of the predicted and experimental relative indentation moduli of the S2-layer of different wood species with respect to the indentation moduli at 16% MC - improved model

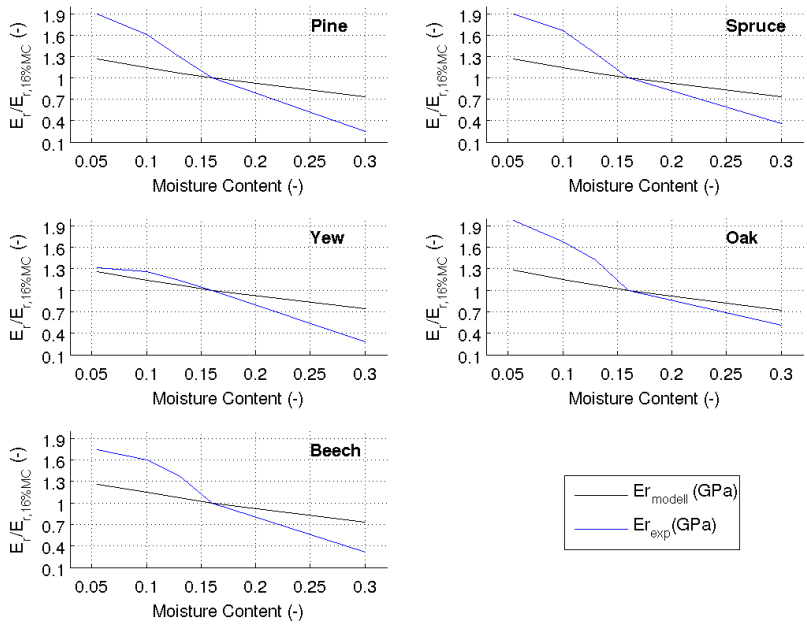

Figure 3.16: Comparison of the predicted and experimental relative indentation moduli the middle lamella of different wood species with respect to the indentation moduli at 16% MC - improved model

Table 3.8: Indentation modulus (GPa) of the middle lamella of beech as determined by experiments, the initial model and the improved model

Relative humidity	10%	40%	60%	80%	100%
Moisture content	5.5%	10%	13%	16%	30%
Experiments	8.7	8.0	6.9	5.0	1.6
Previous model	11.6	10.8	10.2	9.7	7.7
Actual model	11.3	10.3	9.6	9.0	6.6

From these example of beech, it can be concluded that the improved modeling of water modified the results in a positive sense, particularly in the ML. But the effect of the improvement is small and other measures could be taken to optimize the homogenization scheme from the point of view of the moisture-dependency of the cell wall layers.

Conclusion

The aim of this thesis was to determine the dependency of wood cell wall layers (S2 and middle lamella) towards moisture.

Therefore, the latewood wood cell walls were tested by means of nanoindentation measurements in a range of surrounding relative humidities between 10 and 80% RH as well as under water with a fluid cell. It followed that the elastic, viscoelastic and hardness properties of cell wall main layers of the wood microstructure are moisture dependent for the five investigated fresh wood species (three softwood and two hardwood species) and for the deteriorated wood from the Vasa ship. Yew seems to have the lowest indentation modulus and hardness and to be at the same time the lowest moisture-sensitive wood. The softwoods have the most moisture-sensitive mechanical properties among the fresh species. However, the wood from the Vasa ship is even more moisture sensitive than all fresh wood species. It could be shown that the hardness of the S2-layer does not depend of the cellulose microfibrils angle of the layer and is quite similar for all fresh wood specimens, except yew. It varies from 0.04 GPa for pine at 100% RH up to 0.51 GPa for spruce at 10% RH. The stiffness in the S2-layer is homogeneous, except for yew: it varies between 3 and 6 GPa at 100% RH and 20 to 22 GPa at 10% RH. For all wood species, the stiffness for the ML of fresh wood specimens is considerably lower as for the S2-layer, varying between 1.3 to 2.5 GPa at 100% RH and 7.8 to 9.7 GPa at 10% RH. The stiffness for the ML in hardwood seems to be higher as in softwood, yew excepted. Among all investigated wood specimens, pine is the species which encounters the biggest loss of stiffness for both layers between 80% RH and the fibre saturation point. As regards hardness for the ML, expect for yew, the experimental values are similar for all wood species, with a hardness between 0.045 and 0.075 GPa under water and 0.4 and 0.47 GPa at 10% RH. Since yew is more moisture-resistant, its hardness is already higher at 40% RH. For both layers and for hardness as well as for stiffness, the investigated hardwood species are less moisture-sensitive than the investigated softwood species, except yew, in particular for the ML. The creep parameters for the S2-layer of fresh wood species are similar for all wood species, with creep values of 14% and 10% for $Creep1$ and $Creep2$ at 10% RH, respectively, and of 24% and 17% under water, respectively. However, for the ML, beech and yew show a decrease in both creep parameters above 80% RH. No similarity within hardwood or softwood species is visible.

In a further step, the influence of the surrounding relative humidity between 10 and 80% RH on the moisture content of fresh investigated wood samples was investigated at 21 °C. This yielded the moisture desorption curve of the investigated wood species between 10 and 80% RH. For example, a relative humidity of 10% corresponded to a

moisture content of around 5%, while a relative humidity of 80% corresponded to a moisture content of around 16%.

Additionally, a micromechanical model for the cell walls was applied. It gives predictions of the elastic properties of fresh wood. These were compared to the experimental results. The comparison tool from Jäger et al. [30] gives for both investigated wood cell wall layers the relationship between the indentation modulus, the elastic properties and, for the S2-layer, the microfibril angle. Hence, the relationship between indentation modulus (as experimentally investigated), the chemical composition and the wood moisture content of a wood specimen could be predicted by this modeling approach.

The model was tested for both cell wall layer at various wood moisture contents between 5% MC and 30% MC. The stiffness components and thus the indentation modulus from the modeling are moisture-dependent. But the moisture dependency of most investigated wood species did not fit the experimentally determined dependency.

Therefore, the model for each layer was modified to improve the representation of water in a broader range of moisture contents. This included the proportions in which water may be absorbed by the different wood cell wall layers and by the different wood components inside one layer. This improved the model-predicted moisture-dependency of the calculated indentation modulus for the middle lamella. For the S2-layer, however, the moisture-dependency of the indentation modulus was reduced, with slight improvements for moisture contents lower than 16%.

Some points remain unclear at the end of this thesis. First, the ability of the cell walls of a nanoindentation sample embedded in resin to deform with varying moisture content should be quantified and better understood. This could be done with the measurement of the cell wall thickness with SEM under different environmental condition (e.g. a chamber pressure of 5 to 20 mbar). This could shade light on the role of the embedding resin in the moisture uptake of NI samples.

Then, considering e.g. Figure 2.16, the effect of a moisture content between 16 and 30% on the cell wall mechanical properties should be investigated to complement the experimental data. The difficulties for these measurements are the moisture-dependency of the electronic equipments in the Triboindenter and the capacity of the humidity generator to reach the desired relative humidity. The combination of ESEM and nanoindentation in the sams equipment may be a way for these investigations.

Finally, the micromechanical model for the cell wall layers should be further improved, maybe by increasing the precision in the chemical composition of the two investigated layer, by reconsidering the inputs for the mechanical properties of wood constituents or even the way water is represented in this model.

Bibliography

[1] M Arnold. Effect of moisture on the bending properties of thermally modified beech and spruce. *Journal of Materials Science*, 45(3):669–680, 2010.

[2] R Astley, J Harrington, and K Stol. Mechanical modelling of wood microstructure, an engineering approach. *IPENZ Transactions*, 24(1):43–50, 1997.

[3] R Astley, K Stol, and J Harrington. Modelling the elastic properties of softwood. part ii: The cellular microstructure. *Holz als Roh- und Werkstoff*, 56:43–50, 1998.

[4] T Bader, K Hofstetter, J Eberhardsteiner, and D Keunecke. Microstructure-Stiffness Relationships of Common Yew and Norway Spruce. *Strain*, 48(4):306–316, 2012.

[5] T Bader, K Hofstetter, C Hellmich, and J Eberhardsteiner. The poroelastic role of water in cell walls of the hierarchical composite "softwood". *Acta Mechanica*, 217(1-2):75–100, 2010.

[6] J Berthold, J Desbrières, M Rinaudo, and L Salmeń. Types of adsorbed water in relation to the ionic groups and their counter-ions for some cellulose derivatives. *Polymer*, 35(26):5729–5736, 1994.

[7] J Berthold, M Rinaudo, and L Salmeń. Association of water to polar groups; estimations by an adsorption model for ligno-cellulosic materials. *Colloids and Surfaces A Physicochemical and Engineering Aspects*, 112(2-3):117–129, 1996.

[8] University of Cambridge. Water's effect on the mechanical behaviour of wood, 2004-2013, `http://www.doitpoms.ac.uk/tlplib/wood/water_effect.php`.

[9] I Cave. Theory of x-ray measurement of microfibril angles in wood. *Forest Products Journal*, 16(10):37–13, 1966.

[10] W Cousins. Elastic modulus of lignin as related to moisture content. *Wood Science and Technology*, 10(1):9–17, 1976.

[11] W Cousins. Young's modulus of hemicellulose as related to moisture content. *Wood Science and Technology*, 12(3):161–167, 1978.

[12] K de Borst, T Bader, and C Wikete. Microstructure-stiffness relationships of ten european and tropical hardwood species. *Journal of Structural Biology*, 177:532–542, 2012.

[13] JM Dinwoodie. Timber – a review of the structure-mechanical property relationship. *Journal of Microscopy*, 1975.

[14] M Eder, O Arnould, J Dunlop, J Hornatowska, and L Salmeń. Experimental micromechanical characterisation of wood cell walls. *Wood Science and Technology*, 47(1):163–182, 2013.

[15] S Eichhorn and R Young. The young's modulus of a microcrystalline cellulose. *Cellulose*, 8(3):197–207, 2001.

[16] E Engelund. *Wood – water interactions linking molecular level mechanisms with macroscopic performance*. PhD thesis, Technical University of Denmark, 2011.

[17] E Engelund, L Thygesen, S Svensson, and C Hill. A critical discussion of the physics of wood–water interactions. *Wood Science and Technology*, 47(1):141–161, 2013.

[18] D Fengel and G Wegener. *Wood - Chemistry, Ultrastructure, Reactions*. Verlag Kessel, 2003.

[19] A Fischer-Cripps. *Nanoindentation*. Mechanical Engineering Series, 2004.

[20] Forest Products Laboratory. Wood Handbook: Wood as an Engineering Material. Technical report, USDA, Forest Service, 2010.

[21] S Gloimüller. *Multiscale Modeling and Experimental Investigation of the Hygroexpansion Behavior of Softwood*. PhD thesis, Technische Universität Wien, Austria, 2012.

[22] J Harrington, R Booker, and R Astley. Modelling the elastic properties of softwood. part i: The cell-wall lamellae. *Holz als Roh- und Werkstoff*, 56:37–41, 1998.

[23] C Hellmich and F Ulm. Drained and Undrained Poroelastic Properties of Healthy and Pathological Bone: A Poro-Micromechanical Investigation. *Transport in Porous Media*, 58(3):243–268, 2005.

[24] R Hill. Continuum micromechanics of elastoplastic polycrystals. *Journal of the Mechanics and Physics of Solids*, 13(2):89 – 101, 1965.

[25] P Hoffmeyer, E Engelund, and L Thygesen. Equilibrium moisture content (EMC) in Norway spruce during the first and second desorptions. *Holzforschung*, 65(6):875–882, January 2011.

[26] K Hofstetter, Ch Hellmich, and J Eberhardsteiner. Predicting wood strength from composition and microstructure: development and experimental verification of a continuum micromechanics model. In Paris Presses de l'ENPC, editor, *Microstructure et propriétés des matériaux*, 2005.

[27] K Hofstetter, Ch Hellmich, and J Eberhardsteiner. Micromechanical modeling of solid-type and plate-type deformation patterns within softwood materials. a review and an improved approach. *Holzforschung*, 61(4):343–351, 2007.

[28] Hysitron Corporation. *TI 900 Triboindenter® - Information Sheet*, 2010.

[29] CSM Instruments. Surface roughness influence on instrumented indentation testing, 2007, http://www.azonano.com/article.aspx?ArticleID=1930.

[30] A Jäger, T Bader, K Hofstetter, and J Eberhardsteiner. The relation between indentation modulus, microfibril angle, and elastic properties of wood cell walls. *Composites Part A Applied Science and Manufacturing*, 42(6):677–685, 2011.

[31] Y Kojima and H Yamamoto. Effect of moisture content on the longitudinal tensile creep behavior of wood. *Journal of Wood Science*, 51(5):462–467, October 2005.

[32] J Konnerth, N Gierlinger, J Keckes, and W Gindl. Actual versus apparent within cell wall variability of nanoindentation results from wood cell walls related to cellulose microfibril angle. *Journal of Materials Science*, 44(16):4399–4406, 2009.

[33] L&C Science and Technology. *RH-200 Relative Humidity Generator*, 2013.

[34] J Li. On micromechanics approximation for the effective thermoelastic moduli of multi-phase composite materials. *Mechanics of Materials*, 31(2):149–159, February 1999.

[35] Y Meng. Methods for characterizing mechanical properties of wood cell walls via nanoindentation. Master's thesis, University of Tennesee, Knoxville, 2010.

[36] K Nakamura, T Hatakeyama, and H Hatakeyama. Studies on Bound Water of Cellulose by Differential Scanning Calorimetry. *Textile Research Journal*, 51(9):607–613, 1981.

[37] Nasa - Glenn Research Center. *TEM Sample Preparation*, 2013.

[38] W Oliver and G Pharr. An improved technique for determining hardness and elastic modulus using load and displacement sensing indentation experiments. *Journal of Materials Research*, 7(06):1564–1583, January 1992.

[39] T Ovaert, B Kim, and J Wang. Multi-parameter models of the viscoelastic/plastic mechanical properties of coatings via combined nanoindentation and non-linear finite element modeling. *Progress in Organic Coatings*, 47(3–4):312–323, 2003.

[40] D Page, F El-Hosseiny, and K Winkler. Behaviour of single wood fibres under axial tensile strain. *Nature*, 229(5282):252–3, January 1971.

[41] C Plomion, G Le Provost, and A Stokes. Wood formation in trees. *Plant Physiology*, 127(4):1513–1523, 2001.

[42] B Poon, D Rittel, and G Ravichandran. An analysis of nanoindentation in linearly elastic solids. *International Journal of Solids and Structures*, 45:6018–6033, 2008.

[43] A Rafsanjani Abbasi. *Multiscale poroelastic model*. PhD thesis, ETH Zurich, Switzerland, 2013.

[44] A Reuss. Berechnung der fließgrenze von mischkristallen auf grund der plastizitätsbedingung für einkristalle. *Journal of Applier Mathematics and Mechanics*, 9:49–58, 1929.

[45] I Sakurada, Y Nukushina, and T Ito. Experimental determination of the elastic modulus of crystalline regions in oriented polymers. *Journal of Polymer Science*, 57(165):651–660, 1962.

[46] L Salmeǹ. *Temperature and water induced softening behaviour of wood fiber based materials*. PhD thesis, The Royal Institute of Technology, Sweden, 1982.

[47] W Schoch, I Heller, F Schweingruber, and F Kienast. Wood anatomy of central european species. `http://woodanatomy.ch`, 2004.

[48] JF Senft and BA Bendtsen. Measuring microfibrillar angles using light microscopy. *Wood and Fiber Science*, 17(4):564–567, 1985.

[49] C Skaar. *Wood-Water Relationships*, chapter 3, pages 127–172. 1984.

[50] J E Stone and A M Scallan. Effect of component removal upon the porous structure of the cell wall of wood. II. Swelling in water and the fiber saturation point. *Tappi*, pages 496–501, 1967.

[51] A Tamer and A Fauziah. *Cellulose Microfibril Angle in Wood and Its Dynamic Mechanical Significance, Cellulose - Fundamental Aspects*. Dr. Theo G.M. Van De Ven, 2013.

[52] K Tashiro and M Kobayashi. Theoretical evaluation of three-dimensional elastic constants of native and regenerated celluloses: role of hydrogen bonds. *Polymer*, 32(8):1516 – 1526, 1991.

[53] W Tze, S Wang, T Rials, G Pharr, and S Kelley. Nanoindentation of wood cell walls: Continuous stiffness and hardness measurements. *Composites Part A Applied Science and Manufacturing*, 38(3):945–953, 2007.

[54] W Voigt. Theoretische studien über die elasticitätsverhältnisse der krystalle. *Abh. Königliche Gesellschaft der Wissenschaft zu Göttingen, Math. Kl.*, 34:3–51, 1887.

[55] L Wagner, T Bader, D Auty, and K de Borst. Key parameters controlling stiffness variability within trees: a multiscale experimental–numerical approach. *Trees*, 27(1):321–336, 2013.

[56] R Wimmer, B Lucas, T Tsui, and W Oliver. Longitudinal hardness and Young's modulus of spruce tracheid secondary walls using nanoindentation technique. *Wood Science and Technology*, 31(2):131–141, April 1997.

[57] Y Yu, B Fei, H Wang, and G Tian. Longitudinal mechanical properties of cell wall of Masson pine (Pinus massoniana Lamb) as related to moisture content: A nanoindentation study. *Holzforschung*, 65(1):121–126, 2011.

[58] A Zaoui. Continuum micromechanics: Survey. *Journal of Engineering Mechanics*, 128(8):808–816, 2002.